広島大学学位請求論文

Design, Synthesis, and Photoreactions of Near Infrared Two-photon Responsive Caged Compounds Bearing Coumarin Scaffold

(近赤外２光子応答性

クマリン型ケージド化合物の設計、合成、光反応)

2021 年

広島大学大学院理学研究科

化学専攻

千歳　洋平

Table of Contents

1. 主論文

Design, Synthesis, and Photoreactions of Near Infrared Two-photon Responsive Caged Compounds Bearing Coumarin Scaffold
(近赤外２光子応答性
クマリン型ケージド化合物の設計、合成、光反応)

2. 公表論文

(1) “Design, Synthesis, and Reaction of π-Extended Coumarin-based New Caged Compounds with Two-photon Absorption Character in the Near-IR Region”
Youhei Chitose, Manabu Abe,* Ko Furukawa, and Claudine Katan*
Chem. Lett. **2016**, *45*, 1186–1188.

(2) “Design and Synthesis of a Caged Carboxylic Acid with a Donor−π−Donor Coumarin Structure: One-photon and Two-photon Uncaging Reactions Using Visible and Near-Infrared Lights”
Youhei Chitose, Manabu Abe,* Ko Furukawa, Jhe-Yi Lin, Tzu-Chau Lin,* and Claudine Katan*
Org. Lett. **2017**, *19*, 2622−2625.

3. 参考論文

(1) “Design and Synthesis of Two-Photon Responsive Chromophores for Near-Infrared Light-Induced Uncaging Reactions”
Manabu Abe,* Youhei Chitose, Satish Jakkampudi, Pham Thi Thu Thuy, Qianghua Lin, Bui Thi Van, Ayato Yamada, Ryoko Oyama, Miyu Sasaki, and Claudine Katan*
Synthesis, **2017**, *49* (5), 3337-3346.

(2) “２光子応答性ケージド化合物”
千歳　洋平，安倍　学*
光化学, **2017**, *48* (3), 130-138.

(3) “Design and synthesis of two-photon responsive chromophores for application to uncaging reactions”
Youhei Chitose, Manabu Abe*
Photochemistry, **2019**, *46*, 219-241.

(4) “Convenient one-pot access to 2H-3-nitrothiochromenes from 2-bromobenzaldehydes, sodium sulfide and β-nitrostyrenes”
Thi Thu Huong Le, Chitose Youhei, Quy Hien Le, Thanh Binh Nguyen, * Dinh Hung Mac*
Org. Biomol. Chem., **2019**, *17*, 6355-6358.

主論文

Design, Synthesis, and Photoreactions of Near Infrared Two-photon Responsive Caged Compounds Bearing Coumarin Scaffold

2021

Department of Chemistry
Graduate School of Science
Hiroshima University

Youhei Chitose

Contents

Chapter 1

General Introduction

1-1. Caged compounds

Light is a useful tool which can be used not only for generating photoluminescence from molecules but also triggering photoreactions such as photoinduced electron transfer, photolysis and so on. For biological study, two types of techniques with light irradiation have been developed so far. One is "imaging" technique using fluorescent probes.[1] Another is "concentration jump" method, by which the rise of concentration of bioactive compound can be controlled in micro to millisecond scale.[2] In this method, "caged compound" has been used in many physiological experiments. Caged compound is a temporally inactivated compound which can be activated by light irradiation to release a bioactive substance (Figure 1).[3] Photolabile protecting groups (PPGs) are used to make photocleavable covalent bonds with active sites of bioactive substances such as functional groups (-COOH, $-NH_2$, etc.). Caged compound enables spatiotemporal control of the release of bioactive compound only under light irradiation. Masking bioactive sites by PPGs is called "caging" process. On the other hand, the photoinduced regeneration of bioactive compound is "uncaging" process. By utilizing these two processes of caged compound, the "concentration jump" method can be a powerful strategy for investigating the unknown mechanism of cellular dynamics.

Since the first PPGs were developed by Barltrop,[4] Barton,[5,6] Woodward,[7] and Sheehan,[8] several types of PPGs have been introduced in biological study. In 1977, Engels and Schlaeger[9] and Kaplan[10] developed a caged adenosine cyclic 3',5'-phosphate (cAMP). In 1978, Hoffmann et al. developed a caged adenosine 5'-triphosphate used to study the Na/K pump of human red blood cell ghosts.[10]

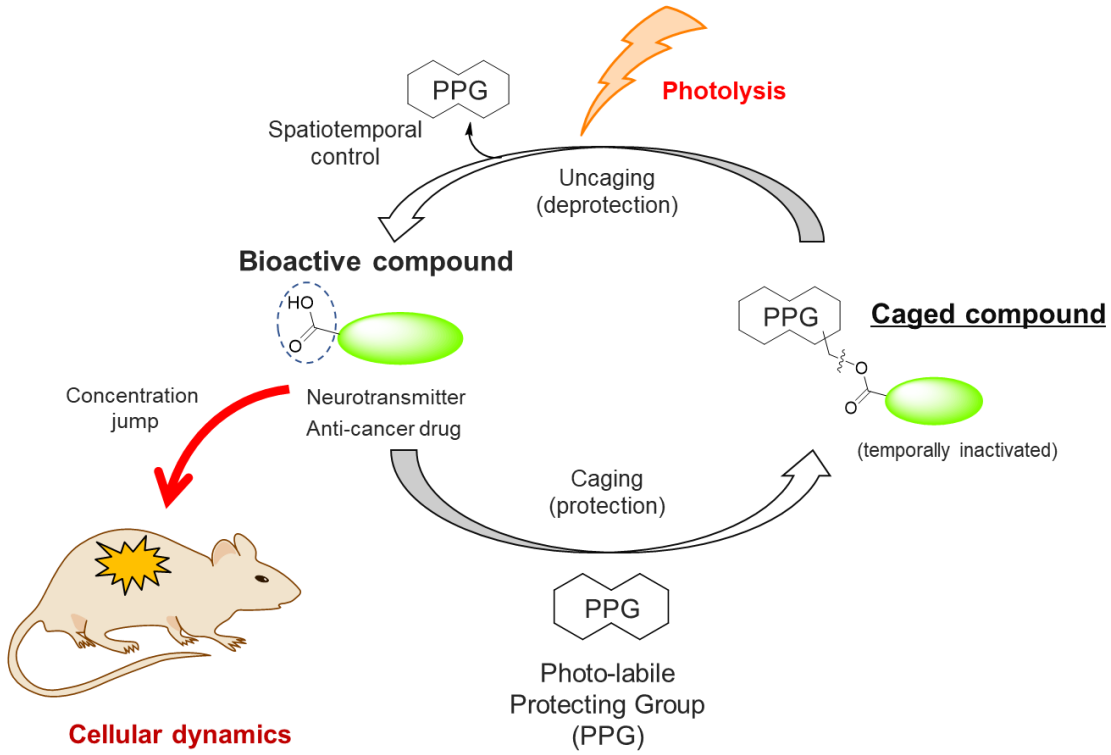

Figure 1. Caging and uncaging process of caged compound.

In the last two decades, there have been several reports on PPGs bearing different molecular structures. The uncaging mechanisms can be roughly classified into two categories. One is intramolecular rearrangement type such as ortho-nitrobenzyl (*o*-NB),[7,11] ortho-nitrophenylethyl (*o*-NPE),[12] ortho-nitroindoline (*o*-NI),[13] para-hydroxyphenacyl (*p*-HP),[14] thiochromone,[15] and stilbene,[16] (Figure 2). The other is photo-S_N1 type such as (coumarin-4yl)methyl,[17] xanthene,[18] quinoline,[19] BODIPY,[20] bimane,[21] and carbazole (CBZ)[22] (Figure 2). For example, the former ortho-nitrobenzyl (*o*-NB) type PPG is known to undergo uncaging reaction along with producing nitroso byproduct, which is thermally unstable and can be cytotoxic.[23] On the other hand, the latter, photo-S_N1 type triggers heterolytic bond-cleavage reaction to release bioactive substances, which can avoid cytotoxic byproducts such as nitroso byproduct (Figure 2). Especially, until recent years, various (coumarin-4yl)methyl (CM) type PPGs have been developed and applied from biological field to material sciences. These studies have been summarized in reviews.[2,3,24] In terms of the photophysical property and uncaging character, [7-(diethylamino)coumarin-4yl]methyl (DEACM) type is relatively

superior to conventional *o*-NB type.[25] In 2011, Heckel et al. reported that uncaging efficiency of DEACM derivative was much higher than that of *o*-NB type.[25] In addition, DEACM type has absorption wavelength over 400 nm, which allows uncaging reaction with less cellular damage compared to the uncaging reaction by UV light irradiation.

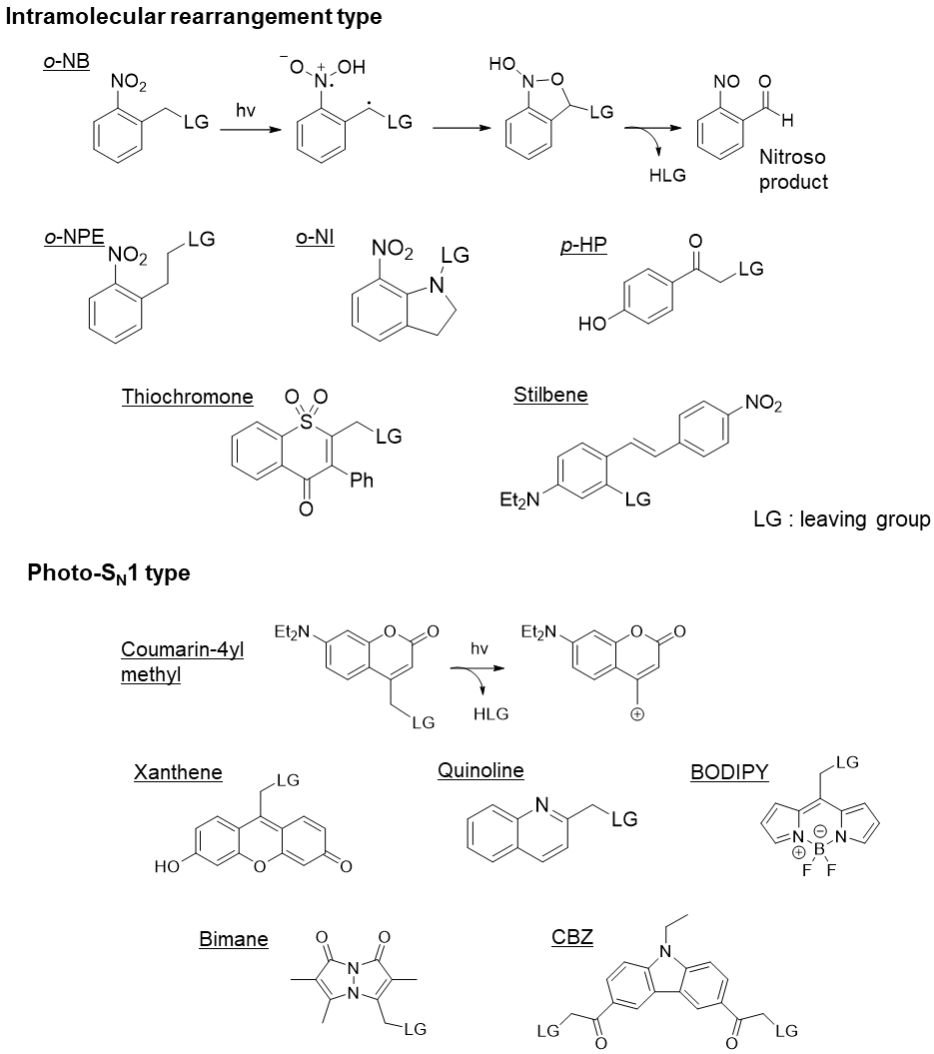

Figure 2. Photolabile protecting groups for uncaging reactions.

For the practicality of PPGs in biological research, there are several important criteria for biological studies: (i) PPGs should be sufficiently soluble in water and permeable in cell membrane. (ii) PPGs themselves and their uncaging by-products should be non-toxic in cellular tissues. (iii) uncaging reaction should be fast to

avoid long time photoirradiation. (iv) their molar extinction coefficients at excitation wavelength should be high for efficient uncaging efficiency. (v) the photobleaching of caged compound should not compete with the absorption of uncaging byproduct at excitation wavelength.

1-2. One-photon (OP) excitation and two-photon (TP) excitation

The uncaging reactions of bioactive substances have been often carried out by OP excitation using ultraviolet or visible light irradiations. However, photoirradiation by UV-vis light can cause invasive and undesired damages to cellular tissues.[26] Moreover, in the OP excitation, the spatial control of uncaging area is limited due to the scattering and low light penetration of UV-vis light. To overcome these practical issues, two-photon (TP) excitation using near infrared light has become important technology in biological study. Compared to UV-vis light, near infrared light in optical window (650-1050 nm) is more suitable because it can penetrate deeper to cellular tissues.[27,28] In the TP excitation process, although high laser intensity is required, a molecule can interact with two photons simultaneously.[29,30] This two-photon absorption (TPA) phenomenon enables an electronic excitation to the same excited state reached by OP excitation using UV-vis light (Figure 3a), even though the molecule does not show near infrared absorption in the OPA process. Approximately half a photon energy of OP excitation can be used in the TPA process. The advantages of near infrared TP excitation for caged compounds in biological study are the highly spatiotemporal control of uncaging reaction and less harmful excitation to cellular tissues. In contrast to OP excitation, the excitation probability of TP excitation is proportional to the square of incident light intensity. Thus, molecules can be excited only in the focal point, providing more spatial control of uncaging reaction (Figure 3a).[31] If chromophore possesses sufficiently high TPA and TP uncaging character, photo-induced damages to the cells can be suppressed.

(a)

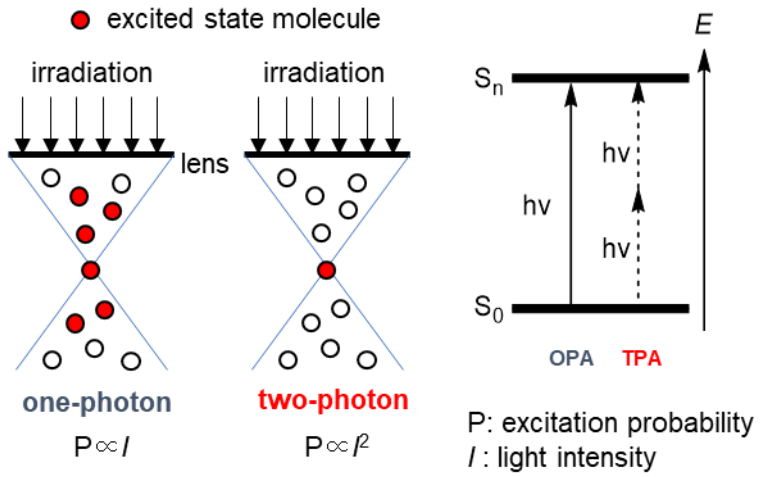

(b)

$$\sigma_2 \approx C \times \left[\frac{\mu_{gi}^2 \times \mu_{if}^2}{((E_{gi}/E_{gf}) - 1)^2 \Gamma} + 4\frac{\Delta\mu_{gf}^2 \times \mu_{gf}^2}{\Gamma}\right] \text{(GM)}$$

σ_2 :TPA cross-section in GM

μ_{gi} : transition dipole moment g → i

μ_{if} : transition dipole moment i → f

μ_{gf} : transition dipole moment g → f

$\Delta\mu_{gf}$: difference between excited and ground state dipole moment

Γ : half width at half maximum of the TPA band

g: ground state
i: intermediate state
f: final state

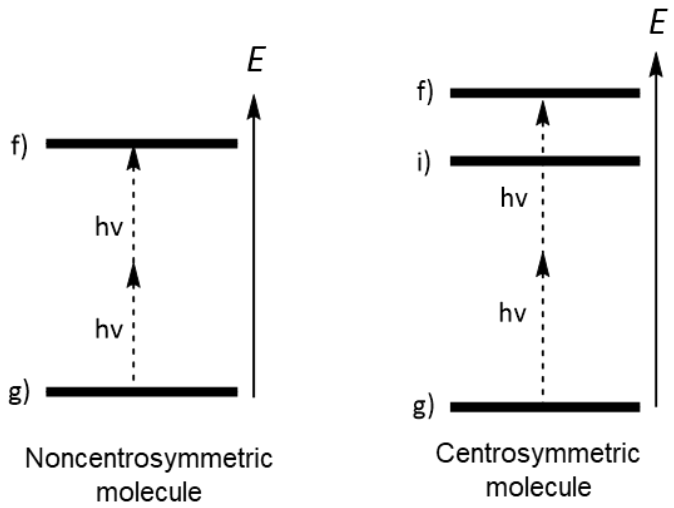

(c) $$\delta_u = \sigma_2 \times \Phi_u$$

δ_u : TP uncaging efficiency
σ_2 :TPA cross-section
Φ_u : uncaging quantum yield

Figure 3. (a) OP and TP excitation process, and the related equations about (b) TPA cross-section and (c) TP uncaging efficiency

TP-induced uncaging efficiency ($\delta_u = \sigma_2 \times \Phi_u$) of caged compound is calculated using TPA cross-section value (σ_2 in GM) (1 GM = 10^{-50} cm^4 s $photon^{-1}$), multiplied by the uncaging quantum yield (Φ_u) (Figure 3c). The unit of GM is in honor of Maria Göppert-Mayer, who originally proposed the theory of TPA in 1931.[32] The phenomenon of TPA was experimentally observed in 1961.[33] TP uncaging techniques has been also developed using several caged compounds.[3] Efficient TP responsive chromophores should be designed for biomedical purpose. Some physiologists suggested that 3 GM of δ_u as an ideal value for biological application.[34] Therefore, caged compound with high TPA cross-section and high uncaging quantum yield will be promising.

1-3. Molecular design for TP responsive chromophores

To design a chromophore with high TPA cross-section, there are several factors that can be tuned by structural modification. The main factors are (i) extension of π-conjugation and (ii) transition dipole moment.

(i) Extension of π-conjugation: This is the basic strategy to increase TPA cross-section. For example, benzene, which is the most common chemical structure, has almost no TPA cross-section. On the other hand, naphthalene shows a slight TPA character (0.9 GM at 530 nm).[35] However, trans-stilbene, which has a double bond between two benzene rings, shows significant increase of TPA cross-section (12 GM at 514 GM) (Figure 4).[36] Based on this fact, π-extended structure is found to be an important key to design TP-responsive chromophore.

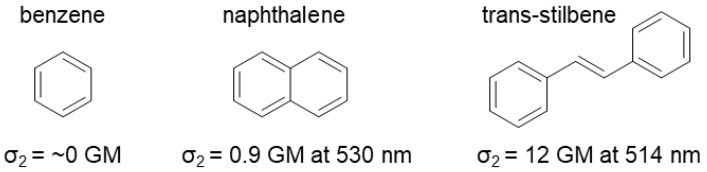

Figure 4. Effect of π-conjugation on TPA cross-section.

(ii) Transition dipole moment: According to the theoretical equation of TPA cross-section (Figure 3b)[37a-b], for noncentrosymmetric molecule, the first term in the square bracket can be omitted and the second term is dominant.[37a] In this case, TPA is proportional to the product of squared transition dipole moment and the squared difference between excited and ground state dipole moment (two-state model). For centrosymmetric molecule, the second term in the square bracket vanishes because the dipole difference ($\Delta\mu_{gf}$) is zero due to the centrosymmetry (three-state model). Thus, increasing intramolecular charge transfer character by introducing strong electron-donor (D) or acceptor (A) substituents is the key strategy to increase TPA cross-section of chromophore. Multipolar systems such as dipolar, quadrupolar, and octupolar have been introduced so far.

The dipolar system is constructed by non-symmetric D-π-A topology. The charge transfer occurs from donor unit to acceptor unit, giving high transition dipole moment. TPA process is explained by using two-state model, in which the TPA maxima are found in the nearly double the OPA maxima.[37c] In the non-symmetric molecules, the 1st electronic transition ($S_0 \rightarrow S_1$) is both OP and TP allowed. The D-π-A based stilbene derivative (Figure 5) shows higher TPA cross-section (100 GM at 830 nm) than that of parent trans-stilbene.[38]

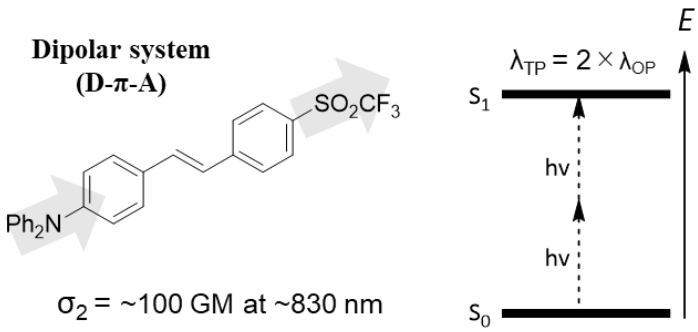

Figure 5. TPA of dipolar system.

The quadrupolar system is constructed by centrosymmetric D-π-D or A-π-A topology. The TPA cross-section of D-π-D analogues (Figure 6) is about 10-100 times higher than that of trans-stilbene.[39,40] The electronic excited states are described by using three-state model. In the centrosymmetric chromophore, the transition from ground state (S_0) to the lowest excited state (S_1) can be achieved by OP excitation. However, the $S_0 \rightarrow S_1$ transition is TP forbidden. On the other hand, the $S_0 \rightarrow S_2$ transition is TP allowed. Hence, TPA maxima are shorter than the double OPA maxima in quadrupolar system.[37c]

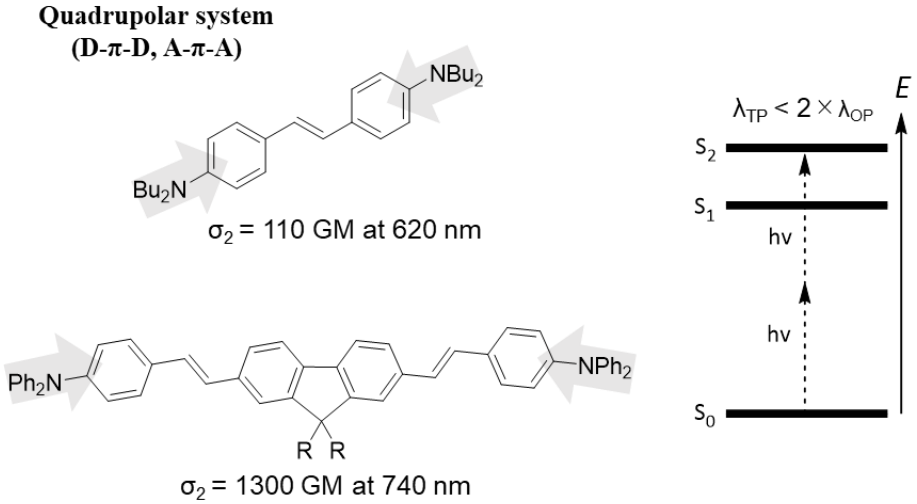

Figure 6. TPA of quadrupolar system.

Octupolar character arises in the trimetric structure (Figure 7). The centrosymmetric chromophore built from three branched dipolar unit is drawn as D(-π-A)$_3$ or A(-π-D)$_3$. Compared to dipolar system, the D(-π-A)$_3$ analogue in Figure 7 shows significantly enhanced TPA cross-section (450 GM at 740 nm).[38] The excited states of octupolar system are divided into the highest excited state (S_3) and two degenerated states (S_1 and S_2). The transition from ground state to the two degenerated states ($S_0 \rightarrow S_1$ and $S_0 \rightarrow S_2$) are OP allowed whereas these transitions are slightly TP allowed.[37c] Despite the vanishing transition dipole moment, the $S_0 \rightarrow S_3$ transition is TP allowed.

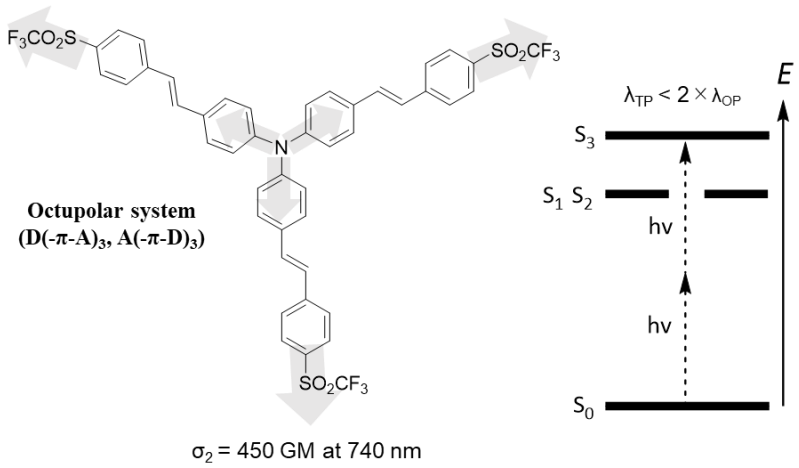

Figure 7. TPA of octupolar system.

1-4. Near infrared TP uncaging of neurotransmitter using (coumarin-4yl)methyl type PPG in biological study

Since Denk et al. developed two-photon microscopy in 1990,[41] many chromophores have been used for caged neurotransmitters.[42] Especially, caged glutamate is one of the most developed caged compounds in biology. Glutamate is the major neurotransmitter in our brain tissues, and the first report of caged glutamate appeared in 1993.[43] However, conventional PPGs showed only effectiveness under UV-vis light but showed few TP sensitivity on their uncaging reactions. In 1999, Tsien and co-workers developed a (6-bromo-7-hydroxycoumarin-4yl)methyl (Bhc) type PPG to investigate glutamate sensitivities over the surface of neuron (Figure 8).[44] Bhc-Glu is the first caged glutamate that allowed near infrared TP photolysis under physiological condition. TP uncaging efficiency of Bhc-Glu was calculated to be ~ 1.0 GM at 740 nm, which was acceptable for their experimental condition. Their work implicated a lot of potential of (coumarin-4yl)methyl PPGs for highly TP responsive uncaging reaction.

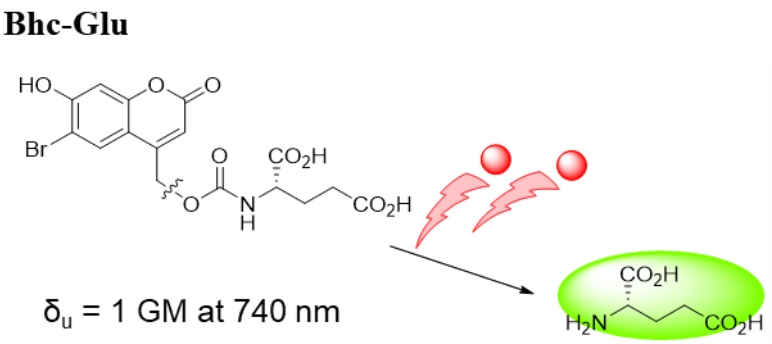

Figure 8. TP uncaging of caged glutamate with coumarin structure.

1-5. Purpose of this research study

So far, either 3-position or 7-postion of coumarin has been frequently modified by introducing electron-donor or electron-acceptor group.[3] This flexibility for structural modification allows us to design TP responsive chromophores based on trans-stilbene backbone. As we described above, multipolar unit can be a key factor to increase TPA character. In this research, we design and synthesize π-extended coumarin based caged compound with dipolar and quadrupolar character.

References:

1) (a) Cornea, A.; Conn, P. M. Eds. In *Fluorescence Microscopy,* Elsevier, 2014. (b) Kim, H. M.; Cho, B. R. Small-Molecule Two-Photon Probes for Bioimaging Applications. *Chem. Rev.* **2015**, *115*, 5014–5055.
2) Corrie, J. E. T.; Furuta, T.; Givens, R.; Yousef, A. L.; Goeldner, M. Photoremovable Protecting Groups Used for the Caging of Biomolecules. *Dynamic Studies in Biology*; Goeldner, M., Givens, R., Eds., 2005.
3) (a) Klán, P.; Šolomek, T.; Bochet, C. G.; Blanc, A.; Givens, R.; Rubina, M.; Popik, V.; Kostikov, A.; Wirz, J. Photoremovable Protecting Groups in Chemistry and Biology: Reaction Mechanisms and Efficacy. *Chem. Rev*. **2013**, *113*, 119–191. (b) Weinstain, R.; Slanina, T.; Kand, D.; Klán, P. Visible-to-NIR-Light Activated Release: From Small Molecules to Nanomaterials. *Chem. Rev*. **2020**, *120*, 13135–13272.
4) Barltrop, J. A.; Schofield, P. PHOTOSENSITIVE PROTECTING GROUP. *Tetrahedron Lett*. **1962**, *16*, 697–699.
5) Barton, D. H. R.; Chow, Y. L.; Cox, A.; Kirby, G. W. Photosensitive Protection of Functional Groups. *Tetrahedron Lett.* **1962**, *23*, 1055–1057.
6) D. H. R. Barton, Y. L. Chow, A. Cox, G. W. K. 654. Photochemical Transformations. Part XIX. Some Photosensitive Protecting Groups. *J. Chem. Soc.* **1965**, 3571–3578.
7) Patchornik, A.; Amit, B.; Woodward, R. B. Photosensitive Protecting Groups. *J. Am. Chem. Soc.* **1970**, *92*, 6333–6335.
8) Sheehan, J. C.; Wilson, R. M. Photolysis of Desyl Compounds. A New Photolytic Cyclization. *J. Am. Chem. Soc.* **1964**, *86*, 5277–5281.
9) Engels, J.; Schlaeger, E. J. Synthesis, Structure, and Reactivity of Adenosine Cyclic 3′,5′-Phosphate-Benzyl Triesters. *J. Med. Chem*. **1977**, *20* (7), 907–911.
10) Kaplan, J. H.; Forbush, B.; Hoffman, J. F. Rapid Photolytic Release of Adenosine 5′-Triphosphate from a Protected Analogue: Utilization by the Na:K Pump of Human Red Blood Cell Ghosts. *Biochemistry* **1978**, *17* (10),

1929–1935.

11) (a) Barltrop, J. A.; Plant, P. J. Photosensitive Protective Groups. *Chem. Commun.* **1966**, *22*, 822–823. (b) Il'ichev, Y. V.; Schwörer, M. A.; Wirz, J. Photochemical Reaction Mechanisms of 2-Nitrobenzyl Compounds: Methyl Ethers and Caged ATP. *J. Am. Chem. Soc.* **2004**, *126* (14), 4581–4595.

12) (a) Foote, R. S.; Cornwell, P.; Isham, K. R.; Gigerich, H.; Stengele, K.-P.; Pfleiderer, W.; Sachleben, R. A. Photolabile Protecting Groups for Nucleosides:Synthesis and Photodeprotection Rates. *Tetrahedron* **1997**, *53* (12), 4247–4264. (b) Gug, S.; Charon, S.; Specht, A.; Alarcon, K.; Ogden, D.; Zietz, B.; Léonard, J.; Haacke, S.; Bolze, F.; Nicoud, J. F.; Goeldner, M. Photolabile Glutamate Protecting Group with High One- and Two-Photon Uncaging Efficiencies. *ChemBioChem* **2008**, *9*, 1303–1307. (c) Donato, L.; Mourot, A.; Davenport, C. M.; Herbivo, C.; Warther, D.; Léonard, J.; Bolze, F.; Nicoud, J. F.; Kramer, R. H.; Goeldner, M.; Specht, A. Water-Soluble, Donor-Acceptor Biphenyl Derivatives in the 2-(o-Nitrophenyl)Propyl Series: Highly Efficient Two-Photon Uncaging of the Neurotransmitter γ-Aminobutyric Acid at λ = 800 nm. *Angew. Chemie. Int. Ed.* **2012**, *51*, 1840–1843. (d) Specht, A.; Bolze, F.; Donato, L.; Herbivo, C.; Charon, S.; Warther, D.; Gug, S.; Nicoud, J. F.; Goeldner, M. The Donor-Acceptor Biphenyl Platform: A Versatile Chromophore for the Engineering of Highly Efficient Two-Photon Sensitive Photoremovable Protecting Groups. *Photochem. Photobiol. Sci*. **2012**, *11*, 578–586.

13) (a) Amit, B.; Patchornik, A. The Photorearrangement of N-Substituted Ortho-Nitroanilides and Nitroveratramides. A Potential Photosensitive Protecting Group. *Tetrahedron Lett.* **1973**, *24*, 2205–2208. (b) Amit, B.; Ben-Efraim, D. A.; Patchornik, A. Light-Sensitive Amides. The Photosolvolysis of Substituted 1-Acyl-7-Nitroindolines. *J. Am. Chem. Soc.* **1976**, *98* (3), 843–844. (c) Morrison, J.; Wan, P.; Corrie, J. E. T.; Papageorgiou, G. Mechanisms of Photorelease of Carboxylic Acids from 1-Acyl-7-Nitroindolines in Solutions of Varying Water Content. *Photochem. Photobiol. Sci*. **2002**, *1*, 960–969. (d) Cohen, A. D.; Helgen, C.; Bochet, C. G.; Toscano, J. P. The Mechanism of Photoinduced Acylation of Amines by N-Acyl-5,7- Dinitroindoline as Determined by

Time-Resolved Infrared Spectroscopy. *Org. Lett.* **2005**, *7* (14), 2845–2848. (e) Corrie, J. E. T.; Barth, A.; Papageorgiou, G. Synthesis and Characterisation of 13C and 15N Isotopomers of a 1-Acyl-7-Nitroindoline. *J. Label. Compd. Radiopharm.* **2001**, *44*, 619–626. (f) Lipshutz, B. H.; Wilhelm, R. S.; Floyd, D. M. Chemistry of Higher Order, Mixed Organocuprates. 1. Substitution Reactions at Unactivated Secondary Centers. *J. Am. Chem. Soc.* **1981**, *103* (25), 7672–7674. (g)Papageorgiou, G.; Ogden, D. C.; Barth, A.; Corrie, J. E. T. Photorelease of Carboxylic Acids from 1-Acyl-7-Nitroindolines in Aqueous Solution: Rapid and Efficient Photorelease of L-Glutamate. *J. Am. Chem. Soc.* **1999**, *121* (27), 6503–6504. (h) Matsuzaki, M.; Hayama, T.; Kasai, H.; Ellis-Davies, G. C. R. *Nat. Chem. Biol.* **2010**, *6*, 255.

14) (a) Givens, R. S.; Park, C. H. P-Hydroxyphenacyl ATP: A New Phototrigger. *Tetrahedron Lett.* **1996**, *37* (35), 6259–6262. (b) Park, C. H.; Givens, R. S. New Photoactivated Protecting Groups. 6. p-Hydroxyphenacyl: A Phototrigger for Chemical and Biochemical Probes. *J. Am. Chem. Soc.* **1997**, *119* (10), 2453–2463. (c) Givens, R. S.; Jung, A.; Park, C. H.; Weber, J.; Bartlett, W. New Photoactivated Protecting Groups. 7. p-Hydroxyphenacyl: A Phototrigger for Excitatory Amino Acids and Peptides. *J. Am. Chem. Soc.* **1997**, *119* (35), 8369–8370. (d) Givens, R. S.; Weber, J. F. W.; Conrad, P. G.; Orosz, G.; Donahue, S. L.; Thayer, S. A. New Phototriggers 9: P-Hydroxyphenacyl as a C-Terminal Photoremovable Protecting Group for Oligopeptides. *J. Am. Chem. Soc.* **2000**, *122* (12), 2687–2697. (e) Bownik, I.; Šebej, P.; Literák, J.; Heger, D.; Šimek, Z.; Givens, R. S.; Klán, P. 4-Hydroxyphenacyl Ammonium Salts: A Photoremovable Protecting Group for Amines in Aqueous Solutions. *J. Org. Chem.* **2015**, *80*, 9713–9721. (f) Slanina, T.; Šebej, P.; Heckel, A.; Givens, R. S.; Klán, P. Caged Fluoride: Photochemistry and Applications of 4-Hydroxyphenacyl Fluoride. *Org. Lett.* **2015**, *17*, 4814–4817.

15) Kitani, S.; Sugawara, K.; Tsutsumi, K.; Morimoto, T.; Kakiuchi, K. Synthesis and Characterization of Thiochromone S,S-Dioxides as New Photolabile Protecting Groups. *Chem. Commun.* **2008**, 2103–2105.

16) Paul, A.; Biswas, A.; Sinha, S.; Shah, S. S.; Bera, M.; Mandal, M.; Singh,

N. D. P. Push-Pull Stilbene: Visible Light Activated Photoremovable Protecting Group for Alcohols and Carboxylic Acids with Fluorescence Reporting Employed for Drug Delivery. *Org. Lett.* **2019**, *21*, 2968–2972.

17) (a) Givens, R. S.; Matuszewski, B. Photochemistry of Phosphate Esters: An Efficient Method for the Generation of Electrophiles. *J. Am. Chem. Soc.* **1984**, *106*, 6860–6861. (b) Kamatham, N.; Mendes, D. C.; Da Silva, J. P.; Givens, R. S.; Ramamurthy, V. Photorelease of Incarcerated Caged Acids from Hydrophobic Coumaryl Esters into Aqueous Solution. *Org. Lett.* **2016**, *18*, 5480–5483.

18) Šebej, P.; Wintner, J.; Müller, P.; Slanina, T.; Al Anshori, J.; Antony, L. A. P.; Klán, P.; Wirz, J. Fluorescein Analogues as Photoremovable Protecting Groups Absorbing at ~520 nm. *J. Org. Chem.* **2013**, *78*, 1833–1843.

19) (a) Fedoryak, O. D.; Dore, T. M. Brominated Hydroxyquinoline as a Photolabile Protecting Group with Sensitivity to Multiphoton Excitation. *Org. Lett.* **2002**, *4* (20), 3419–3422. (b) Zhu, Y.; Pavlos, C. M.; Toscano, J. P.; Dore, T. M. 8-Bromo-7-Hydroxyquinoline as a Photoremovable Protecting Group for Physiological Use: Mechanism and Scope. *J. Am. Chem. Soc.* **2006**, *128* (13), 4267–4276. (c) Jarrett Davis, M.; Kragor, C. H.; Reddie, K. G.; Wilson, H. C.; Zhu, Y.; Dore, T. M. Substituent Effects on the Sensitivity of a Quinoline Photoremovable Protecting Group to One- And Two-Photon Excitation. *J. Org. Chem.* **2009**, *74* (4), 1721–1729. (d) Li, Y. M.; Shi, J.; Cai, R.; Chen, X. Y.; Guo, Q. X.; Liu, L. Development of New Quinoline-Based Photo-Labile Groups for Photo-Regulation of Bioactive Molecules. *Tetrahedron Lett.* **2010**, *51*, 1609–1612.

20) (a) Goswami, P. P.; Syed, A.; Beck, C. L.; Albright, T. R.; Mahoney, K. M.; Unash, R.; Smith, E. A.; Winter, A. H. BODIPY-Derived Photoremovable Protecting Groups Unmasked with Green Light. *J. Am. Chem. Soc.* **2015**, *137*, 3783–3786. (b) Palao, E.; Slanina, T.; Muchová, L.; Šolomek, T.; Vítek, L.; Klán, P. Transition-Metal-Free CO-Releasing BODIPY Derivatives Activatable by Visible to NIR Light as Promising Bioactive Molecules. *J. Am. Chem. Soc.* **2016**, *138*, 126–133. (c) Slanina, T.; Shrestha, P.; Palao, E.; Kand, D.; Peterson, J. A.; Dutton, A. S.;

Rubinstein, N.; Weinstain, R.; Winter, A. H.; Klán, P. In Search of the Perfect Photocage: Structure-Reactivity Relationships in Meso-Methyl BODIPY Photoremovable Protecting Groups. *J. Am. Chem. Soc.* **2017**, *139*, 15168–15175. (d) Toupin, N. P.; Arora, K.; Shrestha, P.; Peterson, J. A.; Fischer, L. J.; Rajagurubandara, E.; Podgorski, I.; Winter, A. H.; Kodanko, J. J. BODIPY-Caged Photoactivated Inhibitors of Cathepsin B Flip the Light Switch on Cancer Cell Apoptosis. *ACS Chem. Biol.* **2019**, *14*, 2833–2840. (e) Kand, D.; Liu, P.; Navarro, M. X.; Fischer, L. J.; Rousso-Noori, L.; Friedmann-Morvinski, D.; Winter, A. H.; Miller, E. W.; Weinstain, R. Water-Soluble BODIPY Photocages with Tunable Cellular Localization. *J. Am. Chem. Soc.* **2020**, *142*, 4970–4974. (f) Shrestha, P.; Dissanayake, K. C.; Gehrmann, E. J.; Wijesooriya, C. S.; Mukhopadhyay, A.; Smith, E. A.; Winter, A. H. Efficient Far-Red/Near-IR Absorbing BODIPY Photocages by Blocking Unproductive Conical Intersections. *J. Am. Chem. Soc.* **2020**, *142*, 15505–15512.

21) Chaudhuri, A.; Venkatesh, Y.; Behara, K. K.; Singh, N. D. P. Bimane: A Visible Light Induced Fluorescent Photoremovable Protecting Group for the Single and Dual Release of Carboxylic and Amino Acids. *Org. Lett.* **2017**, *19*, 1598–1601.

22) (a) Venkatesh, Y.; Rajesh, Y.; Karthik, S.; Chetan, A. C.; Mandal, M.; Jana, A.; Singh, N. D. P. Photocaging of Single and Dual (Similar or Different) Carboxylic and Amino Acids by Acetyl Carbazole and Its Application as Dual Drug Delivery in Cancer Therapy. *J. Org. Chem.* **2016**, *81*, 11168–11175. (b) Venkatesh, Y.; Nandi, S.; Shee, M.; Saha, B.; Anoop, A.; Pradeep Singh, N. D. Bis-Acetyl Carbazole: A Photoremovable Protecting Group for Sequential Release of Two Different Functional Groups and Its Application in Therapeutic Release. *Eur. J. Org. Chem.* **2017**, 6121–6130.

23) Barth, A.; Corrie, J. E. T.; Gradwell, M. J.; Maeda, Y.; Mäntele, W.; Meier, T.; Trentham, D. R. Time-Resolved Infrared Spectroscopy of Intermediates and Products from Photolysis of 1-(2-Nitrophenyl)Ethyl Phosphates: Reaction of the 2- Nitrosoacetophenone Byproduct with Thiols. *J. Am. Chem. Soc.* **1997**, *119* (18), 4149–4159.

24) (a) Hansen, M. J.; Velema, W. A.; Lerch, M. M.; Szymanski, W.; Feringa,

B. L. Wavelength-Selective Cleavage of Photoprotecting Groups: Strategies and Applications in Dynamic Systems. *Chem. Soc. Rev.* **2015**, *44*, 3358–3377. (b) Brieke, C.; Rohrbach, F.; Gottschalk, A.; Mayer, G.; Heckel, A. Light-Controlled Tools. *Angew. Chem. Int. Ed.* **2012**, *51*, 8446–8476. (c) Ankenbruck, N.; Courtney, T.; Naro, Y.; Deiters, A. Optochemical Control of Biological Processes in Cells and Animals. *Angew. Chem. Int. Ed.* **2018**, *57*, 2768–2798. (d) Givens, R. S.; Rubina, M.; Wirz, J. Applications of *p*-hydroxyphenacyl (PHP) and coumarin-4-ylmethyl Photoremovable Protecting Groups. *Photochem. Photobiol. Sci.* **2012**, *11*, 472–488. (e) Olejniczak, J.; Carling, C. J.; Almutairi, A. Photocontrolled Release Using One-Photon Absorption of Visible or NIR Light. *J. Control. Release.* **2015**, *219*, 18–30.

25) Menge, C.; Heckel, A. Coumarin-Caged DG for Improved Wavelength-Selective Uncaging of DNA. *Org. Lett.* **2011**, *13* (17), 4620–4623.

26) Sklar, L. R.; Almutawa, F.; Lim, H. W.; Hamzavi, I. Effects of Ultraviolet Radiation, Visible Light, and Infrared Radiation on Erythema and Pigmentation: A Review. *Photochem. Photobiol. Sci.* **2013**, *12*, 54–64.

27) Villringer, A.; Chance, B. Non-Invasive Optical Spectroscopy and Imaging of Human Brain Function. *Trends Neurosci.* **1997**, *20* (10), 435–442.

28) Strangman, G.; Boas, D. A.; Sutton, J. P. Non-Invasive Neuroimaging Using Near-Infrared Light. *Biol. Psychiatry*. **2002**, *52*, 679–693.

29) Maruo, S.; Nakamura, O.; Kawata, S. Three-dimensional microfabrication with two-photon-absorbed photopolymerization. *Opt. Lett.* **1997**, *22*, 132.

30) Boyd, W. In *Non-Linear Optics*, 2nd ed.; Elsevier, 2003.

31) Abe, M.; Chitose, Y.; Jakkampudi, S.; Thuy, P. T. T.; Lin, Q.; Van, B. T.; Yamada, A.; Oyama, R.; Sasaki, M.; Katan, C. Design and Synthesis of Two-Photon Responsive Chromophores for Near-Infrared Light-Induced Uncaging Reactions. *Synthesis.* **2017**, *49* (15), 3337-3346.

32) Göppert-Mayer, M. Über Elementarakte Mit Zwei Quantensprüngen. *Ann. Phys.* **1931**, *401*, 273–294.

33) Kaiser, W.; Garrett, C. G. B. Two-Photon Excitation in CaF_2: Eu^{2+}. *Phys. Rev. Lett.* **1961**, *7* (6), 229–231.

34) Kiskin, N. I.; Chillingworth, R.; McCray, J. A.; Piston, D.; Ogden, D. The Efficiency of Two-Photon Photolysis of a "Caged" Fluorophore, *o*-1-(2-Nitrophenyl)Ethylpyranine, in Relation to Photodamage of Synaptic Terminals. *Eur. Biophys. J.* **2002**, *30*, 588–604.
35) Weisz, S. Z.; Zahlan, A. B.; Gileeath, J.; Jarnagin, R. C.; Silver, M. Two-Photon Absorption in Crystalline Anthracene and Naphthalene Excited with a Xenon Flash. *J. Chem. Phys.* **1964**, *41* (11), 3491–3495.
36) You, A.; Be, M. A. Y.; In, I. α, ω-Diphenylpolyenes from Stilbene to Diphenyloctatetraene via Three Wave Mixing. *J. Chem. Phys.* **1979**, *70* (9), 4310–4315.
37) (a) Kamada, K.; Iwase, Y.; Sakai, K.; Kondo, K.; Ohta, K. Cationic Two-Photon Absorption Chromophores with Double- and Triple-Bond Cores in Symmetric/Asymmetric Arrangements. *J. Phys. Chem. C.* **2009**, *113* (27), 11469–11474. (b) Ohta, K.; Antonov, L.; Yamada, S.; Kamada, K. Theoretical Study of the Two-Photon Absorption Properties of Several Asymmetrically Substituted Stilbenoid Molecules. *J. Chem. Phys.* **2007**, *127* (8), 084504. (c)Terenziani, F.; Katan, C.; Badaeva, E.; Tretiak, S.; Blanchara-Desce, M. Enhanced Two-Photon Absorption of Organic Chromophores: Theoretical and Experimental Assessments. *Adv. Mater.* **2008**, *20*, 4641-4678.
38) Terenziani, F.; Sissa, C.; Painelli, A. Symmetry Breaking in Octupolar Chromophores: Solvatochromism and Electroabsorption. *J. Phys. Chem. B.* **2008**, *112* (16), 5079–5087.
39) Albota, M.; Beljonne, D.; Brédas, J. L.; Ehrlich, J. E.; Fu, J. Y.; Heikal, A. A.; Hess, S. E.; Kogej, T.; Levin, M. D.; Marder, S. R.; McCord-Maughon, D.; Perry, J. W.; Röckel, H.; Rumi, M.; Subramaniam, G.; Webb, W. W.; Wu, X. L.; Xu, C. Design of Organic Molecules with Large Two-Photon Absorption Cross Sections. *Science.* **1998**, *281* (5383), 1653–1656.
40) Mongin, O.; Porrès, L.; Charlot, M.; Katan, C.; Blanchard-Desce, M. Synthesis, Fluorescence, and Two-Photon Absorption of a Series of Elongated Rodlike and Banana-Shaped Quadrupolar Fluorophores: A Comprehensive Study of Structure-Property Relationships. *Chem. Eur. J.* **2007**, *13*, 1481–1498.

41) Denk, W.; Strickler, J. H.; Webb, W. W. Two-Photon Laser Scanning Fluorescence Microscopy. *Science.* **1990**, *248* (4951), 73–76.
42) Ellis-Davies, G. C. R. Useful Caged Compounds for Cell Physiology. *Acc. Chem. Res.* **2020**, *53*, 1593–1604.
43) Callaway, E. M.; Katzt, L. C. Photostimulation Using Caged Glutamate Reveals Functional Circuitry in Living Brain Slices (Neocortex/Whole-Cell Recording/Intrinsic Circuits). *Proc. Natl. Acad. Sci. USA.* **1993**, *90*, 7661–7665.
44) Furuta, T.; Wang, S. S. H.; Dantzker, J. L.; Dore, T. M.; Bybee, W. J.; Callaway, E. M.; Denk, W.; Tsien, R. Y. Brominated 7-hydroxycoumarin-4-ylmethyls: Photolabile protecting groups with biologically useful cross-sections for two photon photolysis. *Proc. Natl. Acad. Sci. USA.* **1999**, *96*, 1193–1200.

Chapter 2

Design, Synthesis, and Photoreactions of Caged Compounds with D-π-A Coumarin Unit

2-1. Introduction

In this section, near infrared TP responsive D-π-A chromophores were designed and synthesized. D-π-A stilbene unit was introduced into the (coumarin-4yl)methyl PPG to investigate both OP and TP uncaging properties. Theoretical assessments were conducted for TPA character of the dipolar type coumarin chromophores.

2-2. Design and synthesis of D-π-A type coumarin chromophores

First, three coumarin parent chromophores (**3a-c**) were designed and synthesized as shown in Scheme 1. *p*-Nitrobenzene unit was introduced on 3-position as an electron-acceptor part. 7-Position or 7,6-position was substituted by methoxy group as an electron-donor part. The D-π-A chromophores were prepared by one-step Perkin condensation reaction[45] using 2'-hydroxy acetophenone derivatives (**1a-1c**) and 4-nitrophenylacetic acid **2**. The compound **3a** without methoxy group was prepared to compare its OPA and TPA characters with methoxy-substituted D-π-A chromophores (**3b-3c**).

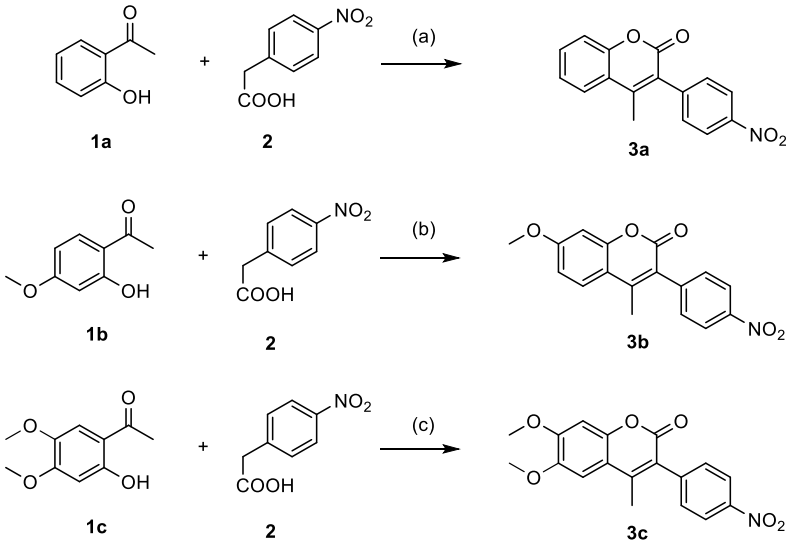

Scheme 1. Synthesis of **3a-c**; Reagents and conditions: (a) Acetic anhydride, triethylamine, 65°C to RT, overnight, 56% yield. (b) Acetic anhydride, triethylamine, 65°C to RT, overnight, 51% yield. (c) Acetic anhydride, triethylamine, 50°C to RT, overnight, 47% yield.

2-3. OP photophysical property

Steady-state OPA spectra of **3a-c** were recorded in DMSO (Figure 9). Compound **3a** shows λ_{max} at 321 nm, while **3b** and **3c** show red-shifted absorption maxima (λ_{max} = 338 nm for **3b**, and 361 nm for **3c**). TDDFT calculation was performed to assign the OP electronic transitions in gas phase. The molecular structures of **3a-3c** were simplified by replacing their 4-methyl group with hydrogen (as shown in the structure of **4a-c**). Single point energy calculation provided vertical excitation energy and the corresponding oscillator strength (*f*). The computed OPA spectra of compound **4a-c** with oscillator strengths are shown in Figure 10. Similar trends with experimental spectra were found on the calculated absorption wavelength for **4a-c**, where **4c** show the lowest excitation energy (3.21 eV = 386 nm) and **4b** show the second lowest excitation energy (3.31 eV = 375 nm). Compound **4a** without methoxy group shows the highest excitation energy (3.53 eV = 351 nm). The 1st electronic transition ($S_0 \rightarrow S_1$) of **4a-c** was assigned to be HOMO (Highest Occupied Molecular Orbital) to LUMO (Lowest Unoccupied Molecular Orbital) transition (Figure 10). The molecular orbitals (MOs) of **4b** and **4c** indicate the reasonable transfer of electron density from donor to acceptor part.

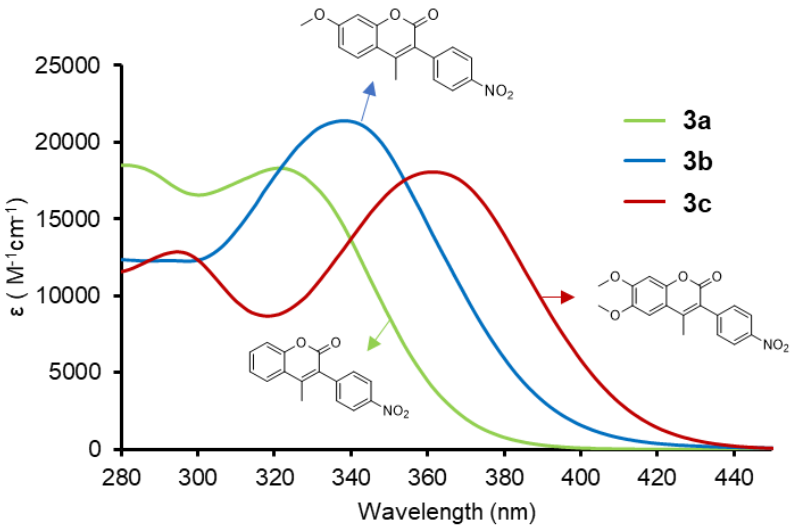

Figure 9. UV-visible absorption spectra of chromophores **3a-c** in DMSO.

(a)

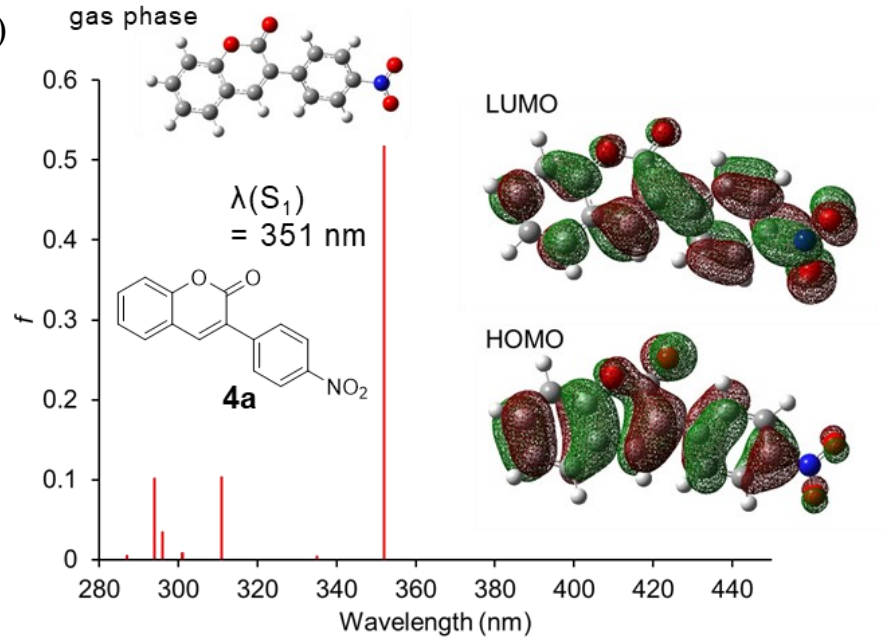
gas phase
λ(S1)
= 351 nm
4a
NO2
LUMO
HOMO
f
Wavelength (nm)

(b)

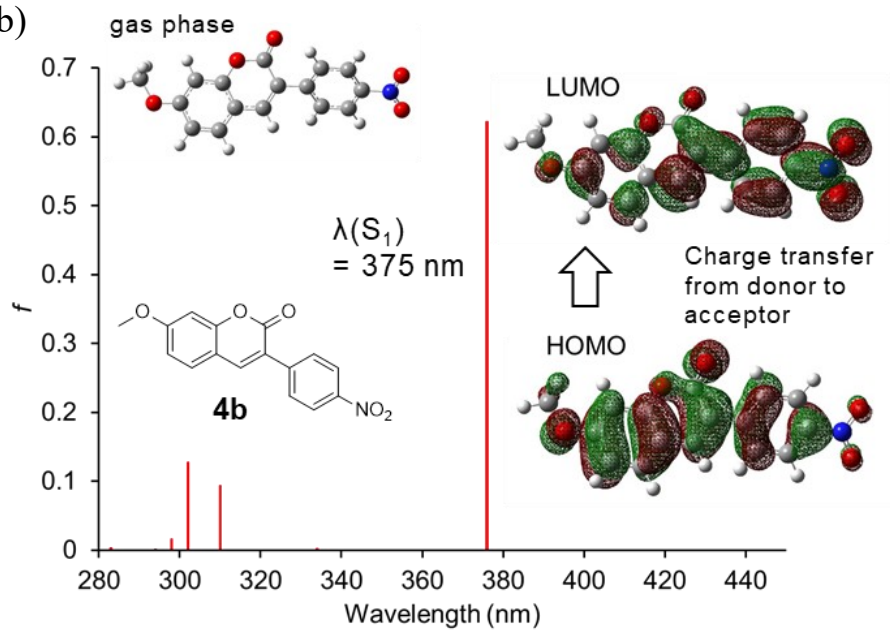
gas phase
λ(S1)
= 375 nm
4b
NO2
LUMO
Charge transfer
from donor to
acceptor
HOMO
f
Wavelength (nm)

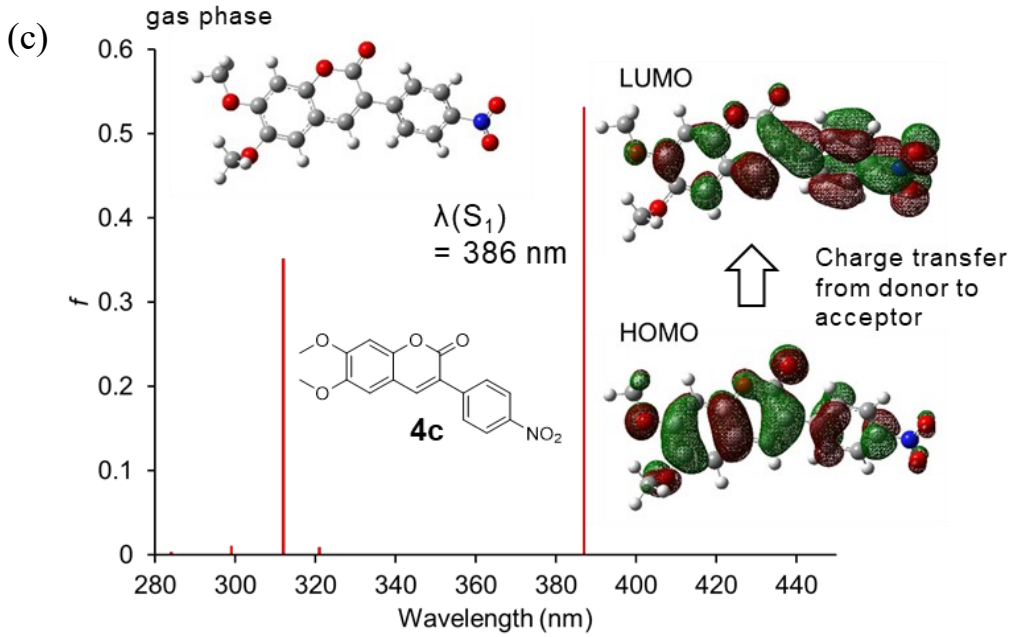

Figure 10. Calculated oscillator strengths (*f*) and MOs of (a) **4a**, (b) **4b**, and (c) **4c**, computed at the TD-RB3LYP/6-31G(d)//RB3LYP/6-31G(d) level of theory.

2-4. Theoretical prediction of TPA cross-section

The predicted OPA and TPA spectra of **4a-c** were shown in Figure 11. The spectra were computed at the TD-B3LYP/6-31G (d)//B3LYP/6-31 (d) level of theory. Two-state model was used to calculate TPA cross-section. As expected, TPA maxima of **4a-4c** exist in 740-780 nm, which are almost double wavelengths of OPA maxima (370-390 nm). This phenomenon is peculiar in the dipolar system. TPA cross-section of ca. 50 GM was calculated for **4a**. TPA cross-sections of methoxy-substituted compound **4b** and **4c** (σ_2 = 170 GM and 179 GM for **4b** and **4c**, respectively) were approximately three times higher than that of **4a**. These computational results suggested that TP excitation of D-π-A chromophores (**4b**, **4c**) in near IR region is feasible. From the next section, we thus focused on the OP and TP uncaging character of caged compound bearing D-π-A coumarin structure.

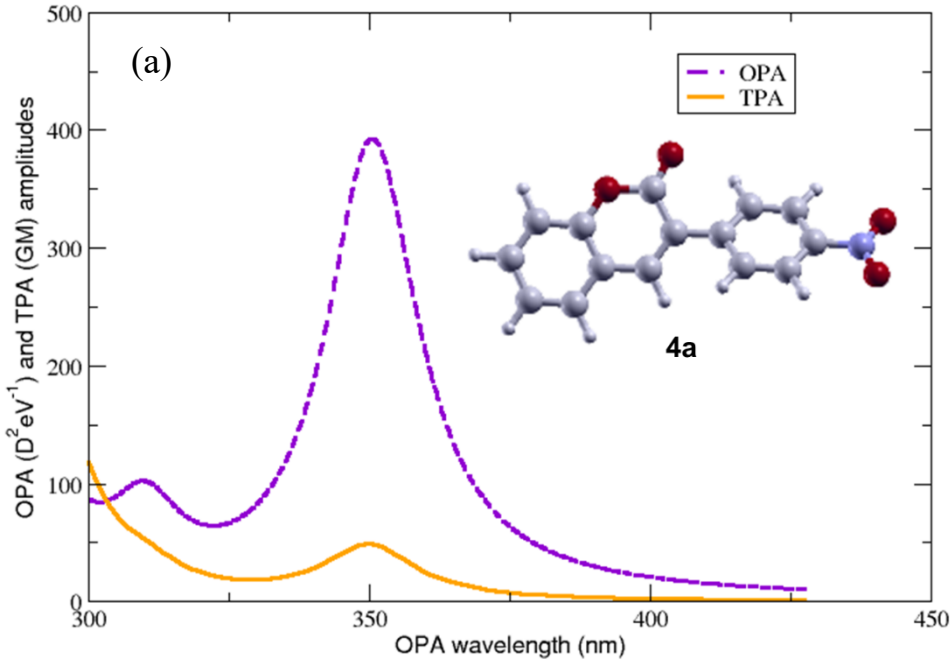
(a)
OPA
TPA
4a
OPA (D^2eV^{-1}) and TPA (GM) amplitudes
OPA wavelength (nm)
0
100
200
300
400
500
300
350
400
450

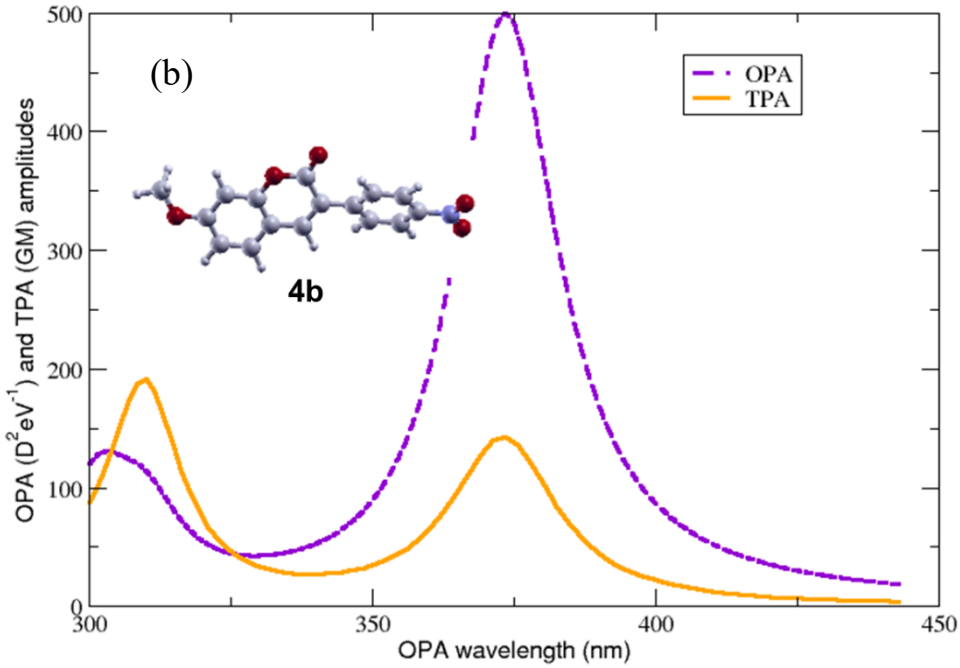
(b)
OPA
TPA
4b
OPA (D^2eV^{-1}) and TPA (GM) amplitudes
OPA wavelength (nm)
0
100
200
300
400
500
300
350
400
450

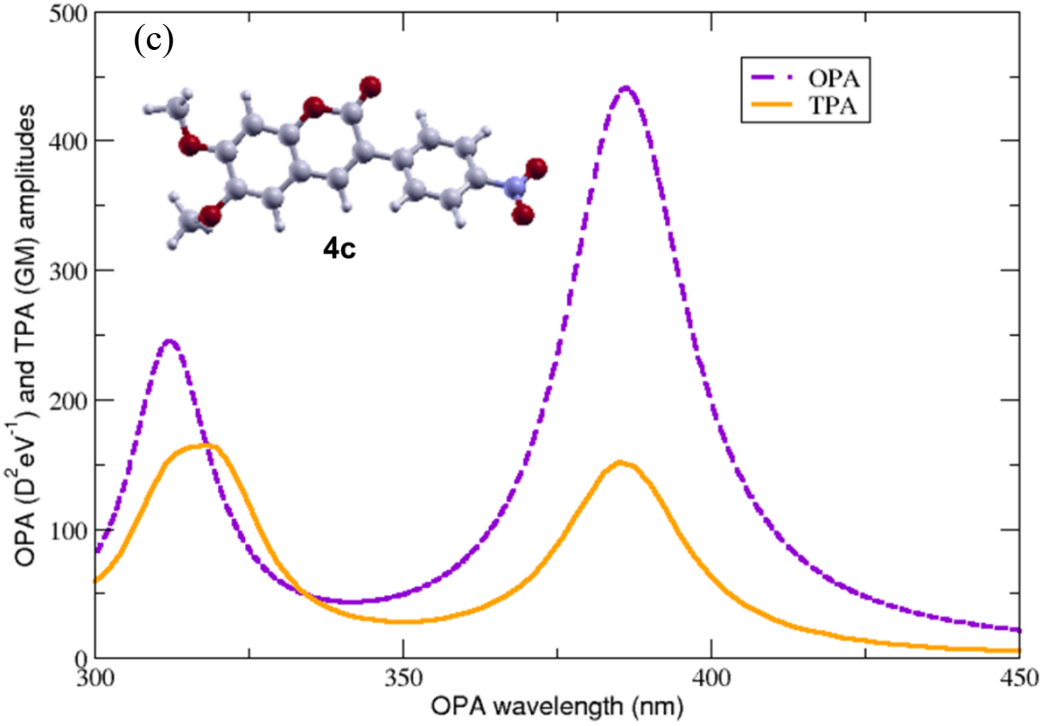

Figure 11. Calculated OPA and TPA spectra of (a) **4a**, (b) **4b**, and (c) **4c**, computed at the TD-B3LYP/6-31G(d)//B3LYP/6-31G(d) level of theory.

2-5. Synthesis of D-π-A caged benzoate

For uncaging reaction, benzoic acid was selected as a simple model instead of bioactive compound. The carboxylic acid moiety of benzoic acid was protected by coumarin PPGs. Starting from parent chromophores (**3b**,**c**), two caged benzoic acids (**7b**,**c**) were synthesized by following the synthetic routes in Scheme 2.

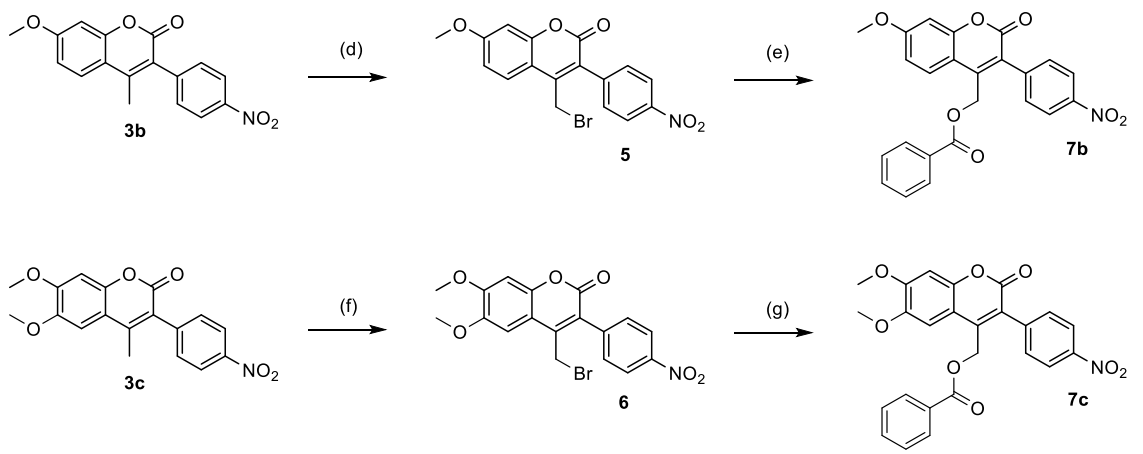

Scheme 2. Synthesis of **7b** and **7c**; Reagents and conditions: (d) NBS, benzoyl peroxide, CCl_4, 90°C, 15h, 40%. (e) Benzoic acid, K_2CO_3, KI, DMF, 50°C, 6h, 20%. (f) NBS, benzoyl peroxide, CCl_4, 90°C, 24h, 59%. (e) Benzoic acid, K_2CO_3, KI, DMF, 50°C, 3h, 42%.

2-6. OP uncaging reaction of D-π-A caged benzoate in DMSO

OP uncaging reactions of caged benzoates **7b** and **7c** were conducted using Xenon lamp (500 W) at 360 ± 10 nm in DMSO-d_6. Based on the ^{1}H NMR spectrum analysis (400 MHz), the peaks of benzoic acid increased under photolysis condition (Figures 12,13). Quantitative release of benzoic acid (> 90%) was observed both for **7b** and **7c**. The photoreaction quantum yield (Φ_u) in DMSO was determined using ferrioxalate as a photochemical actinometer. Quantum yield of **7b** (Φ_u = 0.09) was approximately three times higher than that of **7c** (Φ_u = 0.03). Lower Φ_u of **7c** may be attributed to the strong stabilization of excited state by charge transfer character from dipolar D-π-A unit.

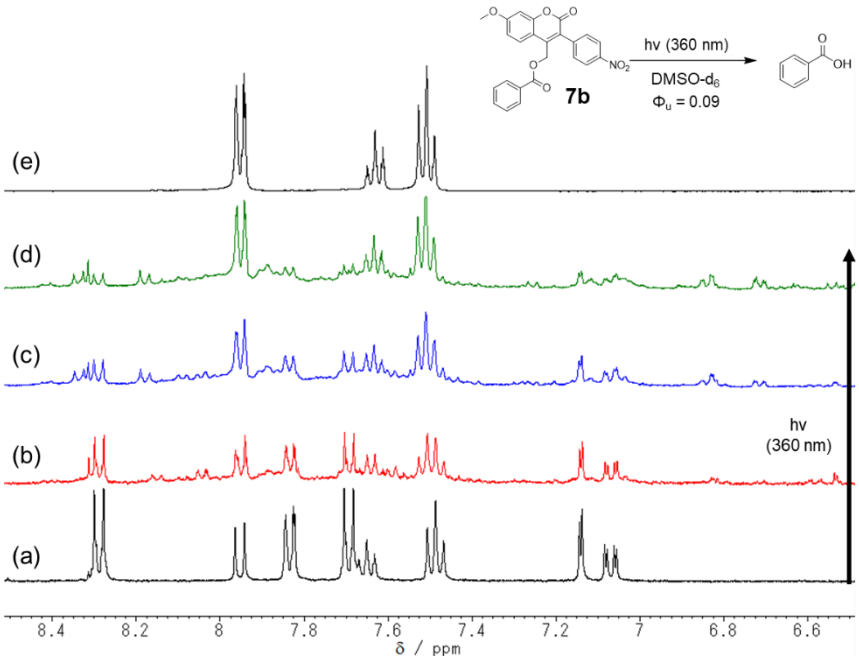

Figure 12. ^{1}H NMR spectra of **7b** in DMSO-d_6 (a) before and after (b) 8, (c) 16, (d) 24h of irradiation at 360 nm; (e) ^{1}H NMR spectra of benzoic acid in DMSO-d_6.

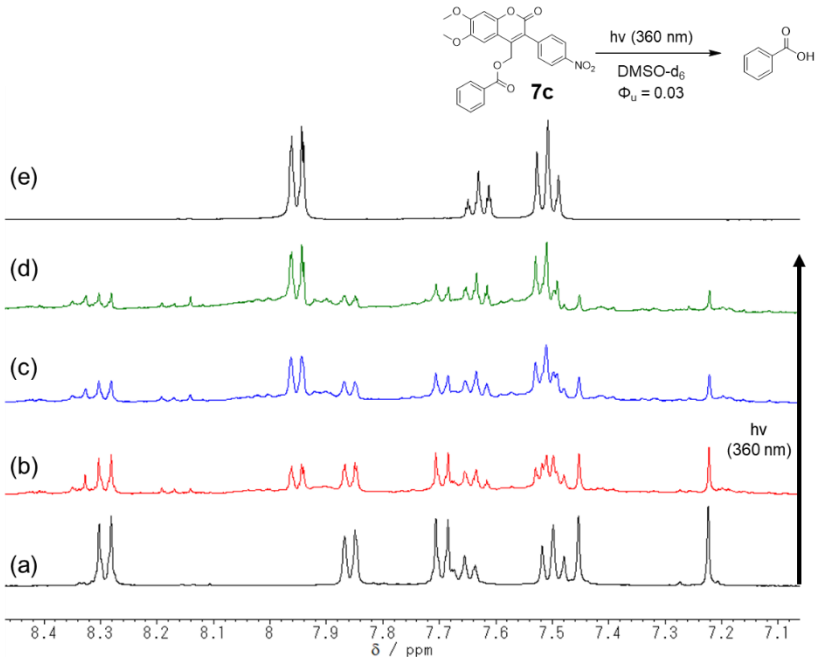

Figure 13. ^{1}H NMR spectra of **7c** in DMSO-d_6 (a) before and after (b) 42, (c) 72, (d) 96h of irradiation at 360 nm; (e) ^{1}H NMR spectra of benzoic acid in DMSO-d_6.

2-7. TP uncaging reaction of D-π-A caged benzoate in DMSO

TP photolysis experiments of **7b** and **7c** were carried out using a Ti: sapphire (pulse width 100 fs, 80 MHz) at an average power of 700 mW at 298 K in DMSO at the wavelengths of 700, 710, 720, 730, 740, 750, and 760 nm (Figure 11a, b). The degradation of starting material **7b** and **7c** was monitored by HPLC analysis. The rate constants of TP photolysis of **7b** and **7c** were extrapolated by comparing with the previous values of NPBF-BA chromophore (k_{740} = 9.4 × 10^{-6} s^{-1}) as a reference.[46] The reported TP uncaging efficiency of NPBF-BA (δ_u = 5.0 GM at 740 nm) allows us to extrapolate TP uncaging efficiency of compound **7b** and **7c**.[47] TPA cross-section values of **7b** and **7c** were determined by following the theoretical equation of $\delta_u = \sigma_2 \times \Phi_u$. The action spectra of TPA cross-section of **7b** and **7c** are shown in Figure 12. Compound **7c** has lower TP uncaging efficiency of δ_u = 2.1 GM at 740 nm than **7b** (δ_u = 3.4 GM at 710 nm) due to the lower photoreaction quantum yield, albeit **7c** shows higher TPA cross-section (σ_2 = 69 GM at 740 nm for **7c**, whereas σ_2 = 38 GM at 710 nm for **7b**). The dipolar character becomes stronger when methoxy groups are introduced on 7- and 6-position, which enhances TPA cross-section but reduces TP uncaging efficiency.

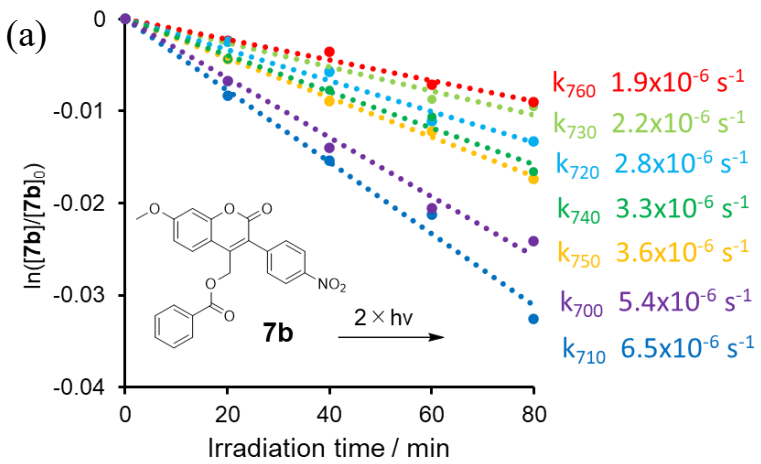

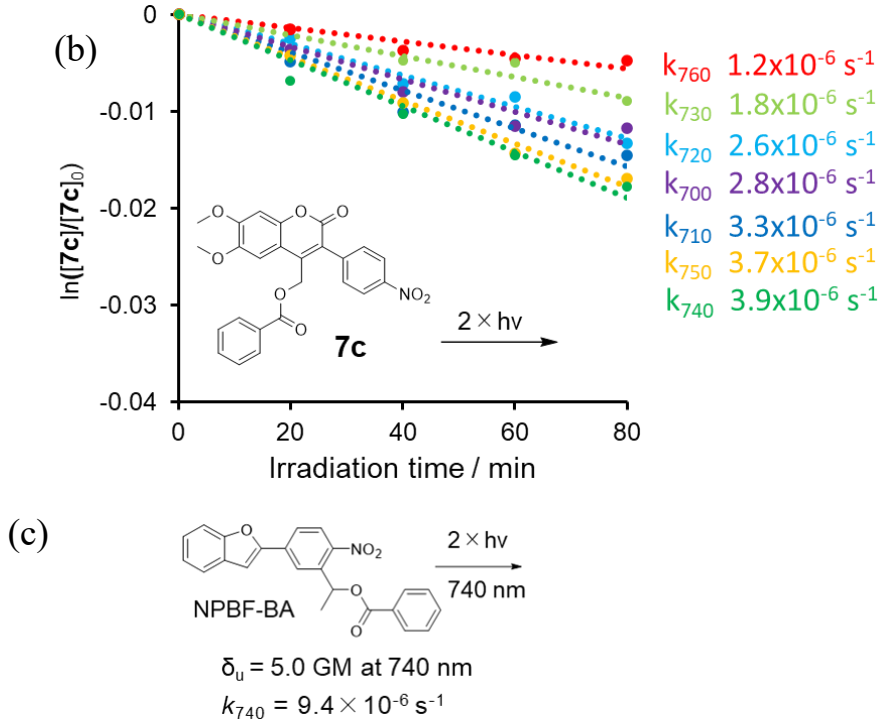

Figure 11. Time profile of the TP uncaging of (a) **7b** and (b) **7c**, ln([sub]/ [sub]$_0$) vs. irradiation time at wavelengths of 700, 710, 720, 730, 740, 750, and 760 nm at 700 mW. (c) TP uncaging reaction of NPBF-BA at 740 nm, δ_u = 5.0 GM at 740 nm.

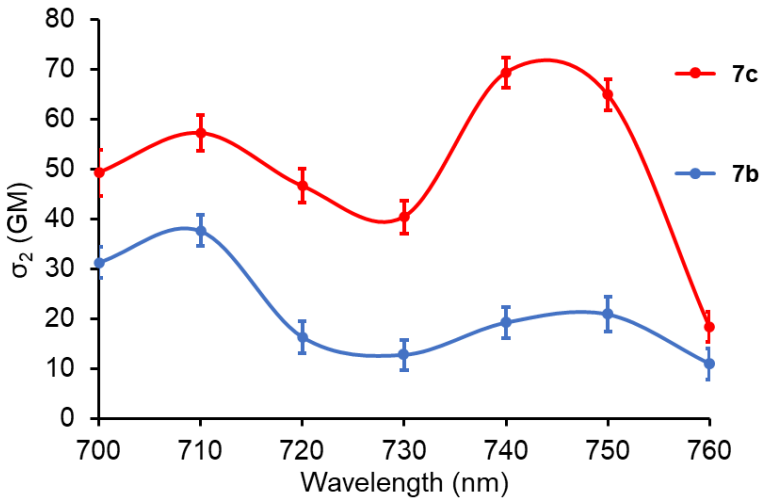

Figure 12. Extrapolated experimental TPA spectra of **7b** (blue) and **7c** (red).

2-8. References

45) Musa, M. A.; Latinwo, L. M.; Virgile, C.; Badisa, V. L. D.; Gbadebo, A. J. Synthesis and in Vitro Evaluation of 3-(4-Nitrophenyl)Coumarin Derivatives in Tumor Cell Lines. *Bioorg. Chem.* **2015**, *58*, 96–103.

46) Komori, N.; Jakkampudi, S.; Motoishi, R.; Abe, M.; Kamada, K.; Furukawa, K.; Katan, C.; Sawada, W.; Takahashi, N.; Kasai, H.; Xue, B.; Kobayashi, T. Design and Synthesis of a New Chromophore, 2-(4-Nitrophenyl)Benzofuran, for Two-Photon Uncaging Using near-IR Light. *Chem. Commun.* **2016**, *52*, 331–334.

47) Donato, L.; Mourot, A.; Davenport, C. M.; Herbivo, C.; Warther, D.; Léonard, J.; Bolze, F.; Nicoud, J. F.; Kramer, R. H.; Goeldner, M.; Specht, A. Water-Soluble, Donor-Acceptor Biphenyl Derivatives in the 2-(o-Nitrophenyl)Propyl Series: Highly Efficient Two-Photon Uncaging of the Neurotransmitter γ-Aminobutyric Acid at λ=800 nm. *Angew. Chem. Int. Ed.* **2012**, *51*, 1840–1843.

2-9. Experimental Section

All reagents and solvent were purchased from commercial source and used without any further purification. Silica Gel 60N (spherical, neutral) 63-210 μm was purchased from Kanto Chemical CO., Inc. to use silica gel column chromatography. Thin layer chromatography (TLC) analysis was performed on silica gel plates and monitored under ultraviolet light. ^{1}H NMR and ^{13}C NMR spectra were recorded on a Bruker ASCENDTM 400 (^{1}H, 400 MHz, ^{13}C, 100 MHz). DMSO-d_6 and $CDCl_3$ (0.03% TMS) was used as deuterated solvents. Signal positions were given in parts per million (ppm) from tetramethylsilane (δ = 0.00) and measured relative to the signal of the solvent ($CDCl_3$: δ = 7.26, ^{1}H NMR; δ = 77.16, ^{13}C NMR). IR spectra were recorded on a PerkinElmer Spectrum One FT-IR spectrometer. UV-vis spectra were taken by a SHIMADZU UV-3600 Plus. Mass-spectrometric data were measured by Mass Spectrometric Thermo Fisher Scientific LTQ Orbitrap XL, whose measurements were supported by National Science Center for Basic Research and Development, Hiroshima Univ. The light source for uncaging reaction of coumarin derivatives was BPS-500B Xe-lamp.

The syntheses of parent chromophore (**3a-3c)** and caged benzoate (7**b**, 7**c)** are described as follows.

4-Methyl-3-(4-nitrophenyl)coumarin (3a)

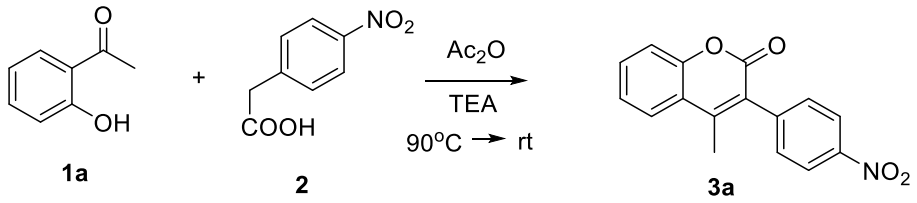

To a mixture of *o*-hydroxyacetophenone **1a** (1.0 g, 7.3 mmol) and 4-nitrophenylacetic acid **2** (1.4 g, 7.9 mmol) in acetic anhydride (10 mL) was added trimethylamine (8 ml). The reaction mixture was then stirred overnight at 65 ℃, allowed to cool to r.t. and 10 mL of ether was added with stirring for another 2-3 h to afford the desire product as a precipitate that was collected using vacuum filtration (1.2 g, 56%). 1H NMR (400MHz, $CDCl_3$): δ 8.34 (d, J = 8.9 Hz, 2H), 7.73 (dd, J = 8.0 Hz, 1H), 7.61 (t, J = 8.0 Hz, 1H), 7.53 (d, J = 8.9 Hz, 2H), 7.42 (d, J = 8.0Hz, 1H), 7.38 (t, J = 8.0Hz, 1H), 2.36 (s, 3H).

7-Methoxy-4-methyl-3-(4-nitrophenyl)coumarin (3b)

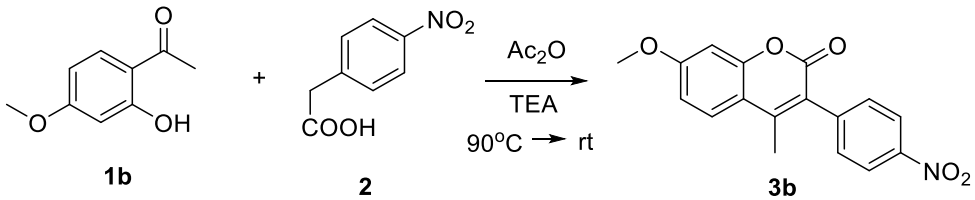

To a mixture of 2'-hydroxy-4'-methoxy acetophenone **1b** (500 mg, 3.0 mmol) and 4-nitrophenylacetic acid **2** (589 mg, 3.3 mmol) in acetic anhydride (2 mL) was added trimethylamine (1 mL). The reaction mixture was then stirred overnight at 65 ℃, allowed to cool to r.t. and 10 mL of ether was added with stirring for another 2-3 h to afford the desire product as a precipitate that was collected using vacuum filtration (475 mg, 51%). ^{1}H NMR (400MHz, $CDCl_3$) *δ* 8.34 (d, J = 8.8 Hz, 2H), 7.63 (d, J = 8.8 Hz, 1H), 7.53 (d, J = 8.8 Hz, 2H), 6.95 (d, J =8.8 Hz, , 2H), 6.91 (s, 1H), 3.94 (s, 3H), 2.33 (s, 3H).

6,7-Dimethoxy-4-methyl-3-(4-nitrophenyl)coumarin (3c)

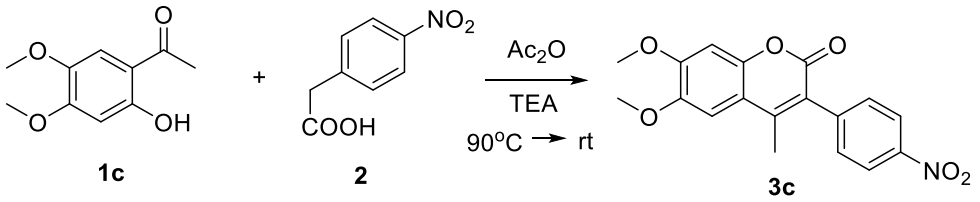

To a mixture of 2'-hydroxy-4',5'-dimethoxy acetophenone **1c** (1.0 g, 5.1 mmol) and 4-nitrophenylacetic acid **2** (996 mg, 5.5 mmol) in acetic anhydride (3 mL) was added trimethylamine (1 mL). The reaction mixture was then stirred overnight at 50 ℃, allowed to cool to r.t. and 10 mL of ether was added with stirring for another 2-3 h to afford the desire product as a precipitate that was collected using vacuum filtration (823 mg, 47%). ^{1}H NMR (400MHz, $CDCl_3$) δ 8.33 (d, J = 8.8 Hz,2H), 7.52 (d, J = 8.8 Hz, 2H), 7.03 (s, 1H), 6.91 (s, 1H), 3.99 (s, 3H), 3.97 (s, 3H), 2.33 (s, 3H). ^{13}C NMR (100 MHz, $CDCl_3$) δ 160.60, 153.26, 148.84, 148.66, 147.53, 146.55, 141.77, 131.58, 123.59, 122.56, 112.57, 105.92, 100.01, 56.57, 56.46, 16.91.; HRMS (ESI) calcd. for $C_{18}H_{15}NO_6$ $[M+Na]^+$; 364.0792 found 364.0793, Mp 255-257℃, IR [cm^{-1}] (KBr) ν_{max} 1701, 1513, 1342, 1273.

7-Methoxy-4-bromomethyl-3-(4-nitrophenyl)coumarin (5)

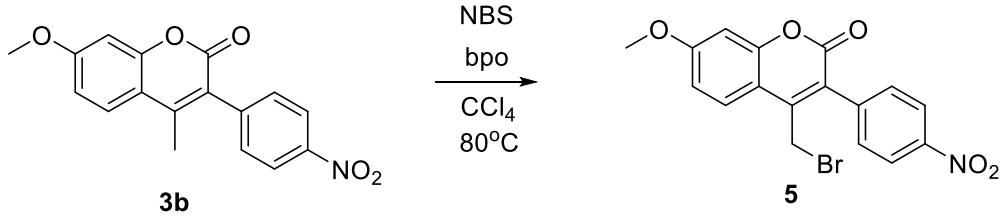

To a suspension of 7-methoxy-4-methyl-3-(4-nitrophenyl)coumarin **3b** (100 mg, 0.32 mmol) and NBS (62.9 mg, 0.35 mmol) in CCl_4 (2 mL), a catalytic amount of benzoyl peroxide (11 mg) was added. The reaction mixture was refluxed for 15h in test tube. The solvent was removed under reduced pressure. The precipitate was stirred with 10 mL of warm water to remove the succinimide, filtered and recrystallized from $CHCl_3$ (50 mg, 40%). ^{1}H NMR (400MHz, $CDCl_3$) δ 8.37 (d, J = 8.8 Hz, 2H), 7.72 (d, J = 8.8 Hz, 1H), 7.67 (d, J = 8.8Hz,

2H) 6.99 (d, J = 8.8Hz , 1H), 6.91 (s, 1H), 4.3 (s, 2H), 3.93 (s, 3H). ^{13}C NMR (100 MHz, $CDCl_3$) δ 163.39, 160.29, 155.32, 148.05, 146.35, 139.96, 130.90, 126.44, 123.82, 122.96, 113.17, 110.68, 101.18, 55.95, 24.53.; HRMS (ESI) calcd. for $C_{17}H_{12}BrNO_5$ $[M+Na]^+$; 411.9791 found 411.9793, Mp 235-238℃, IR [cm^{-1}] (KBr) v_{max} 1719, 1597, 1515, 1346, 1267.

6,7-Dimethoxy-4-bromomethyl-3-(4-nitrophenyl)coumarin (6)

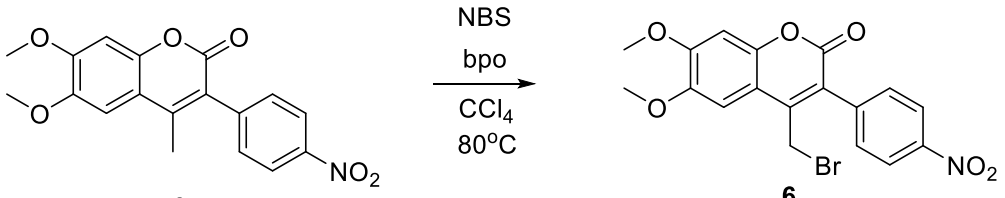

3c **6**

To a suspension of 6,7-dimethoxy-4-methyl-3-(4-nitrophenyl)coumarin **3c** (398 mg, 1.16 mmol) and NBS (374 mg, 2.10 mmol) in CCl_4 (4mL), a catalytic amount of benzoyl peroxide (60 mg) was added. The reaction mixture was refluxed at 90℃ for 24h in test tube. The solvent was removed under reduced pressure. The precipitate was stirred with 10 ml of warm water to remove the succinimide, filtered and purified by silica chromatography (CH_2Cl_2 : EtOAc = 4:1,v/v) and GPC (287 mg, 59%). ^1H NMR (400MHz, $CDCl_3$) δ 8.37 (d, J = 8.8 Hz, 2H), 7.68 (d, J = 8.8 Hz, 2H), 7.14 (s, 1H), 6.92 (s, 1H), 4.32 (s, 2H), 4.00 (s, 3H), 4.00(s, 3H).^{13}C NMR (100 MHz, $CDCl_3$) δ 160.37, 153.72, 149.61, 148.05, 146.71, 146.02, 140.11, 130.91, 123.81, 123.27, 109.82, 105.89, 100.26, 56.59, 56.53, 24.97.; HRMS (ESI) calcd. for $C_{18}H_{14}O_6NBr$ $[M+H]^+$; 420.0077 found 420.0080, Mp 248-250℃, IR [cm^{-1}] (KBr) v_{max} 1712, 1510, 1342, 1276.

7-Methoxy-4-[(benzoyloxy)methyl]-3-(4-nitrophenyl)coumarin (7b)

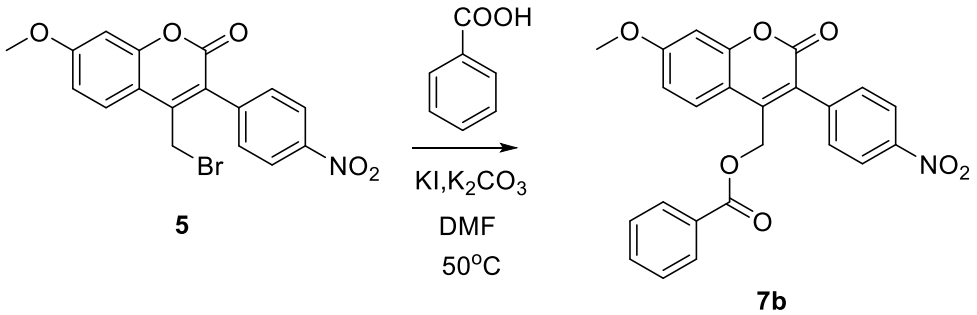

7-Methoxy-4-bromomethyl-3-(4-nitrophenyl)coumarin **5** (129 mg, 0.33 mmol) was dissolved in dry DMF (5 mL). To the solution were added potassium iodide (109 mg, 0.66 mmol), potassium carbonate (91 mg, 0.66 mmol) and benzoic acid (40 mg, 0.33 mmol). The reaction mixture was stirred at 50 ℃ for 6h. After completion of the reaction, solvent was removed under vacuum. To the crude residue was added ethyl acetate, followed by washing with brine water. The organic layer was collected, dried over Na_2SO_4, and evaporated under vacuum to yield crude, which was purified by column chromatography (CH_2Cl_2 : EtOAc ＝ 5:1, v/v) and GPC (28 mg, 20%). ^{1}H NMR (400 MHz, $CDCl_3$) δ 8.33 (d, J = 8.8 Hz, 2H), 7.98 (dd, J = 8.8 Hz, 2H), 7.73 (dd, J = 8.8 Hz, 1H), 7.62 (td, J =3.1 Hz, 1H), 7.61 (d, J = 8.8 Hz, 2H), 7.46 (t, 4.0 Hz, 2H), 6.97 (m, , 1H), 6.94(s, 1H), 5.31(s, 2H), 3.94(s, 3H).^{13}C NMR (100 MHz, $CDCl_3$) δ 165.57, 163.27, 160.46, 155.22, 147.92, 144.80, 140.01, 133.77, 131.47, 129.76, 128.83, 128.66, 126.69, 124.82, 123.67, 113.36, 111.83, 101.07, 60.44, 55.94.;HRMS (ESI) calcd. for $C_{24}H_{17}NO_7$ $[M+H]^+$; 432.1078 found 432.1078, Mp 138-140℃, IR [cm^{-1}] (KBr) ν_{max} 1716, 1606, 1517, 1346, 1264.

6,7-Dimethoxy-4-[(benzoyloxy)methyl]-3-(4-nitrophenyl)coumarin (7c)

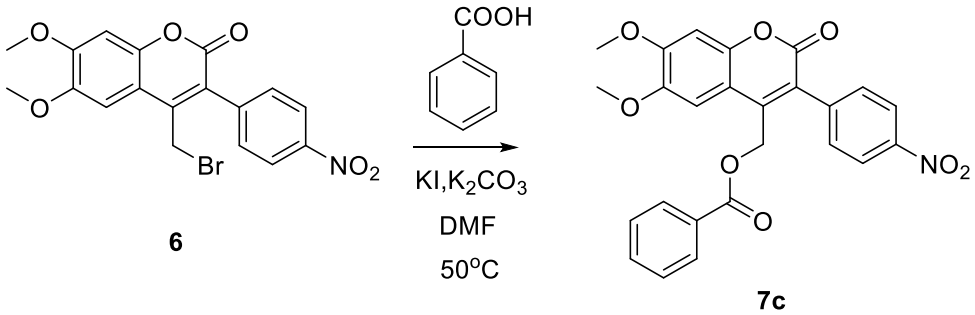

6,7-Dimethoxy-4-bromomethyl-3-(4-nitrophenyl)coumarin **6** (50 mg, 0.12 mmol) was dissolved in dry DMF (2 mL). To the solution were added potassium iodide (40 mg, 0.24 mmol), potassium carbonate (33 mg, 0.24 mmol) and benzoic acid (15 mg, 0.12 mmol). The reaction mixture was stirred at 50 ℃ for 3h. After completion of the reaction, solvent was removed under vacuum. To the crude residue was added ethyl acetate, followed by washing with brine water. The organic layer was collected, dried over Na_2SO_4, and evaporated under vacuum to yield crude, which was purified by column chromatography (CH_2Cl_2 : EtOAc ＝ 5:1, v/v) and GPC (23 mg, 42%). ^{1}H NMR (400 MHz, $CDCl_3$) δ 8.33 (d, J = 8.8 Hz, 2H), 7.99 (d, J = 7.2 Hz, 2H), 7.63 (d, J = 8.8 Hz, 2H), 7.62 (t, J = 3.7 Hz, 1H), 7.46 (t, J = 4.0 Hz, 2H) 7.21 (s, 1H), 6.94 (s, 1H), 5.35 (s, 2H), 3.99 (s, 3H) 3.86 (s, 3H). ^{13}C NMR (100 MHz, $CDCl_3$) δ 165.62, 160.57, 153.46, 149.51, 147.93, 146.78, 144.69, 140.13, 140.09, 133.89, 131.51, 129.71, 128.73, 125.13, 123.68, 110.82, 105.84, 100.10, 60.42, 56.52, 56.39. HRMS (ESI) calcd. for $C_{23}H_{15}NO_7$ $[M+H]^+$; 462.1183 found 462.1184, Mp 162-164℃, IR [cm^{-1}] (KBr) v_{max} 1719,1516, 1347, 1276.

2-10. Supplementary Material

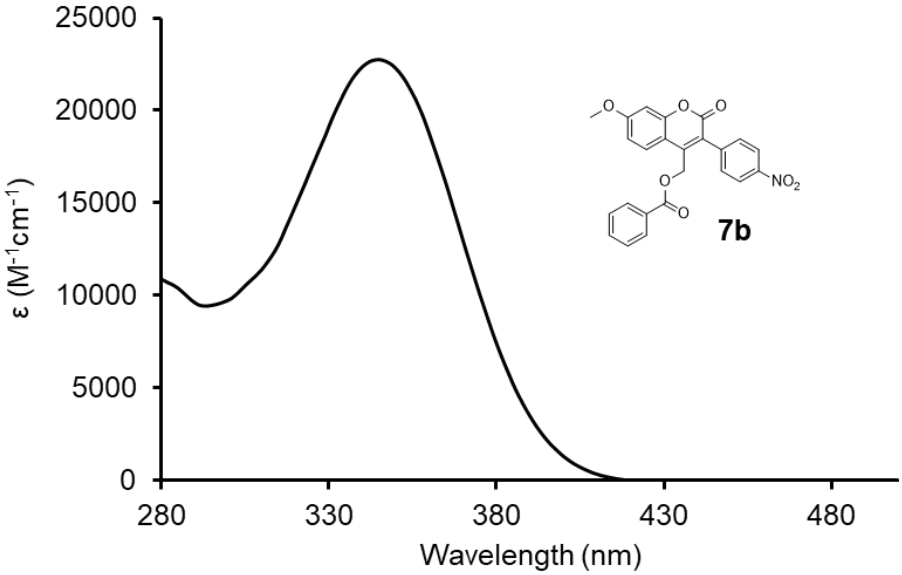

Figure S1. UV-visible absorption spectrum of compound **7b** in DMSO.

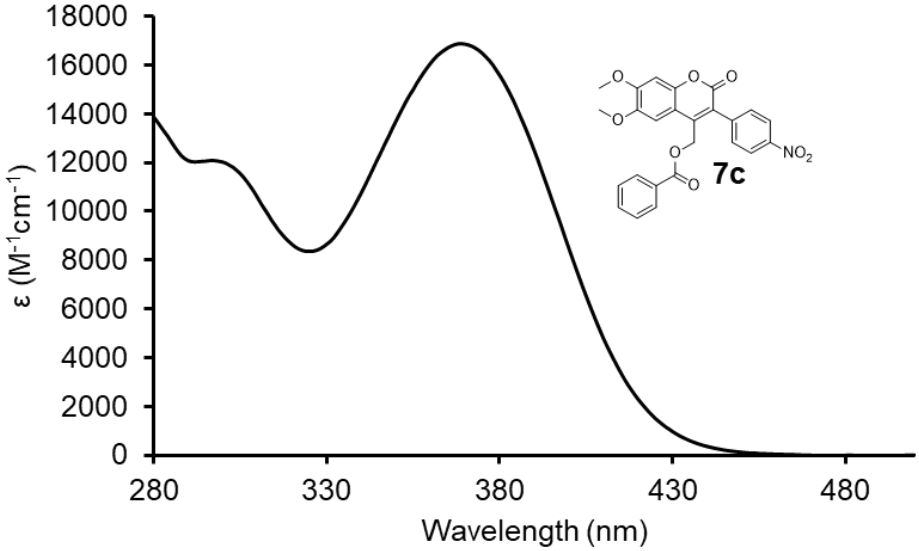

Figure S2. UV-visible absorption spectrum of compound **7c** in DMSO.

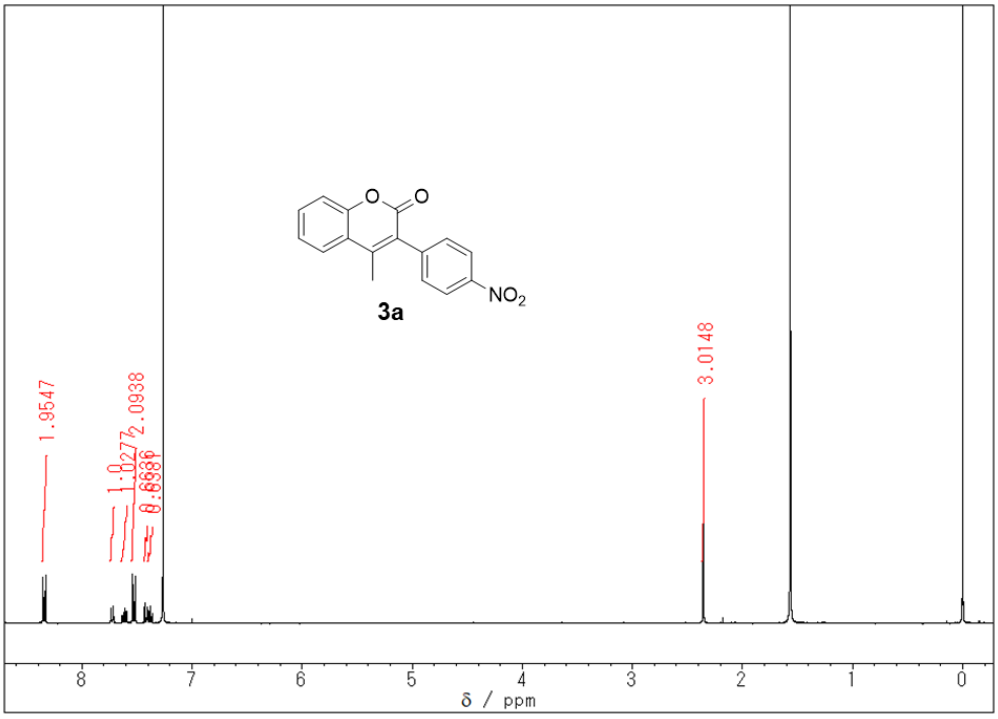

Figure S3. ^{1}H NMR of compound **3a** (400 MHz, $CDCl_3$).

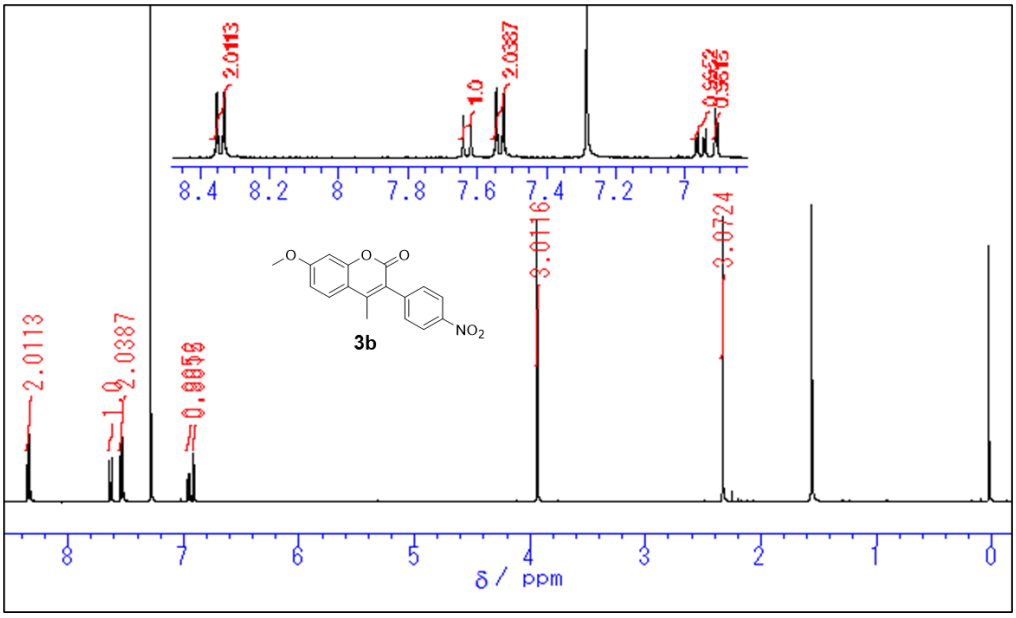

Figure S4. ^{1}H NMR of compound **3b** (400 MHz, $CDCl_3$).

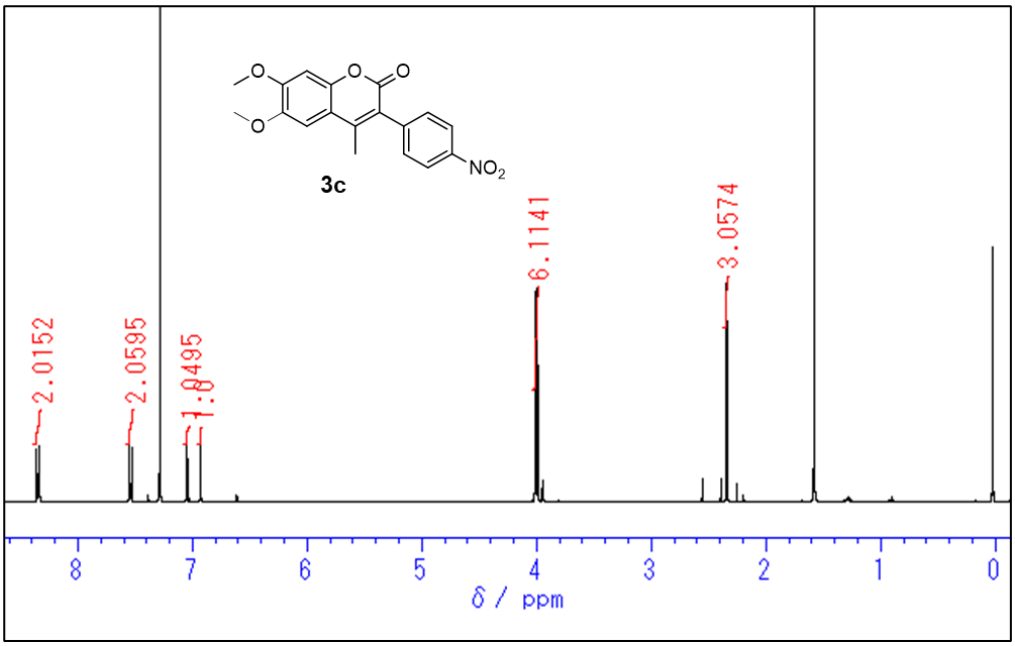

Figure S5. ^{1}H NMR of compound **3c** (400 MHz, $CDCl_3$).

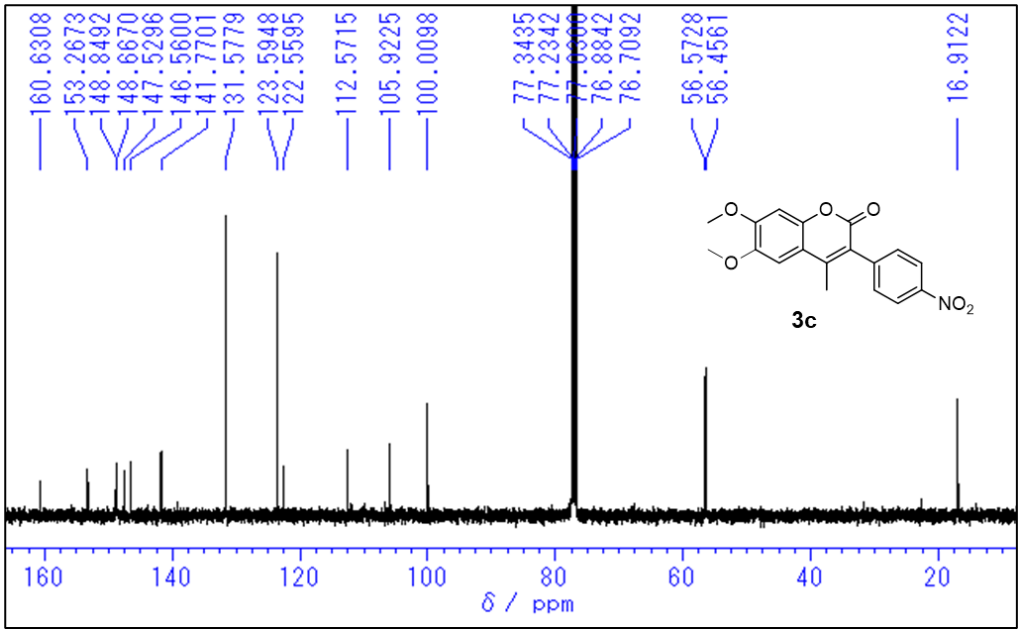

Figure S6. ^{13}C NMR of compound **3c** (100 MHz, $CDCl_3$).

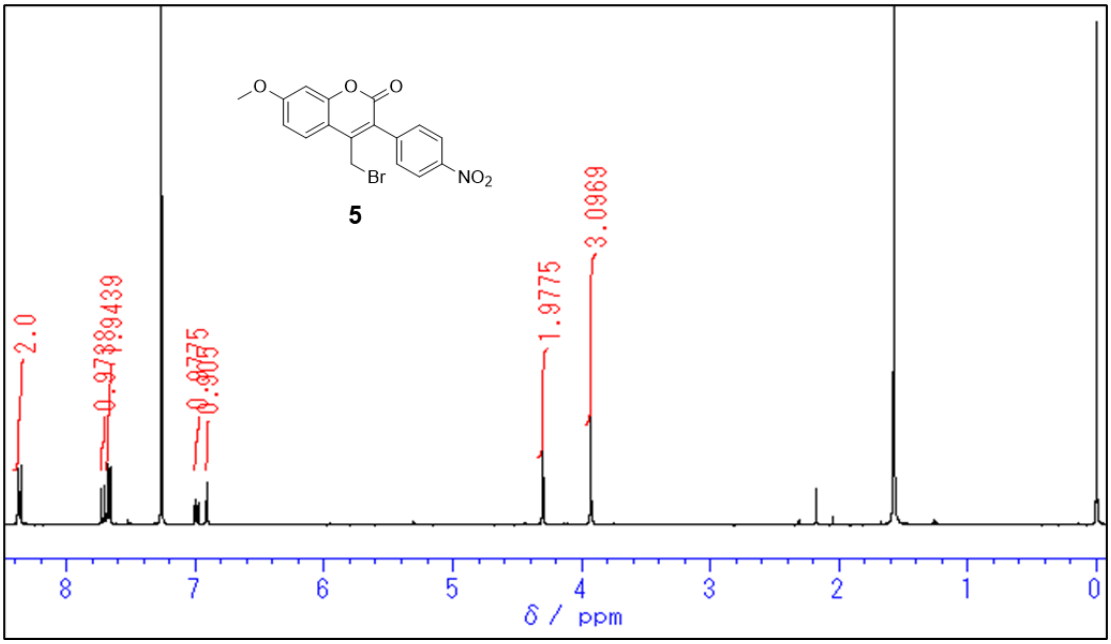

Figure S7. ^{1}H NMR of compound **5** (400 MHz, $CDCl_3$).

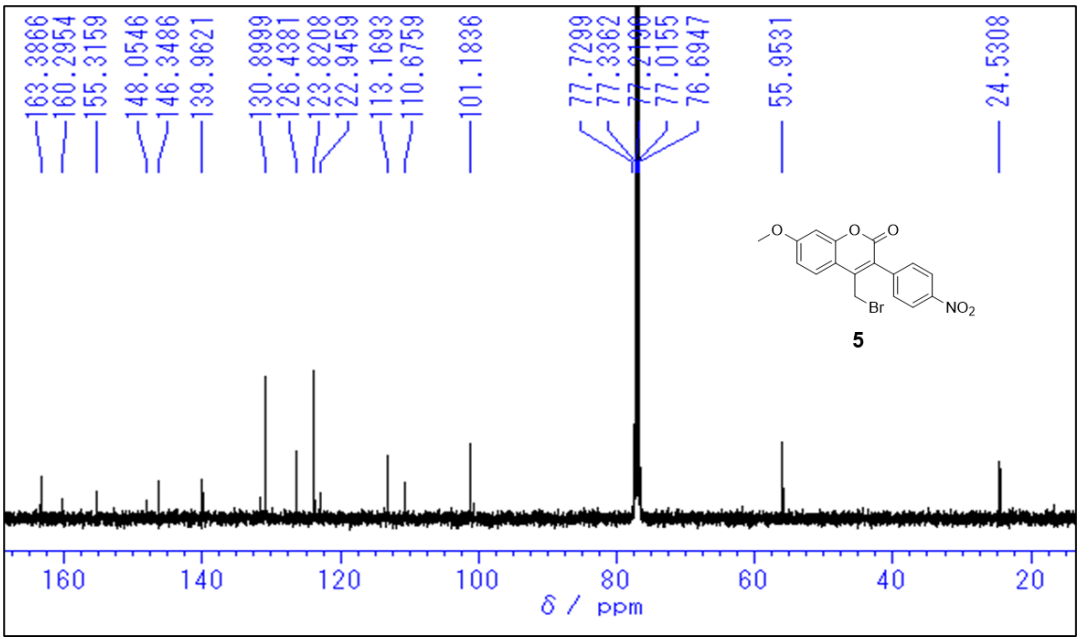

Figure S8. ^{13}C NMR of compound **5** (100 MHz, $CDCl_3$).

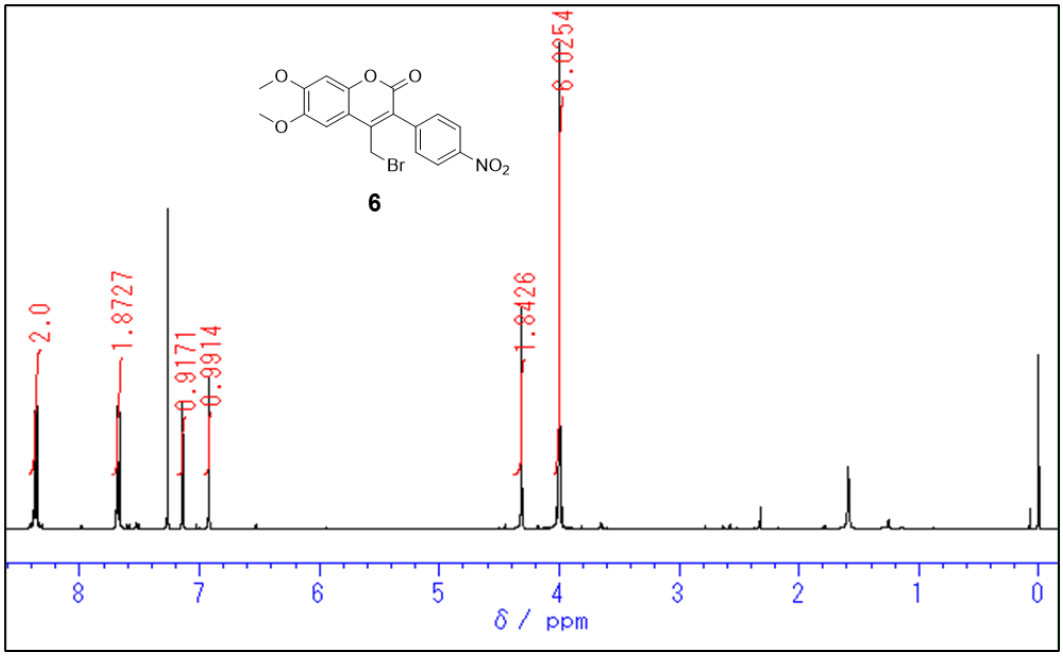

Figure S9. ^{1}H NMR of compound **6** (400 MHz, $CDCl_3$).

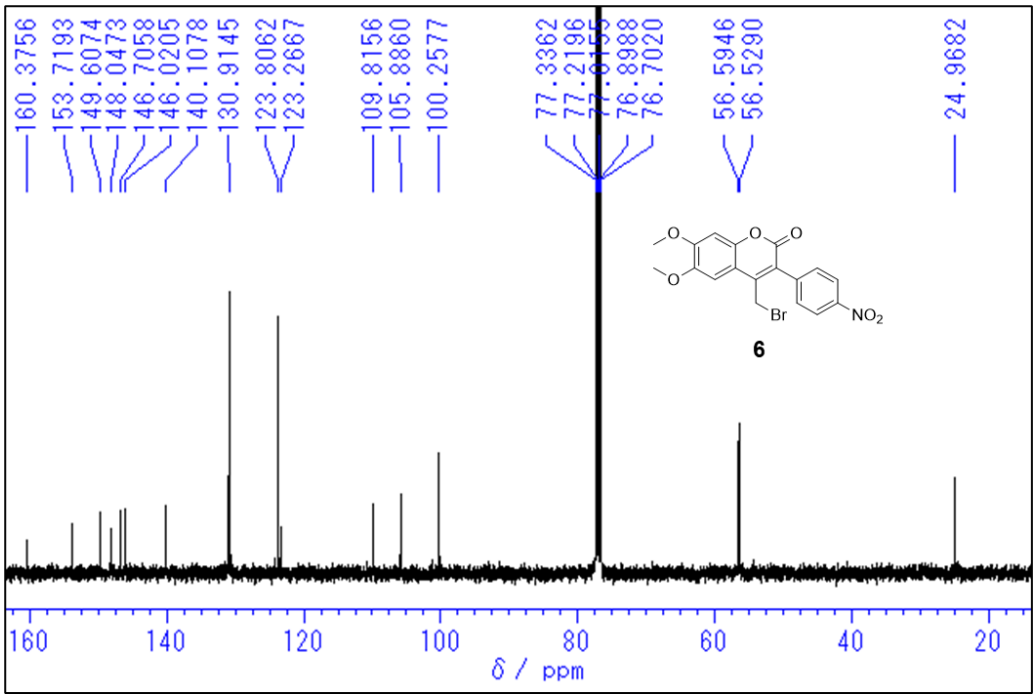

Figure S10. ^{13}C NMR of compound **6** (100 MHz, $CDCl_3$).

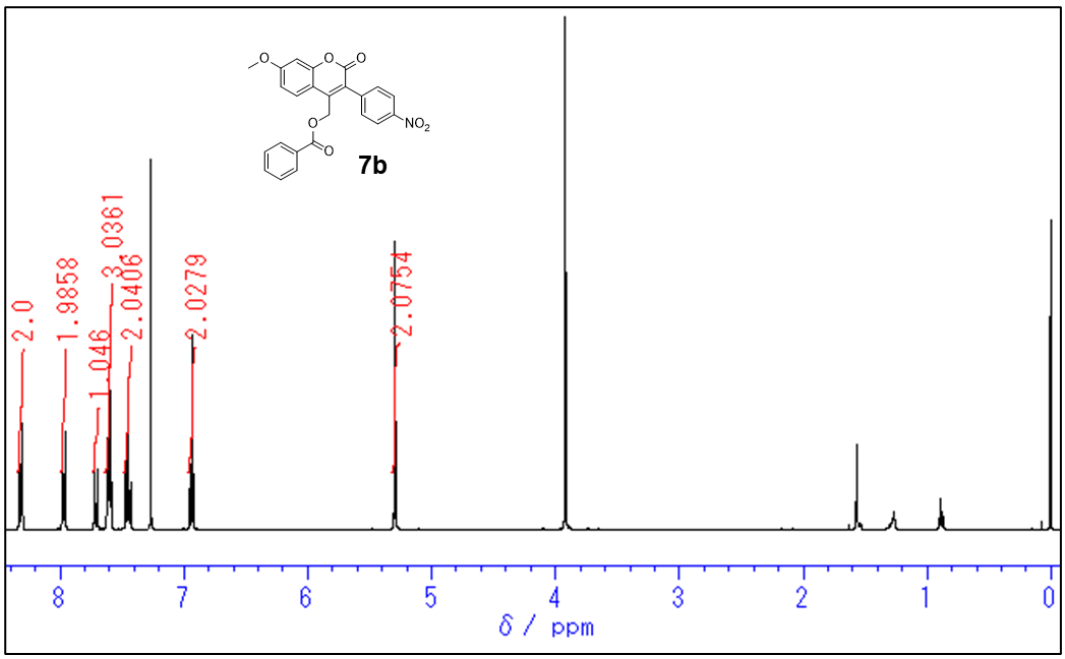

Figure S11. ^{1}H NMR of compound **7b** (400 MHz, $CDCl_3$).

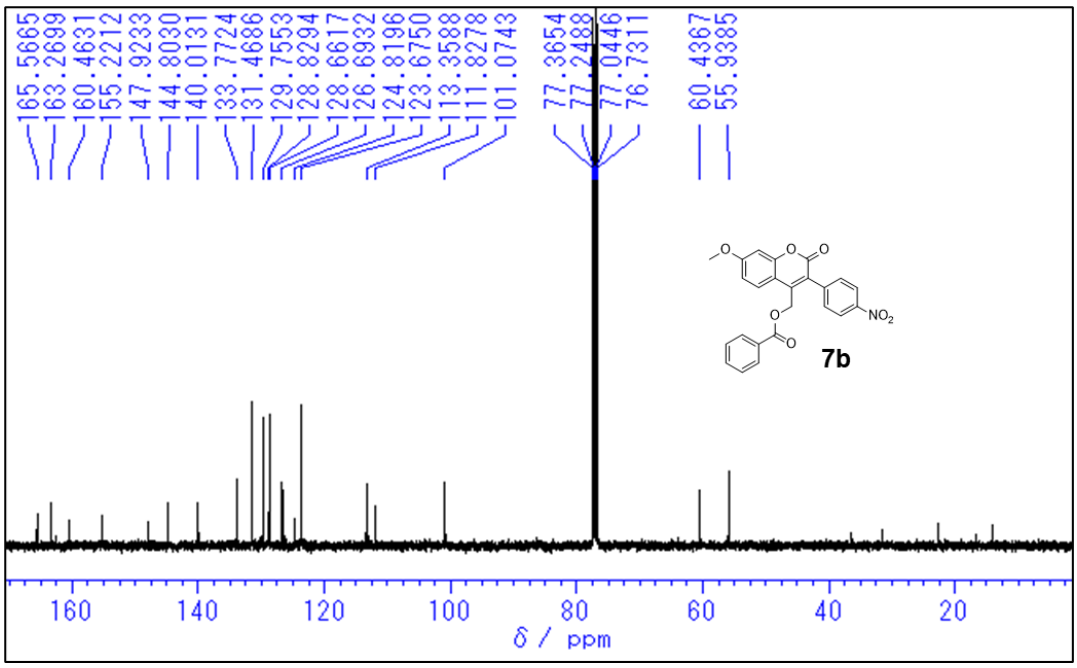

Figure S12. ^{13}C NMR of compound **7b** (100 MHz, $CDCl_3$).

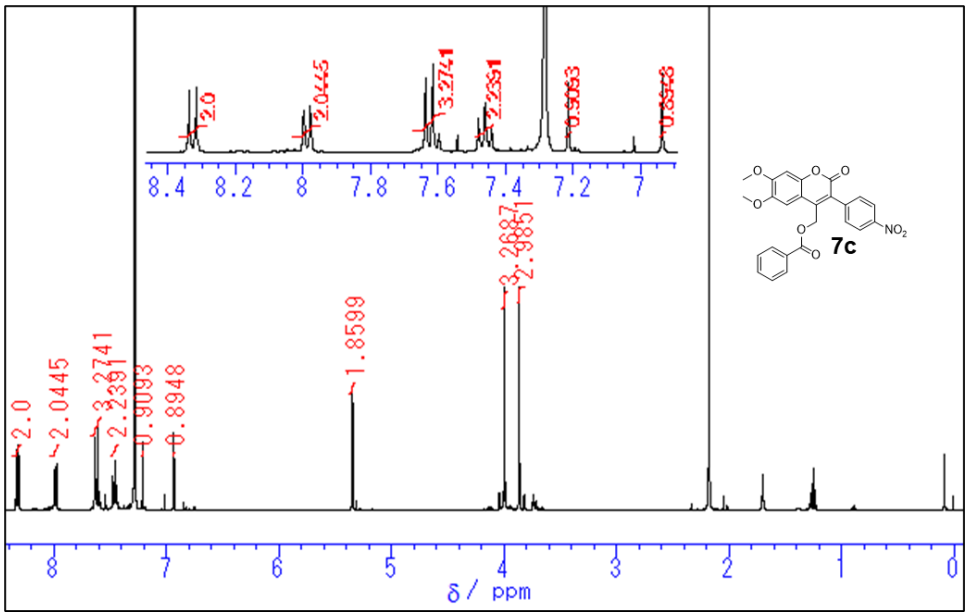

Figure S13. ^{1}H NMR of compound **7c** (400 MHz, $CDCl_3$).

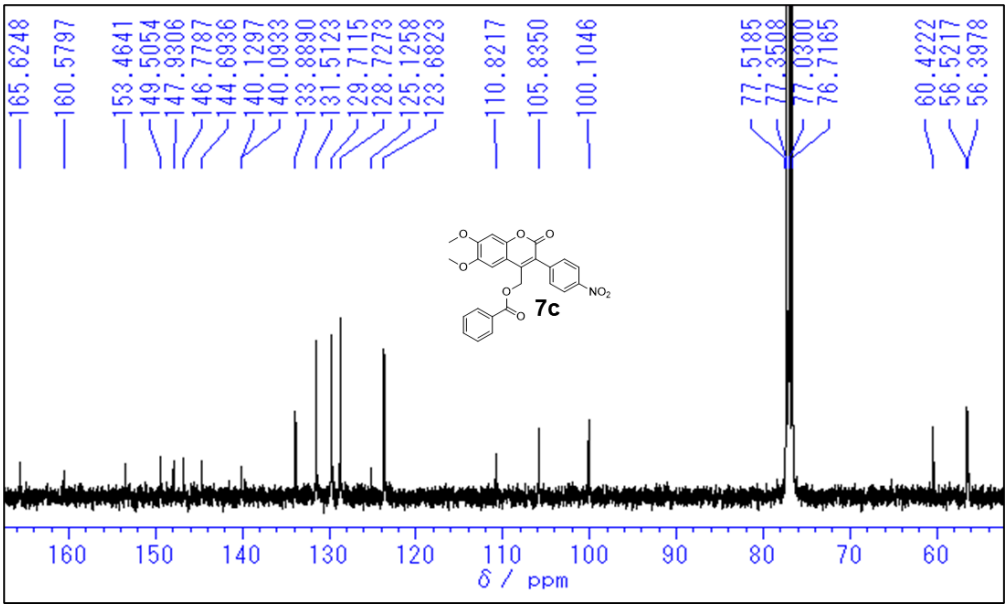

Figure S14. ^{13}C NMR of compound **7c** (100 MHz, $CDCl_3$).

Chemical actinometer for quantum yield measurement:

The rate of photoreaction of caged benzoate **7b** amd **7c** can be quantified by quantum yield (ϕ).

$$\Phi = \frac{\text{number of reacted molecules per time unit}}{\text{number of photons absorbed per time unit}}$$

In this study, ferrioxalate was used as a chemical actinometer to measure photon fluxes. During the light irradiation, the potassium ferrioxalate gives three ion products as shown in the following equations.

$$Fe(C_2O_4)_3^{3+} \xrightarrow{h\nu} Fe^{2+} + C_2O_4^{-} + 2C_2O_4^{2-}$$

$$Fe^{2+} + 3phen \longrightarrow Fe(phen)_3^{2+}$$

The number of ferrous ions that were released by photoreaction is measured by the reaction of ferric ion with phenanthroline to afford the colored tris-phenanthroline compound which has peculiar absorption at 510 nm ($\varepsilon = 11100\ M^{-1}\ cm^{-1}$).

Caged benzoate **7b** and **7c** have absorption maxima around 360 nm. Therefore, we measured the light quantities at 360 nm using a xenon lamp with a monochromator as a light source. The equation is shown as below,

$$I(\text{mol/s}) = \frac{\text{moles of } Fe^{2+}}{\Phi_\lambda \times t \times F} = \frac{V_1 \times V_3 \times \Delta A(510\text{ nm})}{10^3 \times V_2 \times l \times \varepsilon(510\text{ nm}) \times \Phi_\lambda \times t}$$

V_1: the irradiated volume (mL)

V_2: the aliquot of the irradiated solution taken for the determination of the ferrous ions (mL)

V_3: the final volume (mL)

ΔA: the optical difference in absorbance between the irradiated solution and that taken in the dark

l: optical pathlength of the irradiation cell

ε (510 nm): ε of the complex $Fe(phen)_3^{2+}$
Φ_λ: the quantum yield of ferrous ion production at the irradiation wavelength
t: the irradiation time
F: mean function of light absorbed by the ferrioxalate solution

Procedure for measurement:
1) 117.7 mg of $K_3[Fe(C_2O_4)_3] \cdot 3H_2O$ was dissolved in 20 mL of 0.05 M H_2SO_4. (0.012 M Ferrioxalate was prepared)- solution A
2) 10.2 mg of 1,10-phenanthroline monohydrate and 2.25 gm of $CH_3COONa \cdot 3H_2O$ were dissolved in 10 mL of 0.5 M H_2SO_4- solution B
3) To a 3 mL solution A irradiated at 360 nm for 0, 10, 20 and 30 seconds, 0.5 mL of solution B was added. The absorption spectrum of each solution was measured to monitor the change in absorbance at 510 nm. The determined ΔA was used to calculate the light quantity.

The number of photons from Xe-lamp at 360 nm was determined to be I_{360} = 5.52×10^{-9} mol/s = 3.31×10^{-7} mol/min was used. (This value was obtained in previous work in our laboratory)

Procedure for Measurement:
Solution of **7b**, **7c** (**7b**: 0.27 mM, **7c**: 0.32 mM in DMSO) was taken in a cell. Light irradiation was performed using a xenon lamp at 360 nm under ambient atmosphere and the reaction solution after irradiation was injected into HPLC and analyzed. Based on the integral value of peak area before and after light irradiation, the reaction rate was calculated using the following equation.
Reaction rate (%) = (integral value before light irradiation - integral value after light irradiation) ÷ integral value before light irradiation × 100.
The photoreaction quantum yield was calculated using the following equation,
Quantum yield Φ = number of molecules reacted by light irradiation (mol) ÷ amount of light absorbed by the compound (mol).

[HPLC condition]
Solvent : CH_3CN/water =90/10
Intersil ODS-3 5μm 4.6 × 250 mm

flow : 1.0 mL/min, press : 4.2 MPa, detect : 330 nm, range : 0.16

Computational details

We used density functional theory (DFT) and time-dependent (TD) DFT approaches, as implemented in the Gaussian 03 and 09 packages [1,2], to model all chromophores of interest. Calculations have been performed in vacuum and were limited to properties related to the ground state geometry: geometry optimization, one and two-photon absorption related to the electronically excited states (ES). Optical spectra were obtained employing the density matrix formalism for non-linear optical responses as proposed by S. Tretiak and V. Chernyak [3,4].

Figure 11 shows one-photon absorption (OPA) and two-photon absorption (TPA) spectra obtained at the TD-B3LYP/6-31G(d)//B3LYP/6-31G(d) level of theory in conventional quantum chemical notation "single point//optimization level", including up to 20 singlet ES. This level of theory has been shown to provide good predictions for structure-TPA relationships [4-7]. The damping factor introduced to simulate the finite linewidth in the resonant spectra has been fixed to Γ=0.10 eV [4]. The ES structure was further checked for all chromophores at the TD-ωB97XD/6-31G(d)//B3LYP/6-31G(d) level, especially to check for possible spurious charge transfer states.

At the B3LYP/6-31G(d) level, all chromophores show a dihedral angle of about 35° between the phenyl ring and the coumarin core. All chromophores lead to sizable TPA cross sections in the vicinity of twice the wavelength of the first OPA band (Figure 11), which is related to their dipolar nature. Thus, the two-level approximation, which is a standard approach for push-pull chromophores, can be further used to rationalize structure-properties relationships and to gauge quantitatively the various sources of errors on the computed values. Within the two-level model, the TPA cross section σ_2 of a dipolar chromophore at the maximum ($\hbar\omega = \hbar\omega_{0\iota}/2$) reads:

$$\sigma_2 = 2.0757 \times 10^{-3} \frac{\mu_{0i}^2(\mu_{ii}-\mu_{00})^2}{\Gamma} \text{(GM)} \quad (1)$$

where 0 and *i* label the ground and excited state of interest, respectively, and units of the input parameters are eV for Γ (vide supra) and Debye for dipole moments ($\mu_{j\iota}$). Noteworthy, this expression highlights that σ_2 is inversely proportional to the average linewidth broadening parameter Γ, which has been fixed arbitrarily 0.1 eV in our computations. Calculated state and transition dipole moments as well as the values of σ_2 deduced from the two-state model are reported in Table S1.

When using dipole moment matrix elements calculated at the same level of theory, namely TD-B3LYP, the two-state approximation (Table S1) leads to almost quantitative agreement with the calculated TPA maximum obtained (Figure 11). However, the absolute amplitude should be taken with care (*i.e.* as a qualitative result) as stressed in our previous works [6-7]. In fact, considering the ωB97XD exchange-correlation functional to compute dipole moments and transition energies, one notices a dramatic decrease of the excited state dipole moment as compared to B3LYP values (Table S1). This leads to a dramatic decrease of the TPA cross section at the maximum. However, the two to three-fold increase occurring upon substitution, when going from the model nitrocoumarine to the substituted ones, remains indicative of correct qualitative trend. Noteworthy, solvent effects not taken into account here should lead to sizeable increase of σ_2 [4,6,7].

Table S1. Calculated state and transition dipole moments using the 6-31G(d) basis set and for geometries optimized at the B3LYP/6-31G(d) level of theory. The TPA cross section at the maximum is derived within the two-state model (Eq. (1)).

	TD-DFT functional	*i*	μ_{ii} (D)			μ_{00} (D)			μ_{01} (D)			σ_2 (GM)
			x	*y*	*z*	*x*	*y*	*z*	*x*	*y*	*z*	
4a	B3LYP	*1*	16,9	-2,5	0,5	7,1	-3,4	0,8	-6,2	0,3	-0,1	**78**
	ωB97XD	*2*	9,9	-3,0	0,6	7,1	-3,6	0,7	-6,8	0,7	0,2	**8**
4b	B3LYP	*1*	-21,5	-1,5	-1,3	-8,7	-2,1	-1,3	7,0	0,3	0,3	**170**
	ωB97XD	*1*	-12,1	-1,9	-1,3	-8,4	-2,2	-1,3	-7,4	-0,7	-0,5	**16**
4c	B3LYP	*1*	-1,5	20,8	-10,6	-1,3	8,9	-3,2	-0,1	5,8	-3,2	**179**
	ωB97XD	*1*	-1,4	12,6	-5,6	-1,4	8,7	-3,0	0,1	6,8	-3,3	**26**

Table S2. Calculated transition energies using the 6-31G(d) basis set and for geometries optimized at the B3LYP/6-31G(d) level of theory.

	TD-DFT functional	*i*	ω_{0i} (eV)	λ_{OPA} (nm)	λ^{exp}_{OPA} (nm)	λ_{TPA} (nm)	σ_2 (GM)	Δ(eV)
4a	B3LYP	*1*	3,528	351	321[#]	703	**78**	*0,513*
	ωB97XD	*2*	4,041	307		614	**8**	
4b	B3LYP	*1*	3,307	375	338[#]	750	**170**	*0,560*
	ωB97XD	*1*	3,867	321		641	**16**	
4c	B3LYP	*1*	3,212	386	361[#]	772	**179**	*0,596*
	ωB97XD	*1*	3,808	326		651	**26**	

[#] *experiment in DMSO for the Methyl substituted compounds*

Besides, Table S2 also reveals the great sensitivity of transition energies to the

TD-DFT functional used. However, the trends remains the same, for instance : red shift when going from **4a** to **4b** then to **4c**.

In summary theoretical prediction are as follows: there is a sizeable red shift along the above mentionned series; TPA undergoes a two to threefold enhancement as compared to the "*model chromophore*" **4a**, and the position of the first experimental TPA maximum is predicted to show up at twice the OPA absorption band maximum.

References of computational details

[1] Gaussian 03, Revision D.02, M. J. Frisch, G. W. Trucks, H. B. Schlegel, G. E. Scuseria, M. A. Robb, J. R. Cheeseman, J. A. Montgomery, Jr., T. Vreven, K. N. Kudin, J. C. Burant, J. M. Millam, S. S. Iyengar, J. Tomasi, V. Barone, B. Mennucci, M. Cossi, G. Scalmani, N. Rega, G. A. Petersson, H. Nakatsuji, M. Hada, M. Ehara, K. Toyota, R. Fukuda, J. Hasegawa, M. Ishida, T. Nakajima, Y. Honda, O. Kitao, H. Nakai, M. Klene, X. Li, J. E. Knox, H. P. Hratchian, J. B. Cross, V. Bakken, C. Adamo, J. Jaramillo, R. Gomperts, R. E. Stratmann, O. Yazyev, A. J. Austin, R. Cammi, C. Pomelli, J. W. Ochterski, P. Y. Ayala, K. Morokuma, G. A. Voth, P. Salvador, J. J. Dannenberg, V. G. Zakrzewski, S. Dapprich, A. D. Daniels, M. C. Strain, O. Farkas, D. K. Malick, A. D. Rabuck, K. Raghavachari, J. B. Foresman, J. V. Ortiz, Q. Cui, A. G. Baboul, S. Clifford, J. Cioslowski, B. B. Stefanov, G. Liu, A. Liashenko, P. Piskorz, I. Komaromi, R. L. Martin, D. J. Fox, T. Keith, M. A. Al-Laham, C. Y. Peng, A. Nanayakkara, M. Challacombe, P. M. W. Gill, B. Johnson, W. Chen, M. W. Wong, C. Gonzalez, and J. A. Pople, Gaussian, Inc., Wallingford CT, **2004**.

[2] Gaussian 09, Revision A.02, M. J. Frisch, G. W. Trucks, H. B. Schlegel, G. E. Scuseria, M. A. Robb, J. R. Cheeseman, G. Scalmani, V. Barone, B. Mennucci, G. A. Petersson, H. Nakatsuji, M. Caricato, X. Li, H. P. Hratchian, A. F. Izmaylov, J. Bloino, G. Zheng, J. L. Sonnenberg, M. Hada, M. Ehara, K. Toyota, R. Fukuda, J. Hasegawa, M. Ishida, T. Nakajima, Y. Honda, O. Kitao, H. Nakai, T. Vreven, J. A. Montgomery, Jr., J. E. Peralta, F. Ogliaro, M. Bearpark, J. J. Heyd, E. Brothers, K. N. Kudin, V. N. Staroverov, R. Kobayashi, J. Normand, K. Raghavachari, A. Rendell, J. C. Burant, S. S. Iyengar, J. Tomasi, M. Cossi, N.

Rega, J. M. Millam, M. Klene, J. E. Knox, J. B. Cross, V. Bakken, C. Adamo, J. Jaramillo, R. Gomperts, R. E. Stratmann, O. Yazyev, A. J. Austin, R. Cammi, C. Pomelli, J. W. Ochterski, R. L. Martin, K. Morokuma, V. G. Zakrzewski, G. A. Voth, P. Salvador, J. J. Dannenberg, S. Dapprich, A. D. Daniels, Ö. Farkas, J. B. Foresman, J. V. Ortiz, J. Cioslowski, and D. J. Fox, Gaussian, Inc., Wallingford CT, **2009**.

[3] S. Tretiak, V. Chernyak, *J. Chem. Phys.* **2003**, *119*, 8809.

[4] F. Terenziani, C. Katan, E. Badaeva, S. Tretiak, M. Blanchard-Desce, *Advanced Materials* **2008**, *20*, 4641.

[5] S. Boinapally, B. Huang, M. Abe, C. Katan, J. Noguchi, S. Watanabe, H. Kasai, B. Xue and T. Kobayashi, *J. Org. Chem.*, **2014**, *79*, 7822.

[6] B. Xue, C. Katan, J. A. Bjorgaard, T. Kobayashi, *AIP Adv.*, **2015**, *5*, 12.

[7] Komori, N. and Jakkampudi, S. and Motoishi, R. and Abe, M. and Kamada, K. and Furukawa, K. and Katan, C. and Sawada, W. and Takahashi, N. and Kasai, H. and Xue, B. and Kobayashi, T., *Chem. Com.*, **2016,** *52*, 331.

Chapter 3

Design, Synthesis and Photoreactions of Caged Compounds with D-π-D coumarin unit

3-1. Introduction

Dipolar derivative (D-π-A type) **7b** and **7c** as we introduced in Chapter 2 showed an enhanced TPA cross-section, however the uncaging efficiency became lower as the charge transfer character became stronger. In this section, we also designed quadrupolar system (D-π-D type) to overcome this issue of impairing photoreactivity by strong charge transfer character. The photophysical and photochemical properties of D-π-D coumarin chromophore was investigated.

3-2. Design and synthesis of D-π-D coumarin chromophore with strong electron donor group

Amino group was used as an electron-donor part for its strong donating ability from nitrogen. Trans-stilbene structure with amino group is also expected to give high TPA character on chromophores, according to previous research.[48] The target D-π-D chromophore **11** was synthesized by two-steps reaction (Scheme 3). First, the commercially available 7-diethylamino-4-methylcoumarin **8** was brominated by N-bromosuccinimide (NBS) to get the coupling precursor **9**.[49] The subsequent Suzuki-Miyaura coupling reaction with N,N'-dimethylaminophenyl boronic acid pinacol ester **10** produced D-**π**-D chromophore **11**.

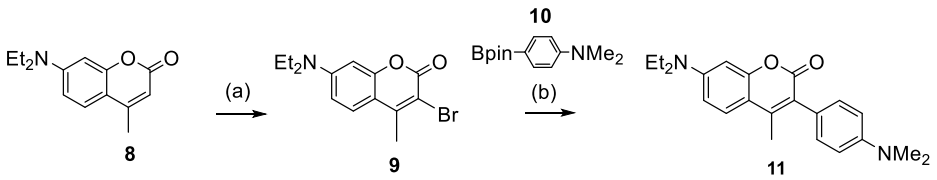

Scheme 3. Synthesis of **11**; Reagents and conditions: (a) NBS, MeCN, RT, 1h, 37%. (b) compound **10**, $PdCl_2(PPh_3)_2$, Na_2CO_3, DMF:H_2O (2:1, v/v), 90°C, 9h, 54%.

3-3. OP photophysical property

Steady-state OPA spectrum of **11** was recorded in DMSO. Compound **11** shows λ_{max} at 386 nm (ε = 28861 $M^{-1}cm^{-1}$) (Figure 13). TDDFT calculation was performed to assign the OP electronic transitions of **11** and the D-**π**-A analogue in gas phase. For calculation, the molecular structures of **11** and D-**π**-A analogue

were simplified by replacing their 7-diethylamino group with 7-dimethylamino group and replacing their 4-methyl group with hydrogen (as shown in the structure of **12a**,**b**). The computed OPA spectra of compound **12a** and **12b** with oscillator strengths are shown in Figure 14. For both compound **12a** and **12b**, a relatively large oscillator strength was found in the 1st electronic transition ($S_0 \rightarrow S_1$) (f = 0.6943 at 402 nm for **12a**, f = 0.6461 at 417 nm for **12b**), which was assigned to the HOMO to LUMO transition. 2nd electronic transition ($S_0 \rightarrow S_2$) was found at 323 nm (f = 0.1909) and 336 nm (f = 0.2496) for **12a** and **12b**, respectively. The 2nd electronic transition was assigned to the HOMO-1 to LUMO transition. In the 1st electronic transition ($S_0 \rightarrow S_1$), the molecular orbital (MO) of **12b** (Figure 14b, HOMO to LUMO) indicates charge transfer character from electron-donor to acceptor part. On the other hand, MO of **12a** in the 1st electronic transition ($S_0 \rightarrow S_1$) (Figure 14a, HOMO to LUMO) shows concentrated MO coefficient on the coumarin core in the LUMO.

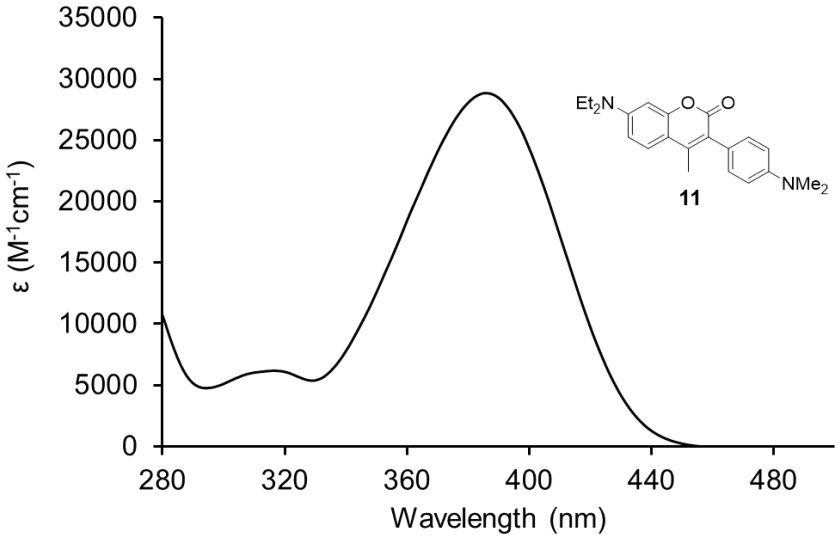

Figure 13. UV-visible absorption spectrum of **11** in DMSO.

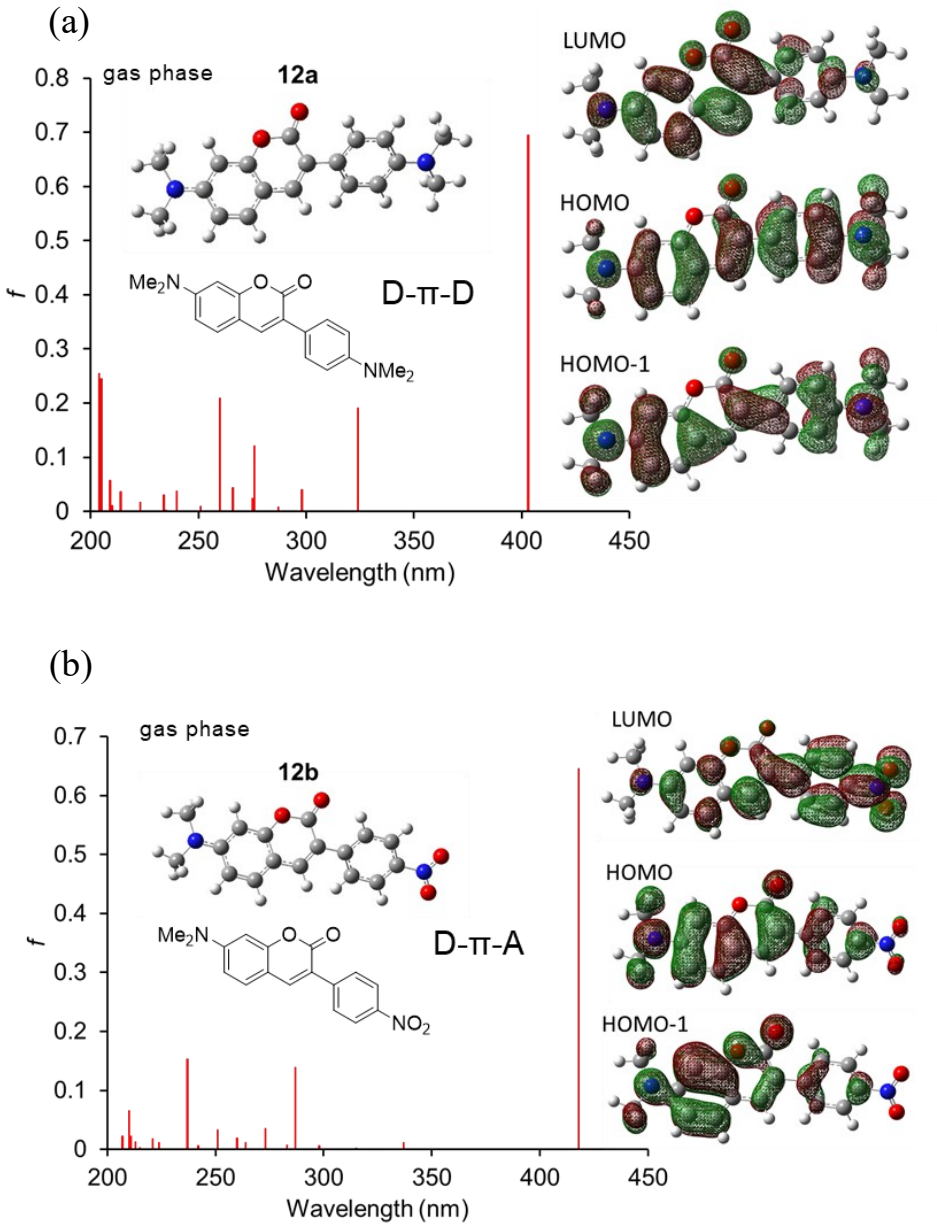

Figure 14. Calculated oscillator strengths and MOs of (a) **12a** (D-**π**-D) and (b) **12b** (D-**π**-A), computed at the TD-RB3LYP/6-31G(d)//RB3LYP/6-31G(d) level of theory.

3-4. Theoretical prediction of TPA cross-section

The predicted OPA and TPA spectra of **12a** and **12b** were shown in Figure 15. All the spectra were computed at the TD-B3LYP/6-31G (d)//B3LYP/6-31 (d) level of theory. Three-state model was used to calculate TPA cross-section. D-π-A analogue **12b** showed TPA cross-section of σ_2 = 309 GM at 834 nm, which is almost double wavelength of OPA maximum (~ 400 nm) (Figure 15b). On the other hand, D-π-D derivative **12a** showed maximum TPA cross-section (ca. 700 GM) near 650 nm, which is blue-shifted from the double wavelength of OPA maximum of **12a** (Figure 15a). The predicted TPA spectrum of **12a** indicates that 1st electronic transition ($S_0 \rightarrow S_1$) is TP forbidden but 2nd electronic transition ($S_0 \rightarrow S_2$) is TP allowed (Figure 15a). Similar phenomenon was observed from quadrupolar 4,4′-bis(di-*n*-butylamino)-*E*-stilbene as reported in the literature.[50] Our computational result suggests that quadrupolar D-π-D chromophore is more TP responsive (2.5-fold increase in TPA cross-section). Such increase can be attributed to the large transition dipole moment in the 2nd electronic transition ($S_0 \rightarrow S_2$) (Table S3). Thus, we selected D-π-D chromophore for next molecular design of TP responsive caged compound.

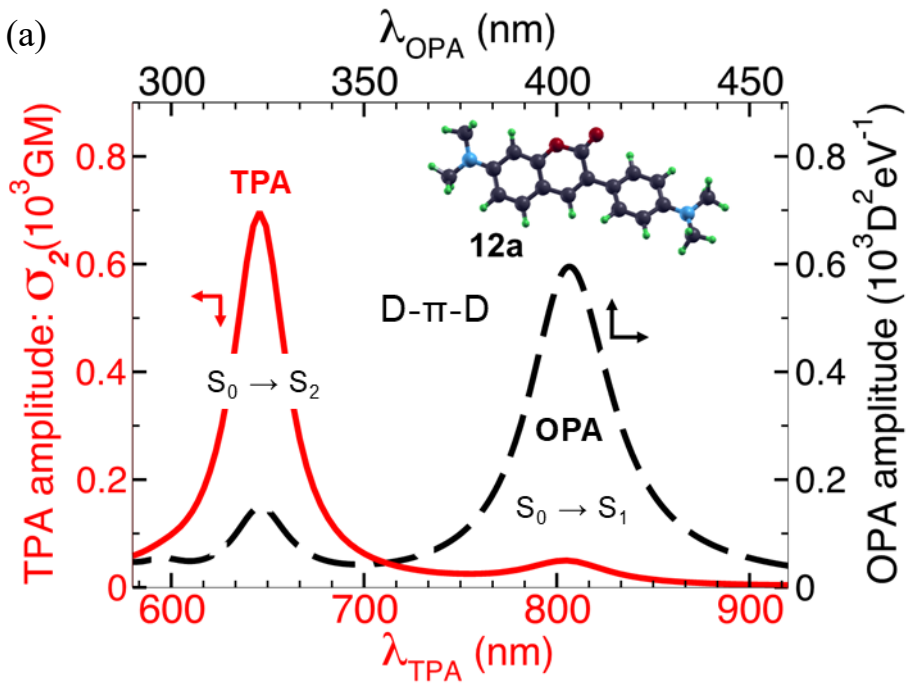

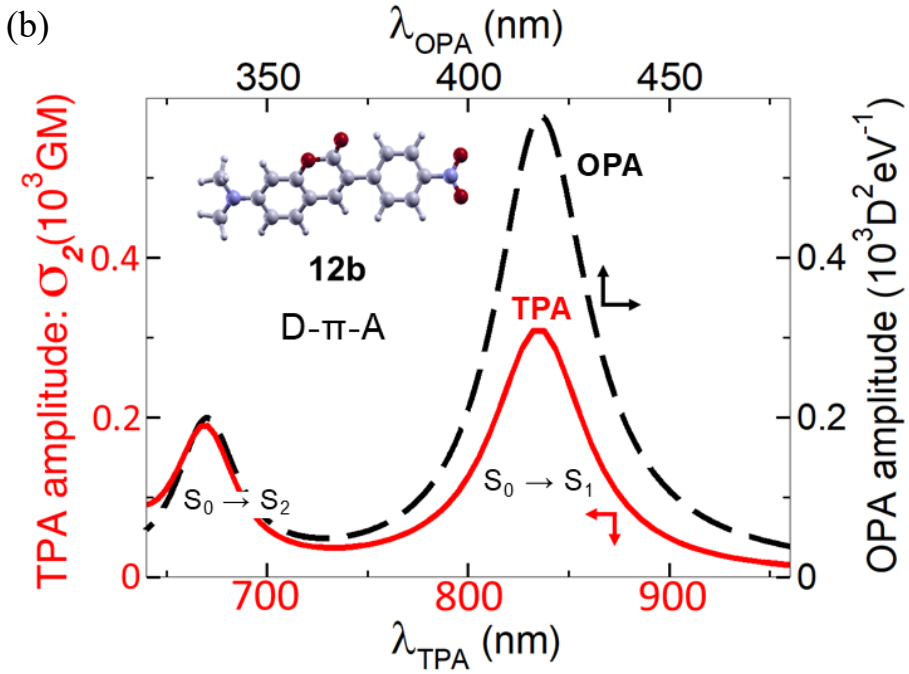

Figure 15. Calculated OPA and TPA spectra of (a) **12a** (D-**π**-D) and (b) **12b** (D-**π**-A), computed at the TD-B3LYP/6-31G(d)//B3LYP/6-31G(d) level of theory.

3-5. Synthesis of D-π-D caged benzoate

Synthetic route of D-π-D caged benzoate **19** is shown in Scheme 4. First, 7-diethylamino-4-methylcoumarin **8** was oxidized by SeO_2 to get aldehyde **13**. 4-hydoxymethyl derivative **14** was afforded by reduction of **13** using $NaBH_4$. The hydroxyl group was protected by tert-butyldimethylsilyl chloride (TBSCl) to give **15**. NBS was used for bromination of **15**, then coupling precursor **16** was obtained.[49] Suzuki-Miyaura coupling reaction of **16** with N,N'-dimethylaminophenyl boronic acid pinacol ester **10** produced D-π-D derivative **17**. Silyl group was deprotected by TBAF to give 4-hydroxymethyl coumarin **18**. D-π-D caged benzoate **19** was obtained by condensation reaction of **18** with benzoic acid using N,N'-dicyclohexylcarbodiimide (DCC) and 4-dimethylaminopyridine (DMAP).

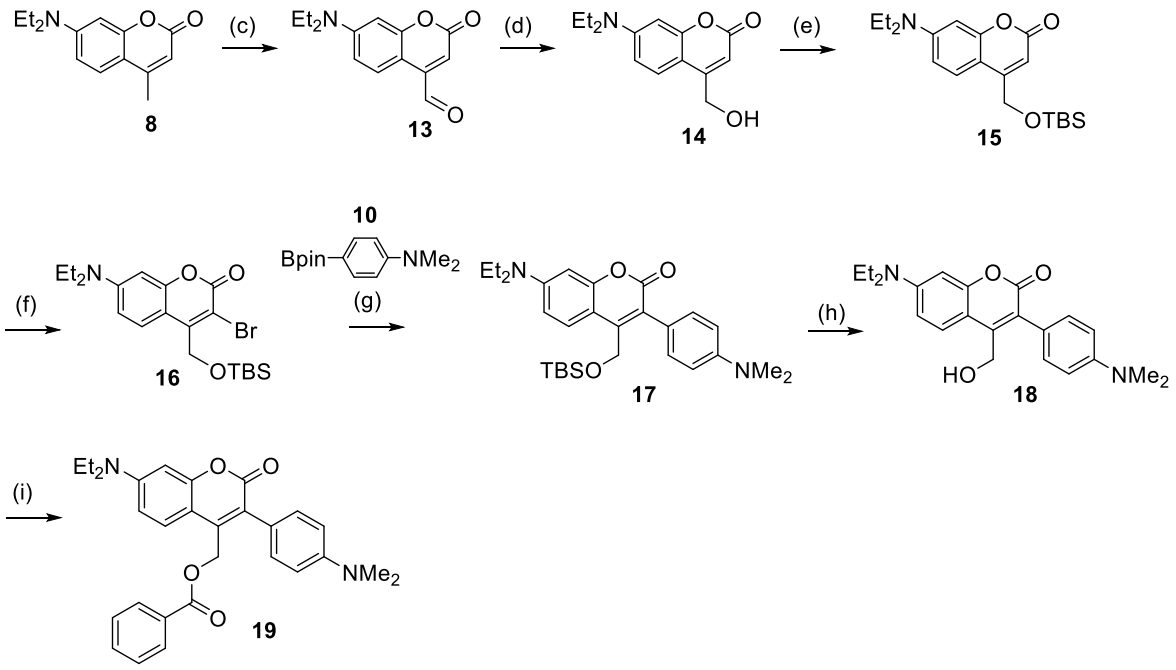

Scheme 4. Synthesis of **19**; Reagents and conditions: (c) SeO2, xylene, 134°C, 24h, 41%. (d) $NaBH_4$, EtOH, RT, 4h, 49%. (e) TBSCl, DMAP, dry DCM, RT, 3h, 90%. (f) NBS, NH_4OAc, MeCN, RT, 1h, 66%. (g) Compound **10**, $PdCl_2(PPh_3)_2$, Na_2CO_3, DMF:H_2O (2:1, v/v), 90°C, 9h, 92%. (h) TBAF, THF, 0°C→RT, 30 min, 40%. (i) Benzoic acid, DCC, DMAP, DCM, RT, 12h, 86%.

3-6. OP uncaging reaction of D-π-D caged benzoate in DMSO

OP uncaging reaction of caged benzoate **19** was conducted using a Xenon lamp (500 W) at 400 ± 10 nm in DMSO-d_6. According to the ^{1}H NMR spectrum analysis (400 MHz), the peaks of benzoic acid and the photolysate increased under photoirradiation (Figure 16). Quantitative release of benzoic acid was observed (> 90%). The photolysis of **19** afforded 4-carboxylaldehyde product in 70% isolated yield. The clean formation of aldehyde **20** was confirmed by UV-vis spectroscopic analysis in DMSO (Figure 17). Concomitant with the depletion of absorption band of **19** with λ_{max} = 407 nm (ε_{407} = 28493 $M^{-1}cm^{-1}$), the absorption band of aldehyde **20** increased with λ_{max} = 482 nm (ε_{482} = 23178 $M^{-1}cm^{-1}$) (Figure 17). Photoreaction quantum yield (Φ_u) of **19** in DMSO was determined using ferrioxalate as a photochemical actinometer. The quantum yield of **19** (Φ_r = 0.16) was higher than that of previous D-π-A derivatives **7b** and **7c**.

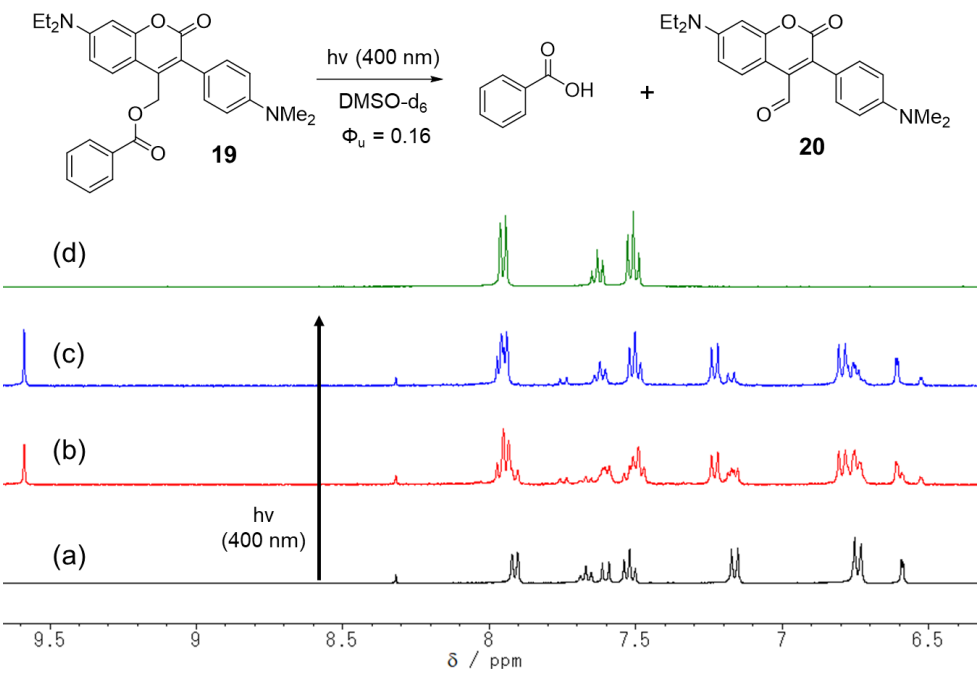

Figure 16. ^{1}H NMR spectra of **19** in DMSO-d_6 (a) before and after (b) 1h, (c) 2h of irradiation at 400 nm; (d) ^{1}H NMR spectra of benzoic acid in DMSO-d_6.

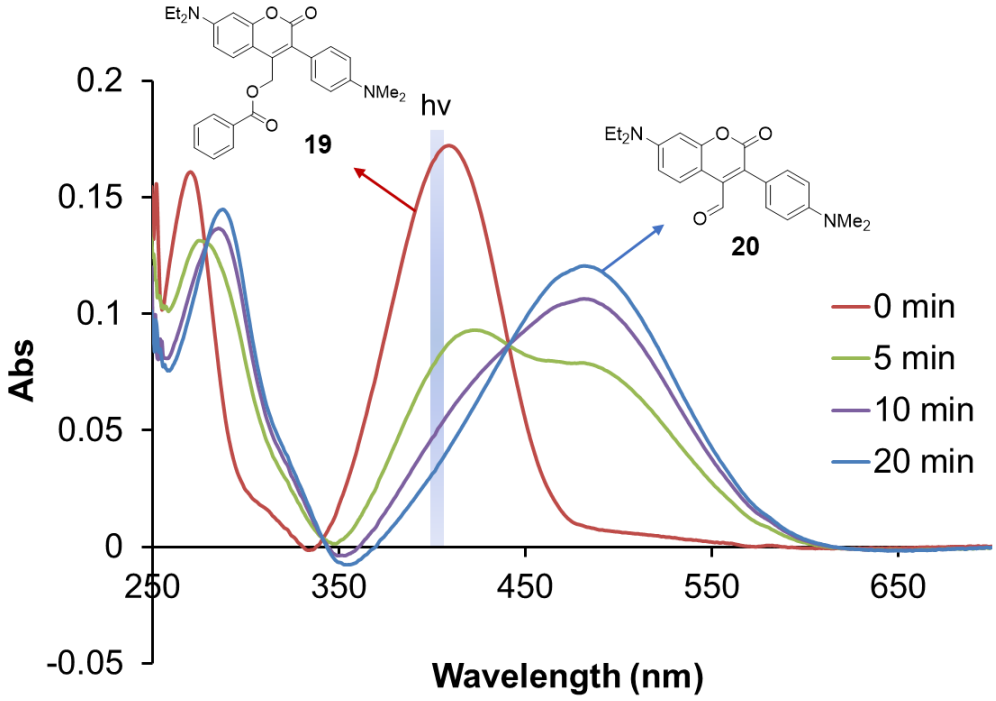

Figure 17. UV-visible spectroscopic analysis of OP uncaging reaction of **19** at 400 ± 10 nm irradiation in DMSO.

It is assumed that uncaging reaction was facilitated by charge transfer on the coumarin core. This hypothesis was supported by computational analysis of MO coefficients. The D-π-D chromophore **12a** showed a larger MO coefficient on the carbon atom at 4-position in the LUMO ($C_{LUMO}^2 = 0.237$) in comparison to the D-π-A analogues ($C_{LUMO}^2 = 0.127$ for **4b**, $C_{LUMO}^2 = 0.126$ for **4c**) (Figure 18). Therefore, it seems that efficient charge transfer to the carbon at 4-position induced higher uncaging quantum yield. Similar principles have been discussed for other photo-S_N1 type chromophores in previous literature.[51]

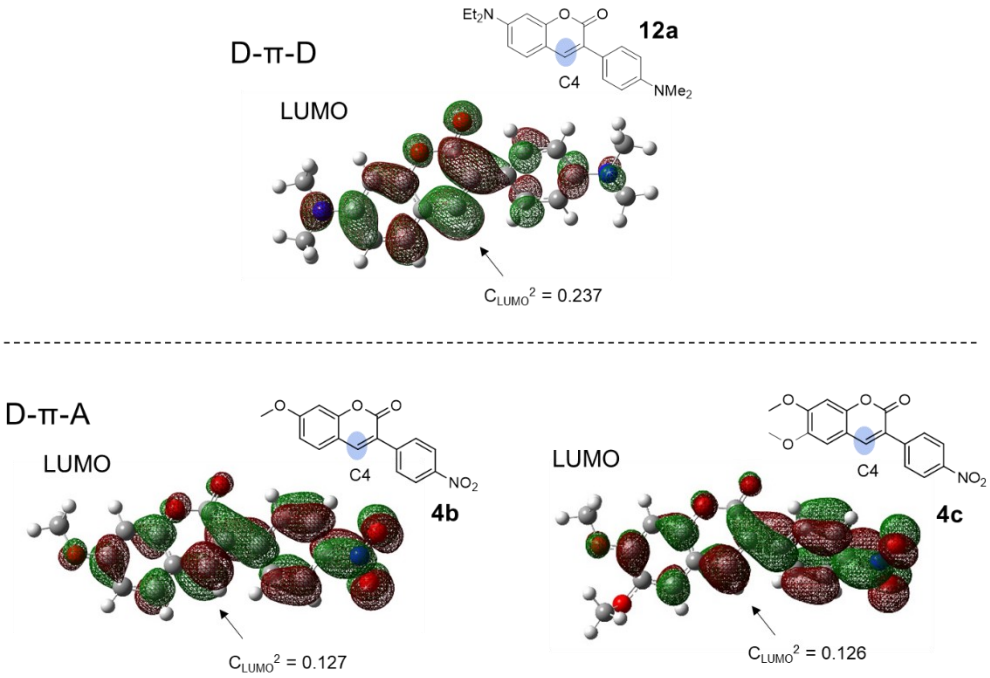

Figure 18. MO coefficients of D-π-D chromophore **12a** and D-π-A analogues **4b** and **4c** in the LUMO.

3-7. Uncaging reaction mechanism of D-π-D caged benzoate

To get more insight into uncaging reaction mechanism of **19**, the solvent effect on OP uncaging reaction of **19**, irradiated at 400 nm using a Xenon lamp, was investigated using methanol, anhydrous DMSO, DMSO with 5% Tris buffer, and DMSO with 5% distilled water. The photoreaction was monitored by HPLC analysis. The rate of reaction that consumed starting material **19** was determined by decreasing of integrated value of peak area. Previously, the uncaging reaction rate of (coumarin-4yl)methyl type PPG was reported to be faster in the presence of water in solvent.[52] The photoreaction of **19** in methanol was interestingly slower than that in anhydrous DMSO or wet DMSO by a factor of 1.6 (Figure 19). On the other hand, the reaction in DMSO with 5% distilled water was slightly faster than that in anhydrous DMSO by a factor of 1.2 (Figure 19). Seemingly, the stronger solvent polarity induced faster photoreaction of **19**, according to dielectric constant of solvents.[53] In the presence of water in anhydrous DMSO, 4-hydroxymethyl product **18** was formed (40% isolated yield) in place of aldehyde **20**. This result indicated the existence of carbocation intermediate **21** generated by heterolytic C-O bond cleavage (Scheme 5). This intermediate **21** was trapped by DMSO or water to give corresponding product (**18** or **20**). From this mechanism, it is also assumed that the higher photoreaction quantum yield of D-π-D caged benzoate **19** (Φ_u = 0.16) than D-π-A analogues (**7b** and **7c** in Chapter 2) may be attributed to the strong stabilization of carbocation intermediate by two electron-donor parts.[54] The shortened fluorescence lifetime of **19** (2.3 ns in DMSO) in comparison with **11** (3.1 ns in DMSO) (Figures S32 and S34) supports the release of benzoic acid from S_1 excited state of **19**.

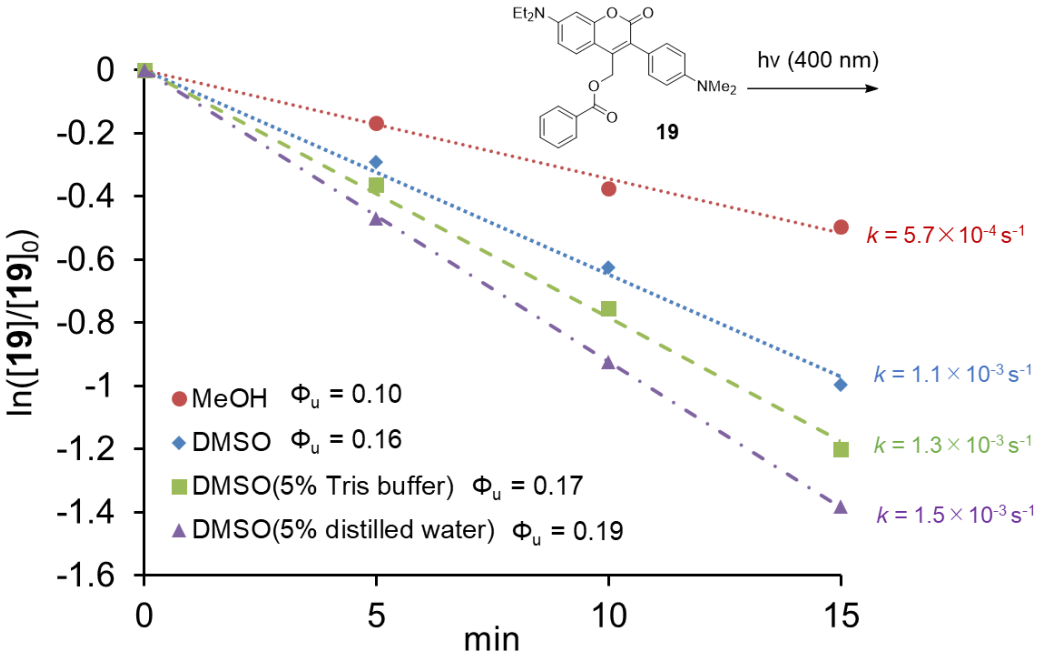

Figure 19. Time profile of the OP uncaging reaction of **19**; ln[**19**]/[**19**]$_0$ vs irradiation time (min) at a wavelength of 400 nm using a Xe lamp in various solvents.

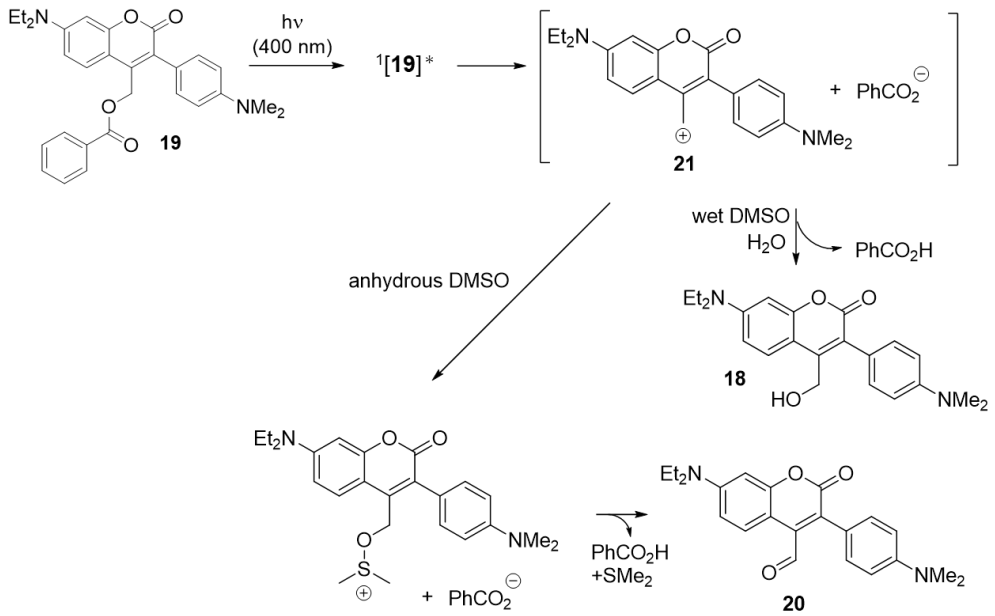

Scheme 5. Mechanism for the Uncaging Reaction of **19** in Anhydrous DMSO and Wet DMSO.

3-8. Measurement of TPA cross-section by TPEF method

TPA cross-section of parent chromophore **11** was determined by two-photon excited fluorescence (TPEF) method. The TPA cross-section in 2nd electronic transition (< 680 nm) was found to be larger than that in 1st electronic transition (~ 760 nm), where σ_2 = 5.6 GM at 760 nm and 18 GM at 680 nm (Figure 20). This is well consistent with our computational result and typical quadrupolar character.

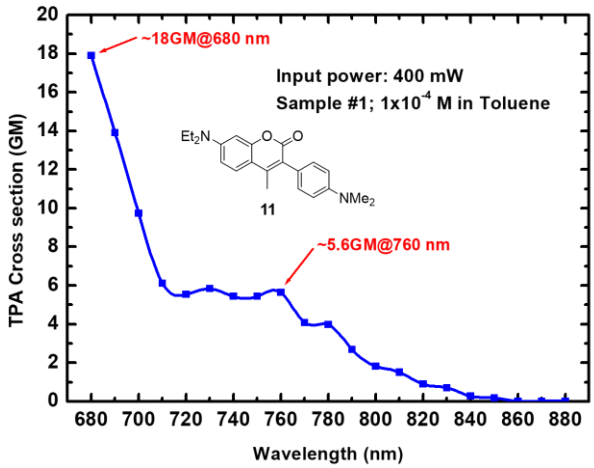

Figure 20. TPA spectrum, 680-880 nm, of compound **11** (1.0×10^{-4} M) in toluene.

3-9. TP uncaging reaction of D-π-D caged benzoate in DMSO

TP photolysis of **19** was performed using a Ti: sapphire (pulse width 100fs, 80MHz) at an average power of 700 mW at 298 K in DMSO at the wavelength of 750 nm (Figure 21). The depletion of **19** was observed by TP photolysis at 750 nm. The rate constants of TP photolysis of **19** at 750 nm was extrapolated to be $k_{750} = 1.9\times10^{-6}$ s^{-1} by comparing with the previous NPBF-BA chromophore[55] ($k_{740} = 9.4\times10^{-6}$ s^{-1}) as a reference.[56] Using the reported TP uncaging efficiency of NPBF-BA (δ_u = 5.0 GM at 740 nm), TPA cross-section of **19** was extrapolated to be 7.0 GM at 750 nm. Although we could not experimentally measure TPA cross-section of **19** below 680 nm, due to the limitation of laser setup, the maximum TPA cross-section was estimated from experimental value σ_2 = 5.6 GM at 760 nm of parent chromophore **11** by using simple proportionality method (see supplementary material). As a result, the maximum TPA cross-section of **19** was extrapolated to be ~ 100 GM at 650 nm. Therefore, the TP uncaging efficiency (δ_u) was estimated to be ~ 16 GM at 650 nm. Further π-extension on

the quadrupolar chromophore **19** will give higher TPA cross-section and more bathochromic shift for TPA wavelength.

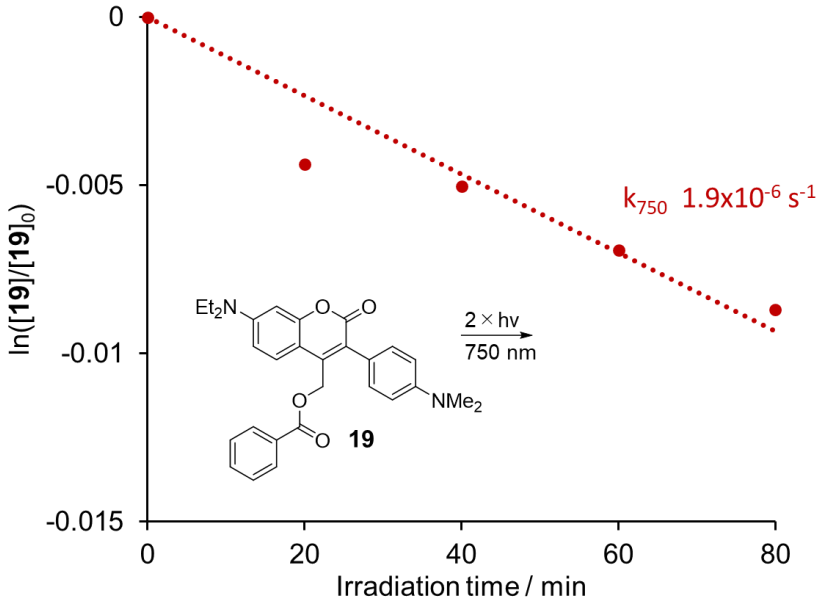

Figure 21. Time profile of the TP uncaging of **19**, ln([sub]/ $[sub]_0$) vs. irradiation time at wavelengths of 750 nm at 700 mW.

3-10. References

48) Boinapally, S.; Huang, B.; Abe, M.; Katan, C.; Noguchi, J.; Watanabe, S.; Kasai, H.; Xue, B.; Kobayashi, T. Caged Glutamates with π-Extended 1,2-Dihydronaphthalene Chromophore: Design, Synthesis, Two-Photon Absorption Property, and Photochemical Reactivity. *J. Org. Chem.* **2014**, *79*, 7822–7830.

49) Olson, J. P.; Banghart, M. R.; Sabatini, B. L.; Ellis-Davies, G. C. R. Spectral Evolution of a Photochemical Protecting Group for Orthogonal Two-Color Uncaging with Visible Light. *J. Am. Chem. Soc.* **2013**, *135*, 15948–15954.

50) Albota, M.; Beljonne, D.; Brédas, J. L.; Ehrlich, J. E.; Fu, J. Y.; Heikal, A. A.; Hess, S. E.; Kogej, T.; Levin, M. D.; Marder, S. R.; McCord-Maughon, D.; Perry, J. W.; Röckel, H.; Rumi, M.; Subramaniam, G.; Webb, W. W.; Wu, X. L.; Xu, C. Design of Organic Molecules with Large Two-Photon Absorption Cross

Sections. *Science.* **1998**, *281* (5383), 1653–1656.

51) Šolomek, T.; Wirz, J.; Klán, P. Searching for Improved Photoreleasing Abilities of Organic Molecules. *Acc. Chem. Res.* **2015**, *48*, 3064–3072.

52) Suzuki, A. Z.; Watanabe, T.; Kawamoto, M.; Nishiyama, K.; Yamashita, H.; Ishii, M.; Iwamura, M.; Furuta, T. Coumarin-4-ylmethoxycarbonyls as Phototriggers for Alcohols and Phenols. *Org. Lett.* **2003**, *5* (25), 4867–4870.

53) Furniss, B. S.; Hannaford, A. J.; Smith, P. W. G.; Tatchell, A. R., Eds., In *Vogel's Textbook of Practical Organic Chemistry,* 5th ed.; Longman Scientific & Technical, 1989.

54) Lin, Q.; Yang, L.; Wang, Z.; Hua, Y.; Zhang, D.; Bao, B.; Bao, C.; Gong, X.; Zhu, L. Coumarin Photocaging Groups Modified with an Electron-Rich Styryl Moiety at the 3-Position: Long-Wavelength Excitation, Rapid Photolysis, and Photobleaching. *Angew. Chem. Int. Ed.* **2018**, *57*, 3722–3726.

55) Komori, N.; Jakkampudi, S.; Motoishi, R.; Abe, M.; Kamada, K.; Furukawa, K.; Katan, C.; Sawada, W.; Takahashi, N.; Kasai, H.; Xue, B.; Kobayashi, T. Design and Synthesis of a New Chromophore, 2-(4-Nitrophenyl)Benzofuran, for Two-Photon Uncaging Using near-IR Light. *Chem. Commun.* **2016**, *52*, 331–334.

56) Donato, L.; Mourot, A.; Davenport, C. M.; Herbivo, C.; Warther, D.; Léonard, J.; Bolze, F.; Nicoud, J. F.; Kramer, R. H.; Goeldner, M.; Specht, A. Water-Soluble, Donor-Acceptor Biphenyl Derivatives in the 2-(o-Nitrophenyl)Propyl Series: Highly Efficient Two-Photon Uncaging of the Neurotransmitter γ-Aminobutyric Acid at λ= 800 nm. *Angew. Chem. Int. Ed.* **2012**, *51*, 1840–1843.

3-11. Experimental Section

7-(Diethylamino)-4-methyl-3-bromocoumarin (9)

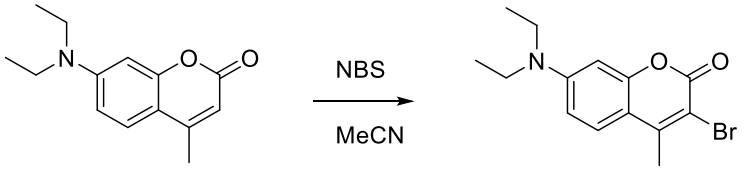

8 9

The solution of 7-(diethylamino)-4-methylcoumarin **8** (1.01 g, 4.4 mmol) and NBS (848 mg, 4.8 mmol) in MeCN (20 mL) was stirred at room temperature for 1h. After addition of water, the mixture was extracted with EtOAc, dried over $MgSO_4$, filtered, and evaporated to obtain crude material. The crude was purified by column chromatography (hexane : EtOAc = 4:1, v/v) (497 mg, 37 %). ^{1}H NMR (400 MHz, $CDCl_3$): δ (ppm) 7.45 (d, J = 9.1 Hz, 1H), 6.63 (dd, J = 9.1 Hz, 1H), 6.52 (d, J = 2.5 Hz, 1H), 3.44 (q, J = 7.1 Hz, 4H), 1.23 (t, J = 7.1 Hz, 6H).

7-(Diethylamino)-4-methyl-3-(4-dimethylaminophenyl) coumarin (11)

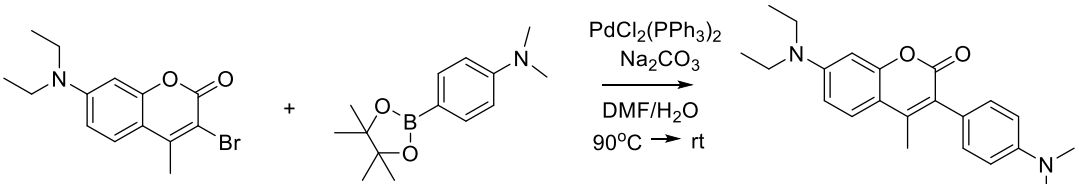

9 10 11

To a solution of 7-(diethylamino)-4-methyl-3-bromocoumarin **9** (50 mg, 0.16 mmol) and N,N'-dimethylaminophenyl boronic acid pinacol ester **10** (40 mg, 0.16 mmol) in DMF-H2O (2:1, v/v) 6 mL, sodium carbonate (34 mg, 0.32 mmol) and $PdCl_2(PPh_3)_2$ (3 mg, 0.0032 mmol) were added and the reaction was heated at 90℃ for 9 hours under N_2. The reaction was then cooled to room temperature, poured into water and extracted in CH_2Cl_2. The organic layer was dried over $MgSO_4$, filtered and concentrated to obtain the crude product. The crude material was purified by column chromatography (hexane : EtOAc = 2:1, v/v) (30 mg, 54%). ^{1}H NMR (400 MHz, $CDCl_3$): δ (ppm) 7.46 (d, J = 9.1 Hz, 1H), 7.20 (d, J = 8.7Hz, 2H), 6.81 (d, J = 8.7 Hz, 2H), 6.63(dd, J = 9.1 Hz, 1H), 6.56(d, J = 2.6 Hz,

1H), 3.44 (q, J = 7.1 Hz, 4H), 3.01 (s, 6H), 2.29 (s, 3H) 1.24 (t, J = 7.1 Hz, 6H). ^{13}C NMR (100 MHz, $CDCl_3$): δ (ppm) 162.52, 154.89, 149.89, 149.88, 147.44, 131.27, 125.95, 123.06, 121.38, 112.17, 109.95, 108.48, 97.57, 44.73, 40.54, 16.38, 12.50. HRMS (ESI) calcd. for $C_{22}H_{26}N_2O_2$ $[M+H]^+$; 351.2067 found 351.2072, Mp:152-156℃, IR(cm^{-1}) (KBr) 1069, 1143, 1191, 1273, 1355, 1414, 1528, 1587, 1619, 1706, 2896, 2972.

7-(Diethylamino)-4-(hydroxymethyl) coumarin (14)

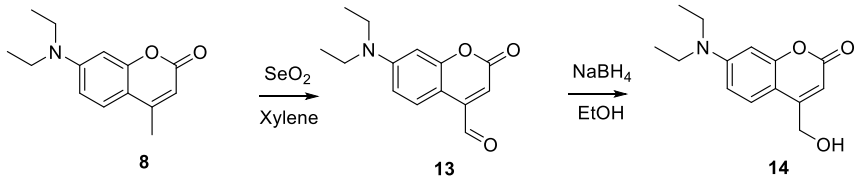

Selenium dioxide (414 mg, 3.7 mmol) was added to a solution of 7-(diethylamino)-4-methylcoumarin **8** (570 mg, 2.5 mmol) in xylene (70 mL). The solution was refluxed for 24h. After cooled to room temperature, filtered through celite and evaporated. Ethanol (100 mL) and sodium borohydride (46 mg, 1.2 mmol) were added and the mixture was stirred for 4h. The solution was neutralized with 1M HCl and extracted three times with CH_2Cl_2, dried over $MgSO_4$ and evaporated. The brown residue was purified by column chromatography (CH_2Cl_2 : EtOAc = 4:1, v/v) to afford **14** (300 mg, 49%) ^1H NMR (400 MHz, $CDCl_3$): δ (ppm) 7.33 (d, J = 8.8 Hz, 1H), 6.58 (dd, J = 8.8 Hz, 1H), 6.52 (d, J = 2.6 Hz, 1H), 6.28 (s), 4.85(s, 2H) 3.42 (q, J = 7.1 Hz, 4H), 2.21(s, 1H), 1.23 (t, J = 7.1 Hz, 6H)

7-(Diethylamino)-4-[[[(1,1-dimethylethyl)dimethylsilyl]oxy]methyl] coumarin (15)

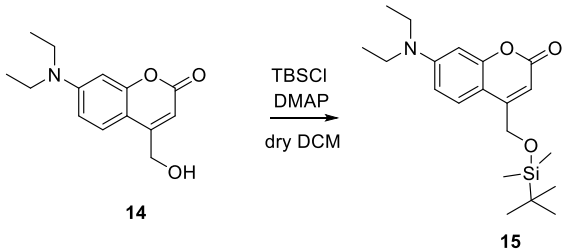

To a solution of 7-(diethylamino)-4-(hydroxymethyl) coumarin **14** (382 mg, 1.5 mmol) in dry DCM (30 mL), TBSCl (283 mg, 1.88 mmol) and DMAP (55 mg,

0.45 mmol) were added before treated with trimethylamine. The solution was stirred at room temperature for 3h and then quenched by satured NH_4Claq, extracted with DCM. The combined organics were dried over $MgSO_4$, evaporated to afford crude material. The crude was purified by column chromatography (hexane : EtOAc = 4:1, v/v) to give **15** (505 mg, 90%). ^1H NMR (400 MHz, $CDCl_3$): δ (ppm) 7.27 (d, J = 8.8 Hz, 1H), 6.57 (dd, J = 8.8 Hz, 1H), 6.54 (d, J = 2.6 Hz, 1H), 6.31 (s, 1H), 4.84(s, 2H) 3.43 (q, J = 7.1 Hz, 4H), 1.22 (t, J = 7.1 Hz, 6H), 0.98 (s, 9H), 0.16 (s, 6H).

7-(Diethylamino)-4-[[[(1,1-dimethylethyl)dimethylsilyl]oxy]methyl]-3-bromo coumarin (16)

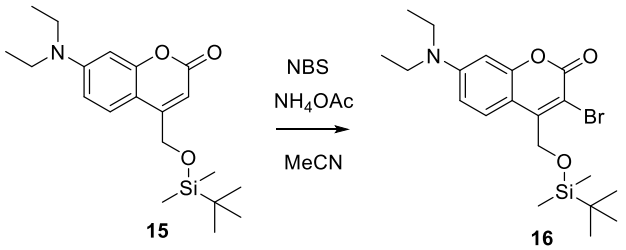

To a solution of 7-(diethylamino)-4-[[[(1,1-dimethylethyl)dimethylsilyl]oxy] methyl]coumarin **15** (195 mg, 0.54 mmol) and NBS (105 mg, 0.59 mmol) in MeCN (4 mL) was added NH_4OAc (5 mg, 0.054 mmol), stirred at room temperature for 1h. After addition of water, the mixture was extracted with EtOAc, dried over $MgSO_4$, filtered and evaporated to obtain crude material. The crude was The crude material was purified by column chromatography (hexane : EtOAc = 2:1, v/v) (157 mg, 66%). ^1H NMR (400 MHz, $CDCl_3$): δ (ppm) 7.78 (d, J = 9.2 Hz, 1H), 6.64 (dd, J = 9.2 Hz, 1H), 6.50 (d, J = 2.6 Hz, 1H), 5.02 (s, 2H), 3.44 (q, J=7.1Hz, 4H), 1.23 (t, J = 7.1 Hz, 6H), 0.92 (s, 9H), 0.16 (s, 6H).

7-(Diethylamino)-4-[[[(1,1-dimethylethyl)dimethylsilyl]oxy]methyl]-3-(4-dimethylaminophenyl)coumarin (17)

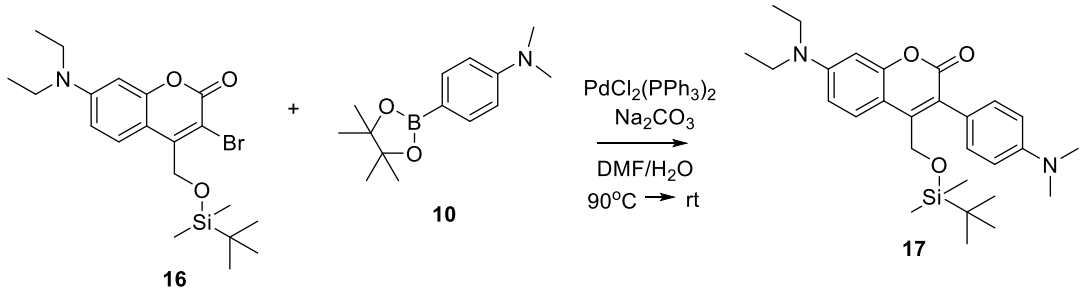

To a solution of 7-(diethylamino)-4-[[[(1,1-dimethylethyl)dimethylsilyl]oxy]methyl]-3-bromocoumarin **16** (206 mg, 0.47 mmol) and N,N'-dimethylaminophenyl boronic acid pinacol ester **10** (116 mg, 0.47 mmol) in DMF-H_2O (2:1, v/v) 6 mL, sodium carbonate (99 mg, 0.94 mmol) and $PdCl_2(PPh_3)_2$ (7 mg, 0.0094 mmol) were added and the reaction was heated at 90℃ for 9 hours under N_2. The reaction was then cooled to room temperature, poured into water and extracted in CH_2Cl_2. The organic layer was dried over MgSO4, filtered and concentrated to obtain the crude product. The crude material was purified by column chromatography (hexane : EtOAc = 2:1, v/v) (206 mg, 92%). ^{1}H NMR (400 MHz, $CDCl_3$): δ (ppm) 7.70 (d, J = 9.1 Hz, 1H), 7.26 (d, J = 8.7Hz, 2H), 6.78 (d, J = 8.7Hz, 2H), 6.63(dd, J = 9.1 Hz, 1H), 6.55(d, J = 2.6 Hz , 1H), 4.66 (s, 2H), 3.44 (q, J = 7.1 Hz, 4H), 3.01 (s, 6H), 1.24 (t, J = 7.1 Hz, 6H), 0.90 (s, 9H), 0.04 (s, 6H). ^{13}C NMR (100 MHz, $CDCl_3$): δ (ppm) 162.93, 155.46, 150.24, 149.77, 147.26, 131.37, 127.27, 122.05, 121.74, 112.03, 108.86, 108.51, 97.48, 60.29, 44.68, 40.54, 25.82, 18.23, 12.52, -5.35 HRMS (ESI) calcd. for $C_{28}H_{40}N_2O_3Si$ $[M+H]^+$; 481.2879 found 481.2881, Mp:70-75℃, IR(cm^{-1}) (KBr) 754, 779, 836, 939, 1057, 1145, 1193, 1276, 1359, 1408, 1525, 1590, 1618, 1715, 2856, 2927.

7-(Diethylamino)-4-(hydroxymethyl)-3-(4-dimethylaminophenyl)coumarin (18)

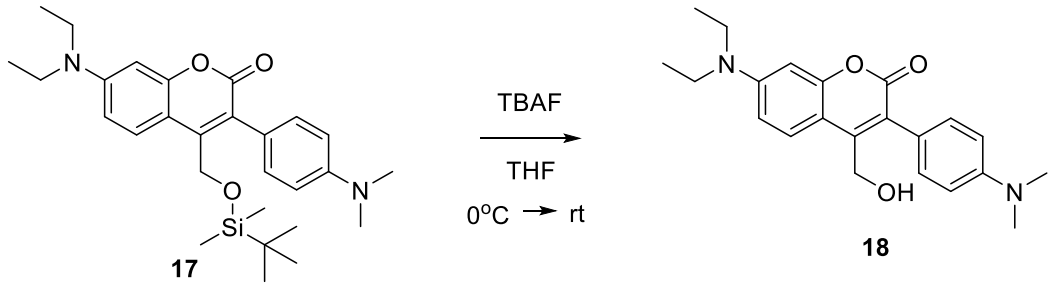

To a solution of 7-(diethylamino)-4-[[[(1,1-dimethylethyl)dimethylsilyl]oxy]methyl]-3-(4-dimethylaminophenyl)coumarin **17** (130 mg, 0.026 mmol) in THF (15 mL) was added tetrabutylammonium fluoride (1M in THF) (0.54 ml, 0.54 mmol). The reaction was stirred for 30 minutes, quenched with sat. NH_4Cl and extracted with EtOAc. The combined organics were dried over $MgSO_4$, filtered and concentrated to obtain the crude product. The crude material was then purified by column chromatography (hexane : EtOAc = 2:1, v/v) (40 mg, 40%). ^{1}H NMR (400 MHz, acetone-d_6): δ (ppm) 7.84 (d, J = 9.1 Hz, 1H), 7.25 (d, J = 8.9 Hz, 2H), 6.78 (d, J = 8.9 Hz, 2H), 6.75(dd, J = 9.0 Hz, 1H), 6.52(d, J = 2.6 Hz , 1H), 4.63 (d, J = 5.3 Hz, 2H), 4.36 (t, J = 5.2 Hz, 1H) 3.53 (q, J = 7.0Hz, 4H), 2.99 (s, 6H) 1.24 (t, J = 7.0 Hz, 6H).^{13}C NMR (100 MHz, DMSO-d_6): δ (ppm) 162.04, 155.38, 150.21, 150.05, 148.63, 131.67, 128.22, 122.17, 120.90, 111.94, 109.17, 108.37, 96.93, 58.35, 40.53, 12.84. HRMS (ESI) calcd. for $C_{22}H_{26}N_2O_3$ $[M+H]^+$; 367.2016 found 367.2019, Mp:232-235℃, IR(cm^{-1}) (KBr) 804, 819, 1069, 1141, 1274, 1363, 1410, 1528, 1588, 1617, 1685, 2931, 3422.

7-(Diethylamino)-4-[(benzoyloxy)methyl]-3-(4-dimethylaminophenyl) coumarin (19)

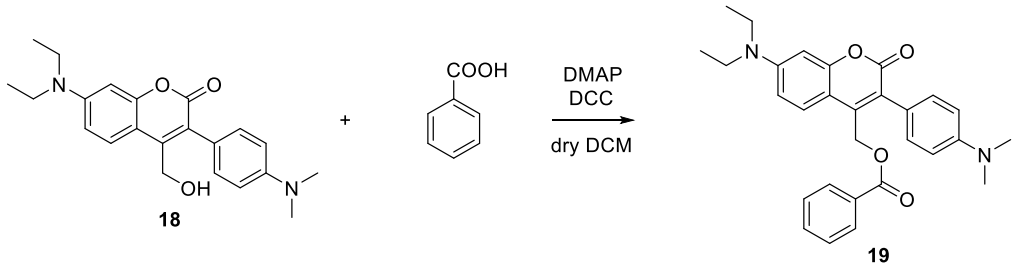

To a solution of 7-(diethylamino)-4-(hydroxymethyl)-3-(4-dimethylaminophenyl)coumarin **18** (30 mg, 0.082 mmol) and benzoic acid (10 mg, 0.082 mg) in dry DCM (4 ml) was added DMAP (1 mg, 0.0082 mmol) and stirred for 10 min. DCC (17 mg, 0.082 mmol) was added and the mixture was stirred at room temperature for 12 hours in the dark. The reaction was then poured into water and extracted in CH_2Cl_2. The organic layer was dried over $MgSO_4$, filtered and concentrated to obtain the crude product. The crude material was purified by column chromatography (hexane : EtOAc = 2:1, v/v) (33 mg, 86%). ^{1}H NMR (400 MHz, $CDCl_3$): δ (ppm) 8.06 (dd, J = 7.4 Hz, 2H), 7.60 (td, J = 7.4 Hz, 1H), 7.48 (d, J = 8.9 Hz, 2H), 7.46 (t, J = 7.4 Hz, 2H), 7.29 (d, J = 8.9 Hz, 2H), 6.60 (dd, J = 8.9 Hz, 1H) 6.59 (s, 1H), 5.35 (s, 2H), 3.43 (q, J=7.1Hz, 4H) 2.99 (s, 6H) 1.23 (t, J=7.1Hz, 6H). ^{13}C NMR (100 MHz, CDCl3): δ (ppm) 166.02, 162.43, 155.37, 150.01, 142.46, 133.26, 131.22, 129.82, 128.55, 128.48, 126.10, 124.39, 121.22, 112.08, 108.94, 108.31, 97.67, 61.37, 44.74, 40.39, 12.49. HRMS (ESI) calcd. for $C_{29}H_{30}N_2O_4$ $[M+H]^+$; 471.2277 found 471.2278, Mp:192-195℃, IR(cm^{-1}) (KBr) 713, 821, 1029, 1069, 1110, 1144, 1193, 1271, 1355, 1416, 1528, 1591, 1619, 1720, 2906, 2979.

7-(Diethylamino)-4-carboxaldehyde-3-(4-dimethylaminophenyl)coumarin (20)

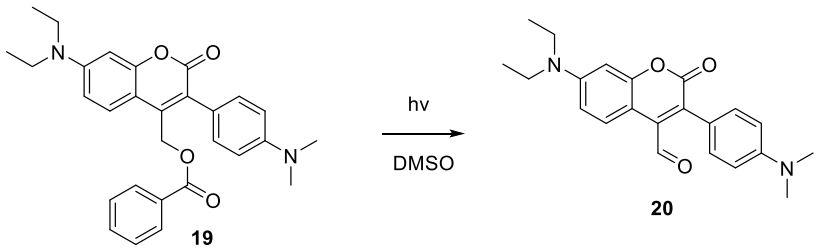

The solution of 7-(diethylamino) -4-[(benzoyloxy)methyl]-3-(4-dimethylaminophenyl)coumarin **19** (11 mg, 0.023 mmol) in DMSO (3 ml) was irradiated for 1 hour with vigorous stirring. The reaction was then poured into water and extracted in CH_2Cl_2. The organic layer was dried over $MgSO_4$, filtered and concentrated to obtain the crude product. The crude material was purified by column chromatography (hexane : EtOAc = 2:1, v/v) and GPC (6 mg, 70%).
^{1}H NMR (400 MHz, acetone-d_6): δ (ppm) 9.71 (s, 1H), 8.10 (d, J = 9.1 Hz, 1H), 7.31 (d, J = 8.9 Hz, 2H), 6.83 (d, J = 8.9 Hz, 2H), 6.77 (dd, J = 9.0 Hz, 1H), 6.58 (d, J = 2.6 Hz , 1H), 3.54 (q, J = 7.0 Hz, 4H), 3.06 (s, 6H) 1.24 (t, J = 7.0Hz, 6H).
^{13}C NMR (100 MHz, acetone-d_6): δ (ppm) 192.86, 161.62, 155.69, 151.30, 150.17, 138.96, 132.78, 127.15, 126.94, 118.95, 111.22, 109.21, 104.71, 97.13, 44.27, 39.35, 11.89. HRMS (ESI) calcd. for $C_{22}H_{24}N_2O_3$ $[M+H]^+$; 365.1859 found 365.1859, Mp:160-163℃, IR(cm^{-1}) (KBr) 802, 816, 1058, 1142, 1191, 1274, 1358, 1413, 1528, 1615, 1685, 1718, 2851, 2922, 2966.

3-12. Supplementary Material

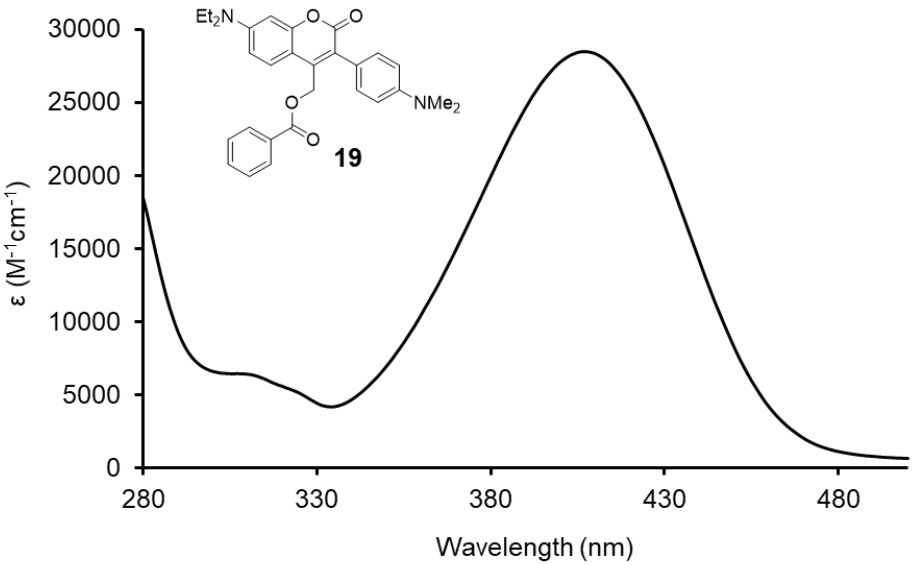

Figure S15. UV-visible absorption spectrum of compound **19** in DMSO.

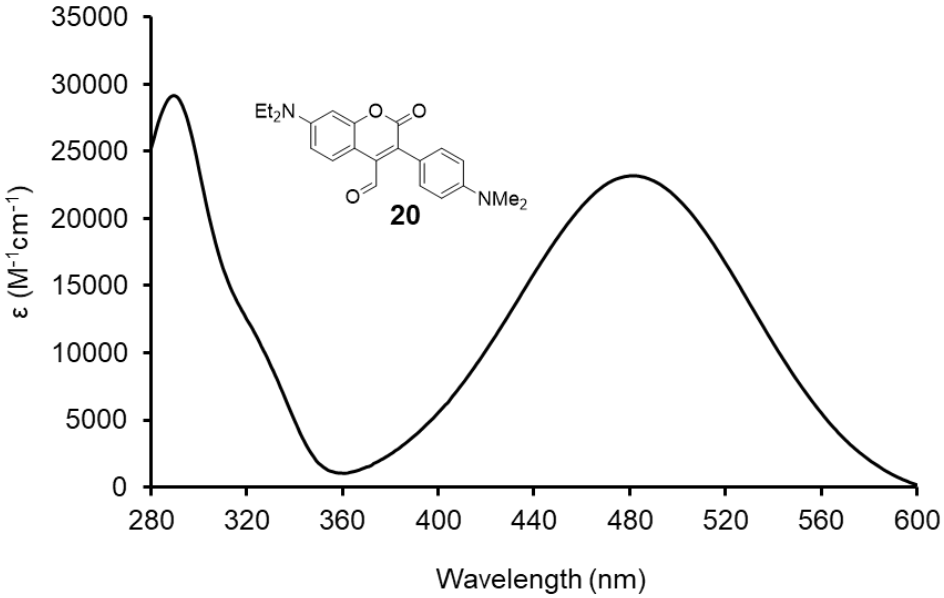

Figure S16. UV-visible absorption spectrum of compound **20** in DMSO.

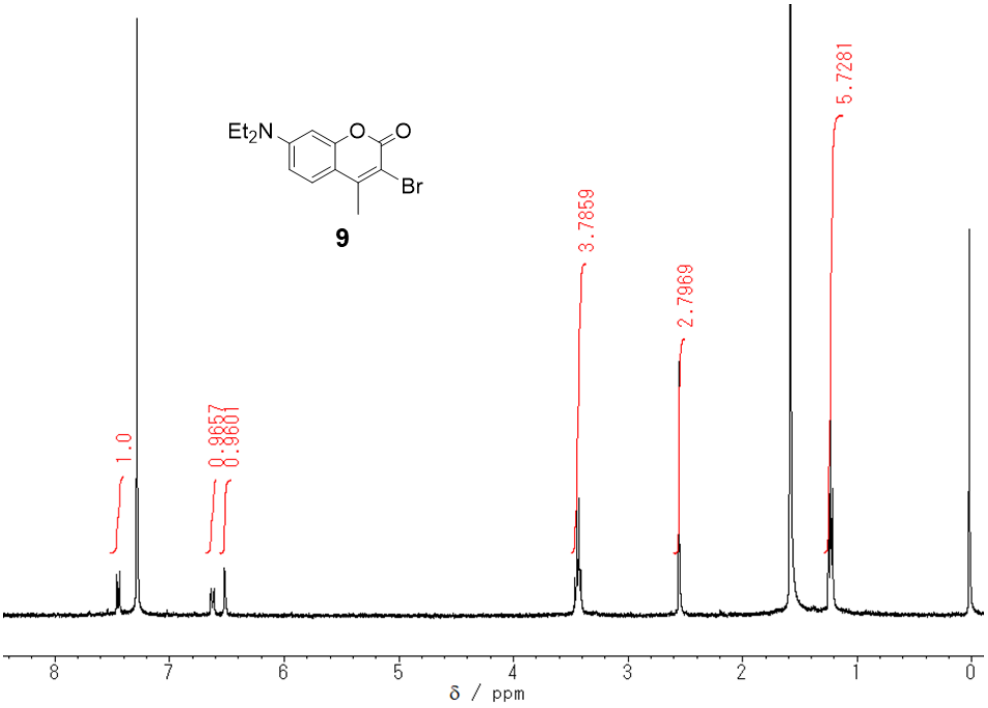

Figure S17. ^{1}H NMR of compound **9** (400 MHz, $CDCl_3$).

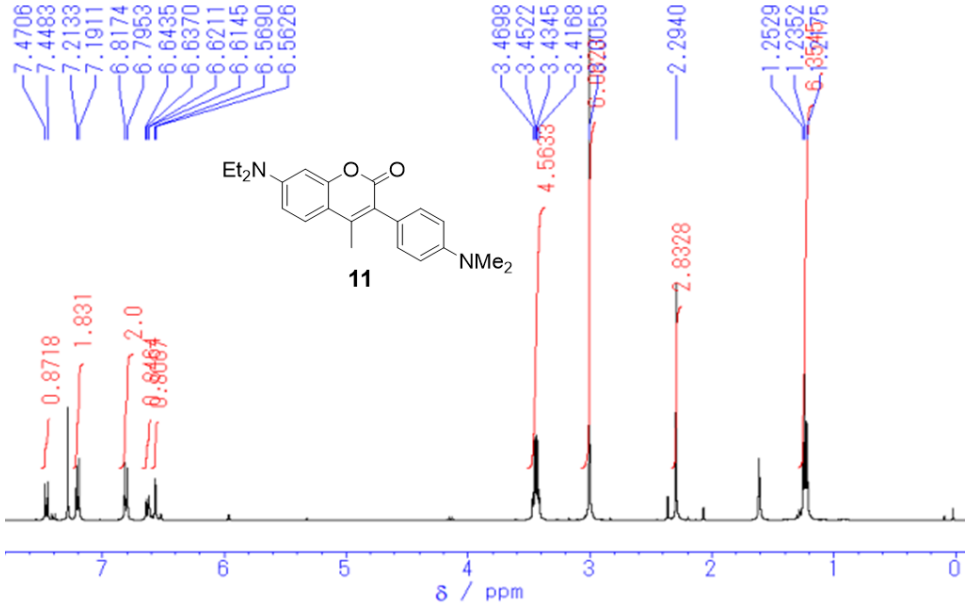

Figure S18. ^{1}H NMR of compound **11** (400 MHz, $CDCl_3$).

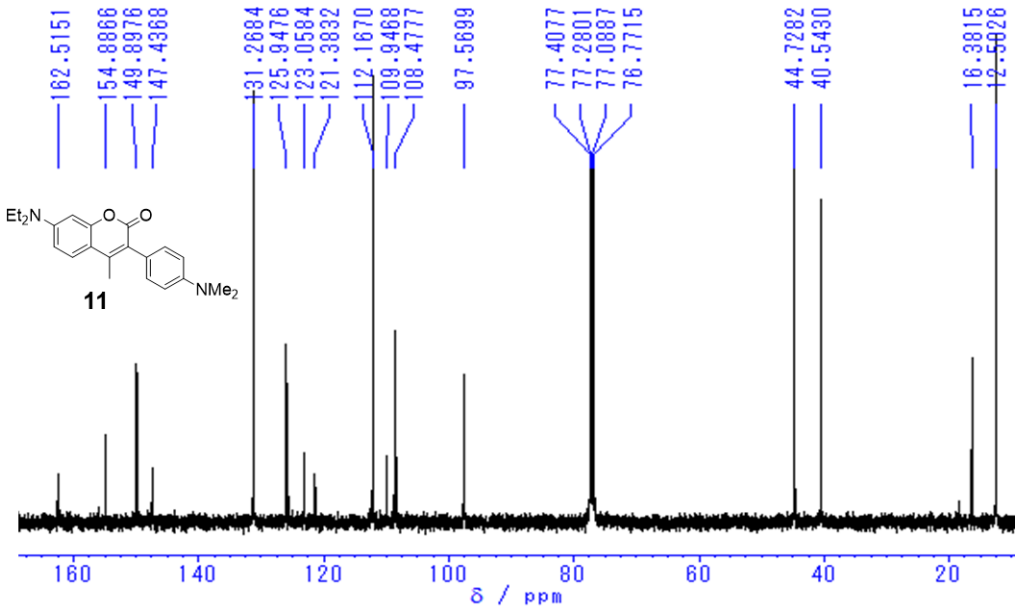

Figure S19. ^{13}C NMR of compound **11** (100 MHz, $CDCl_3$).

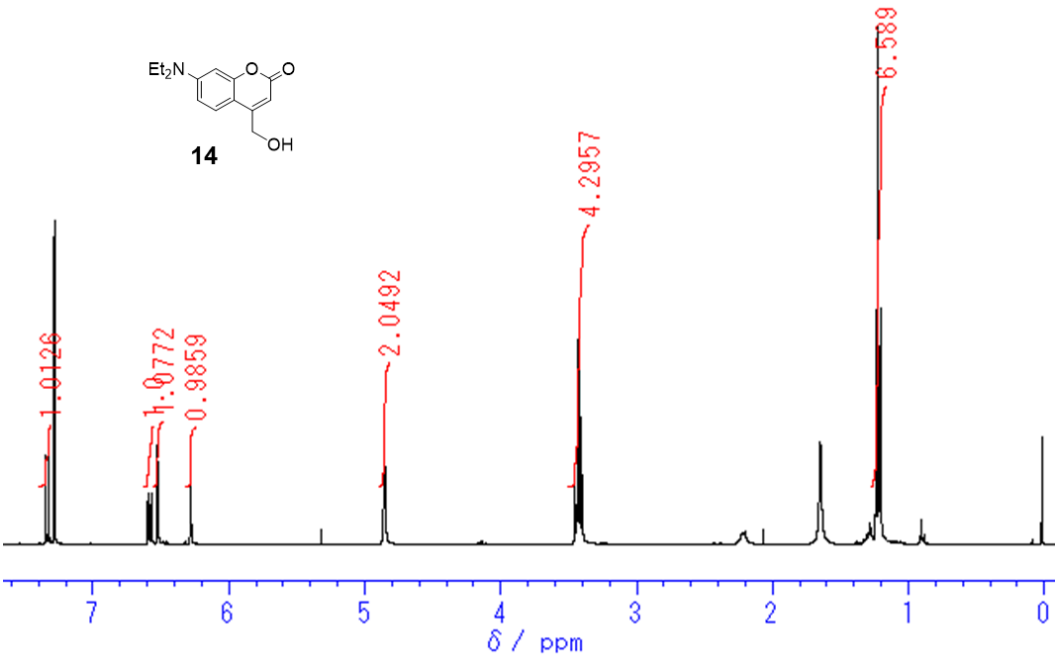

Figure S20. ^{1}H NMR of compound **14** (400 MHz, $CDCl_3$).

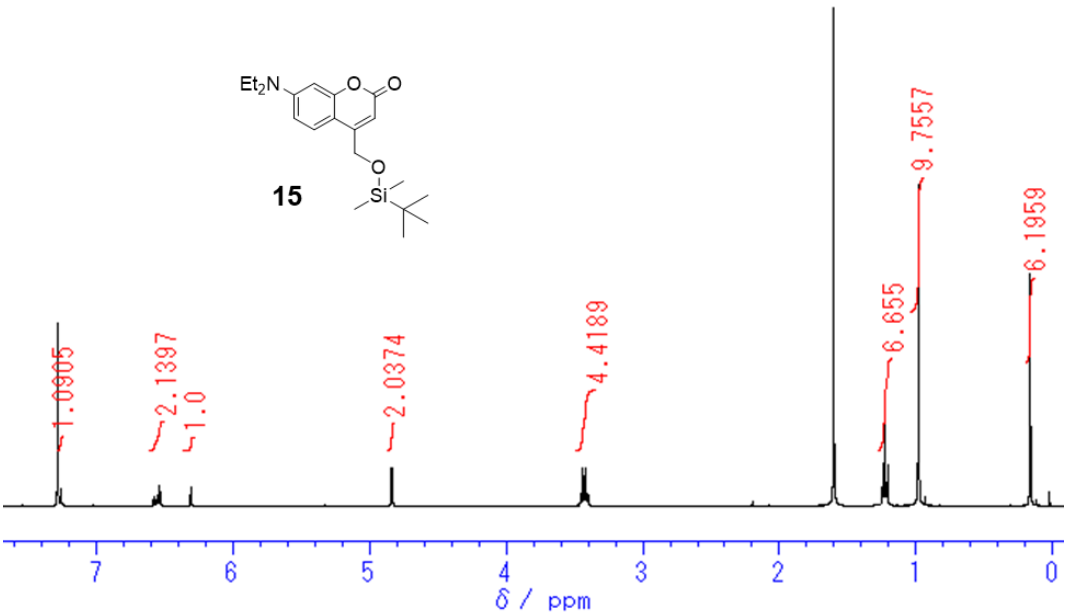

Figure S21. ^{1}H NMR of compound **15** (400 MHz, $CDCl_3$).

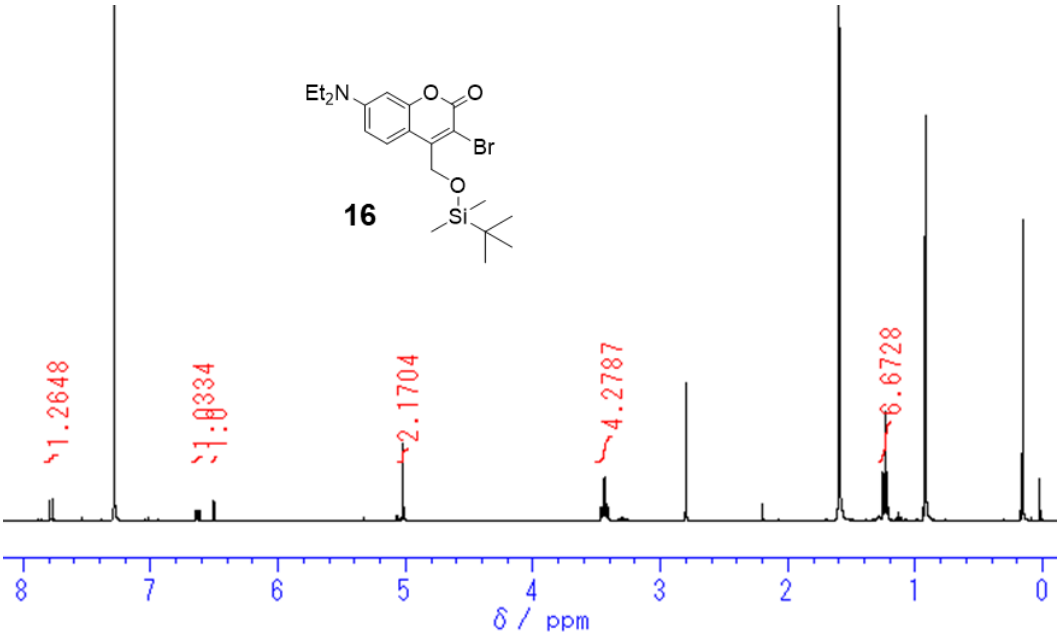

Figure S22. ^{1}H NMR of compound **16** (400 MHz, $CDCl_3$).

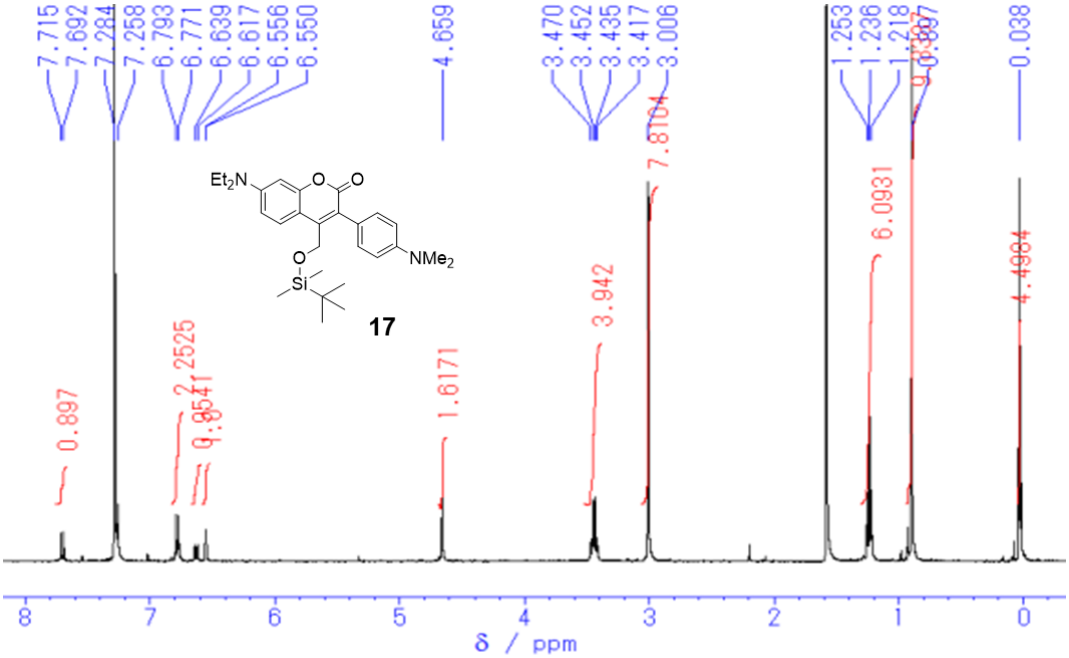

Figure S23. ^{1}H NMR of compound **17** (400 MHz, $CDCl_3$).

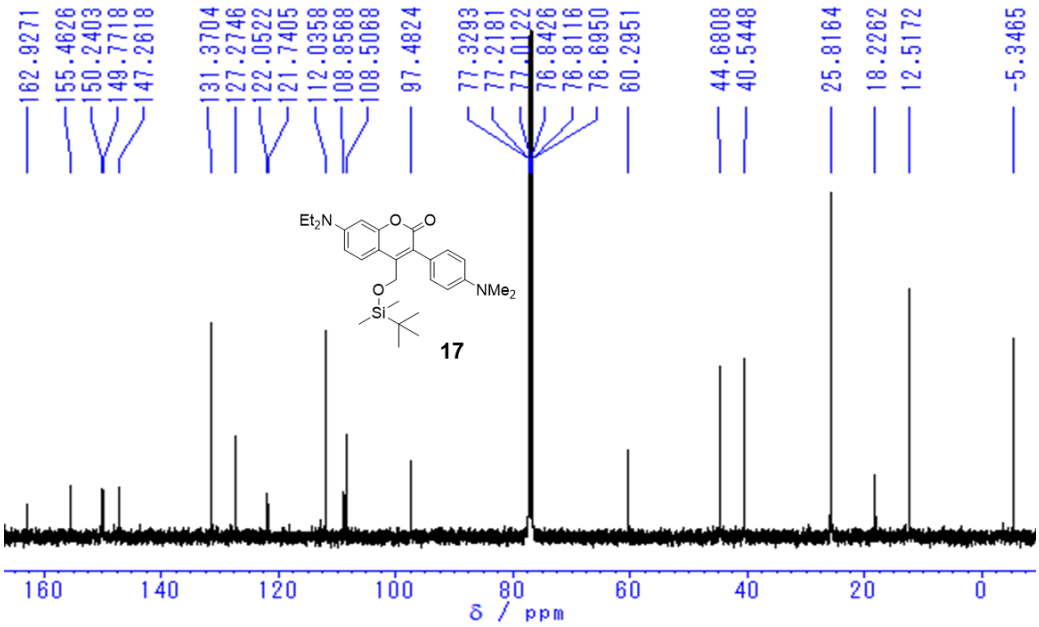

Figure S24. ^{13}C NMR of compound **17** (100 MHz, $CDCl_3$).

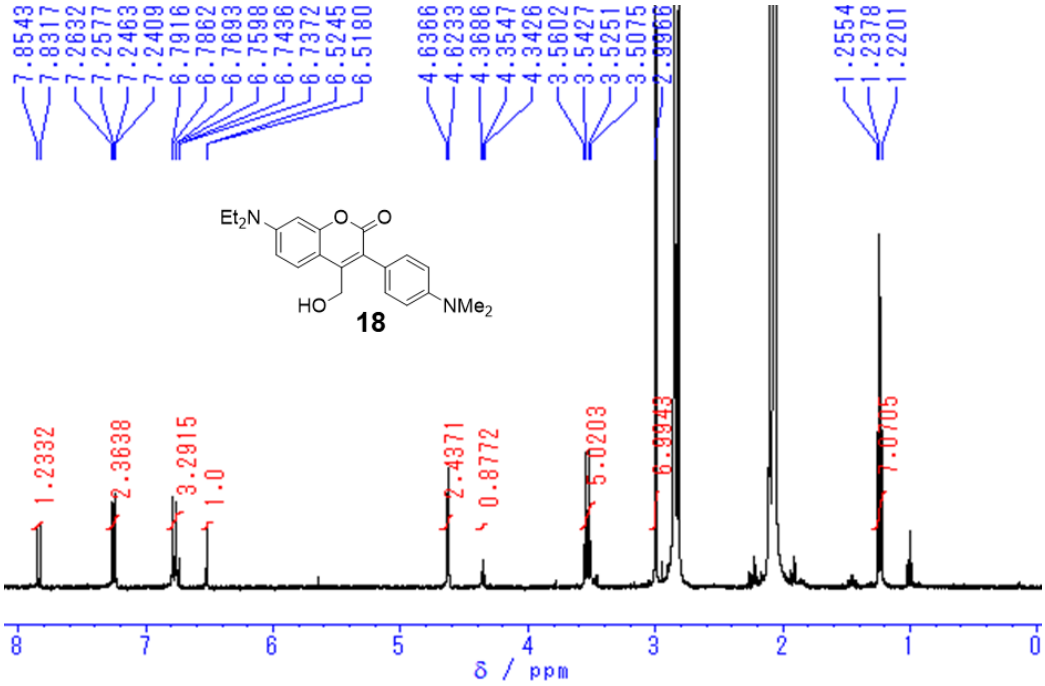

Figure S25. ^{1}H NMR of compound **18** (400 MHz, acetone-d_6).

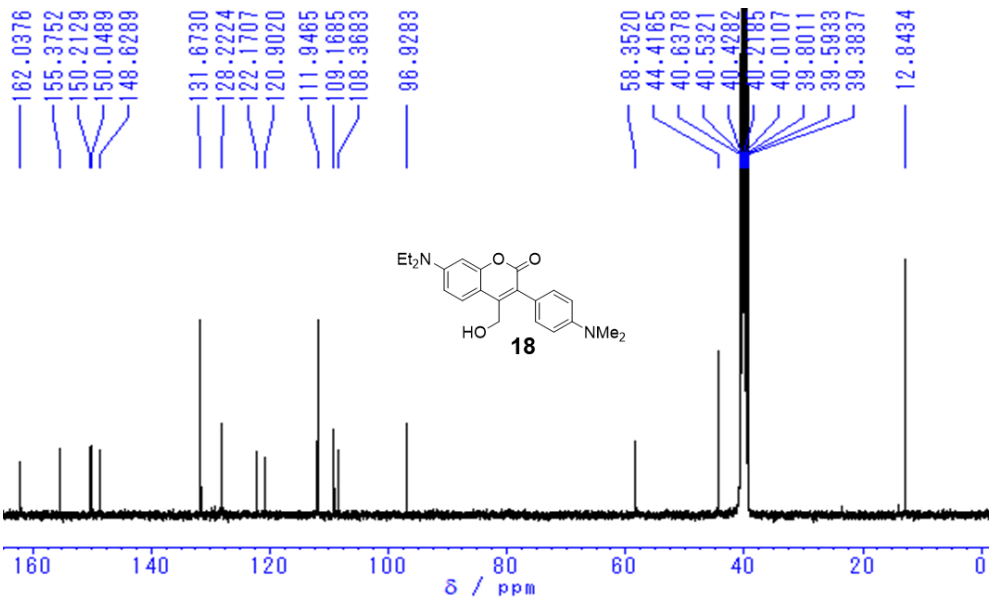

Figure S26. ^{13}C NMR of compound **18** (100 MHz, DMSO-d_6).

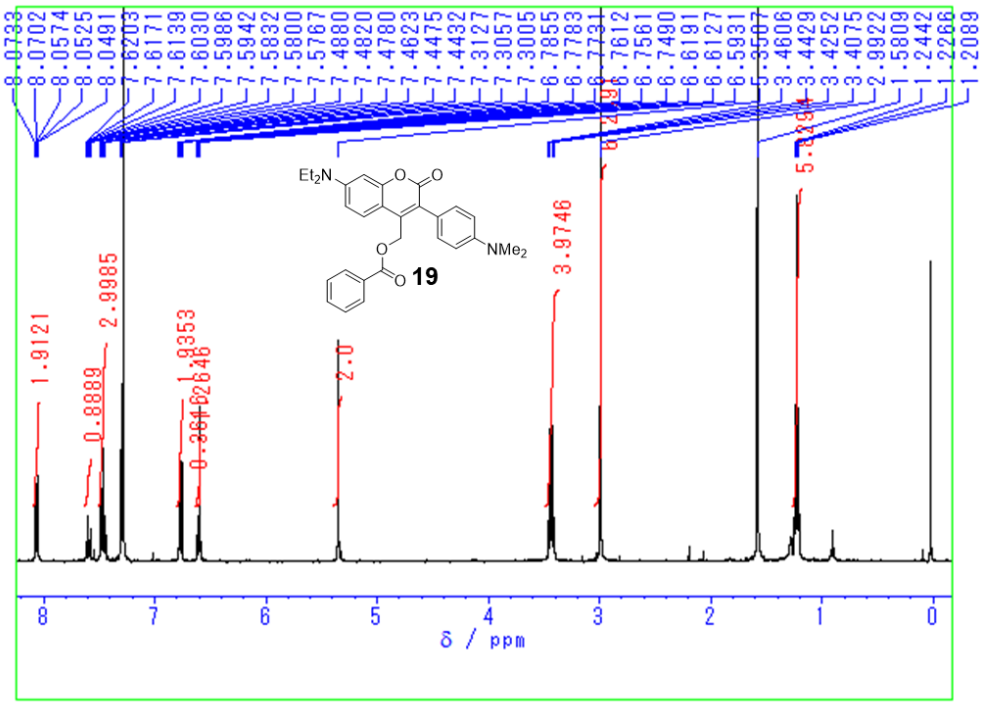

Figure S27. ^{1}H NMR of compound **19** (400 MHz, $CDCl_3$).

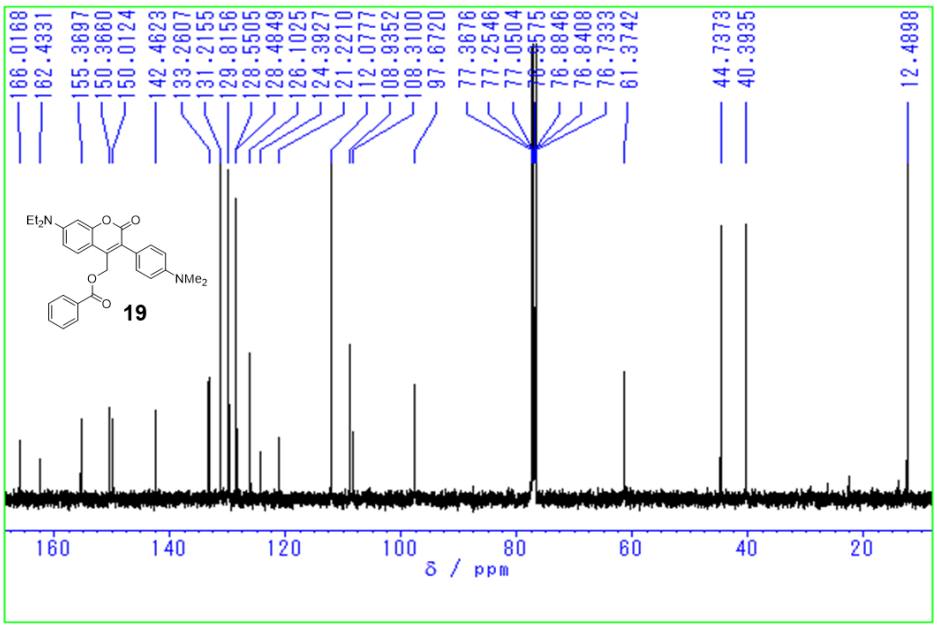

Figure S28. ^{13}C NMR of compound **19** (100 MHz, $CDCl_3$).

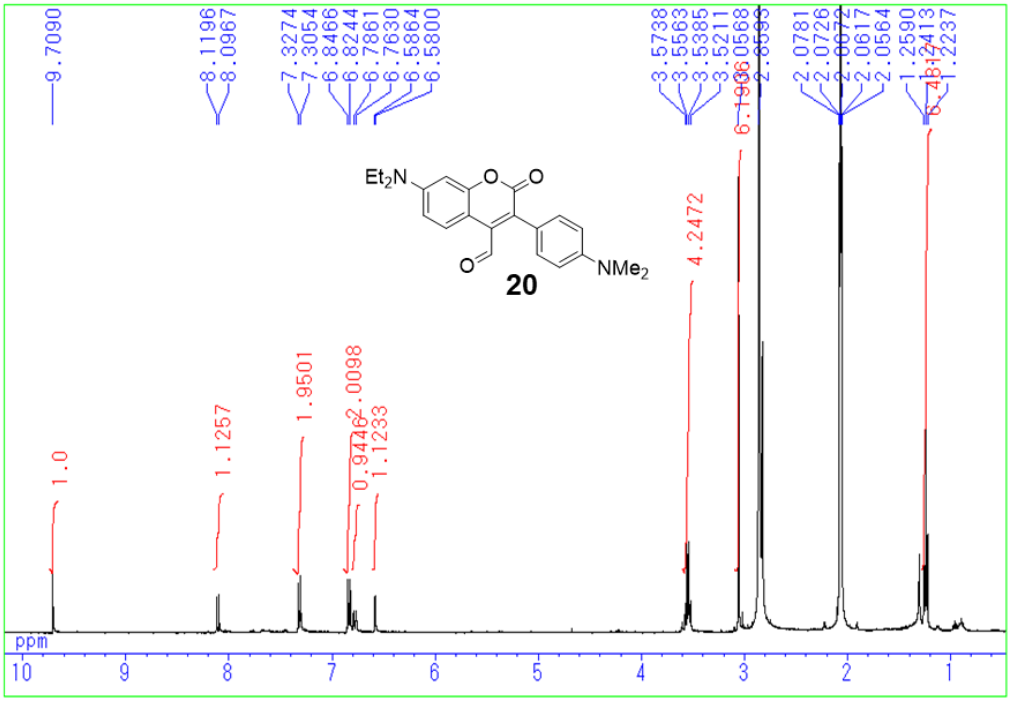

Figure S29. ^{1}H NMR of compound **20** (400 MHz, acetone-d_6).

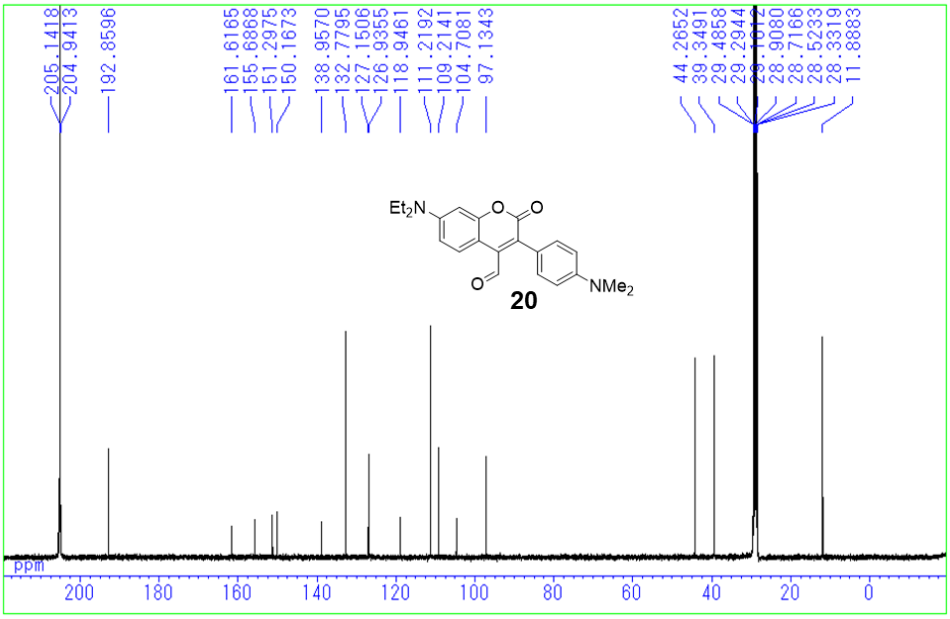

Figure S30. ^{13}C NMR of compound **20** (100 MHz, acetone-d_6).

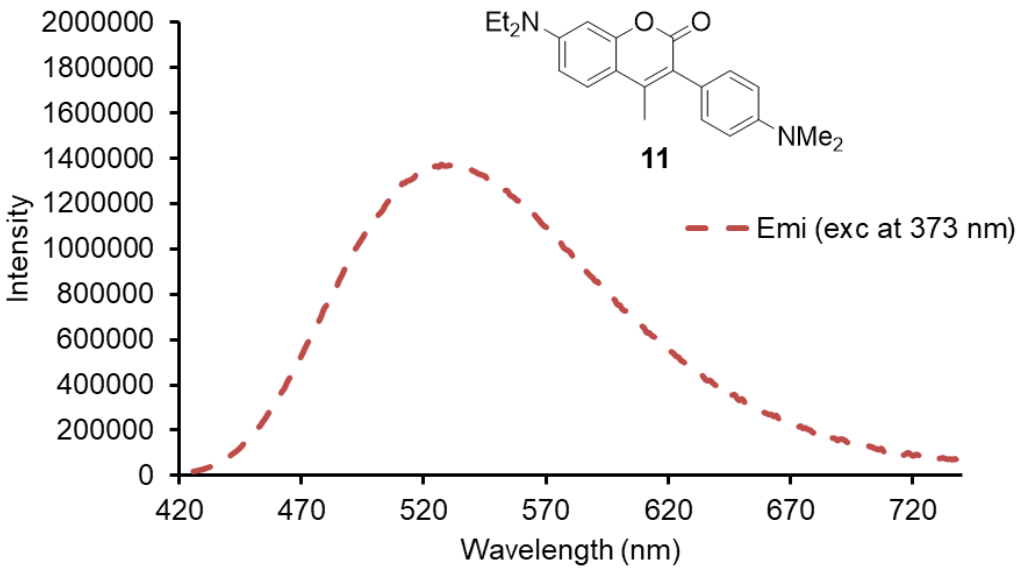

Figure S31. Fluorescence spectrum of compound **11** in DMSO (λ_{exc} = 373 nm).

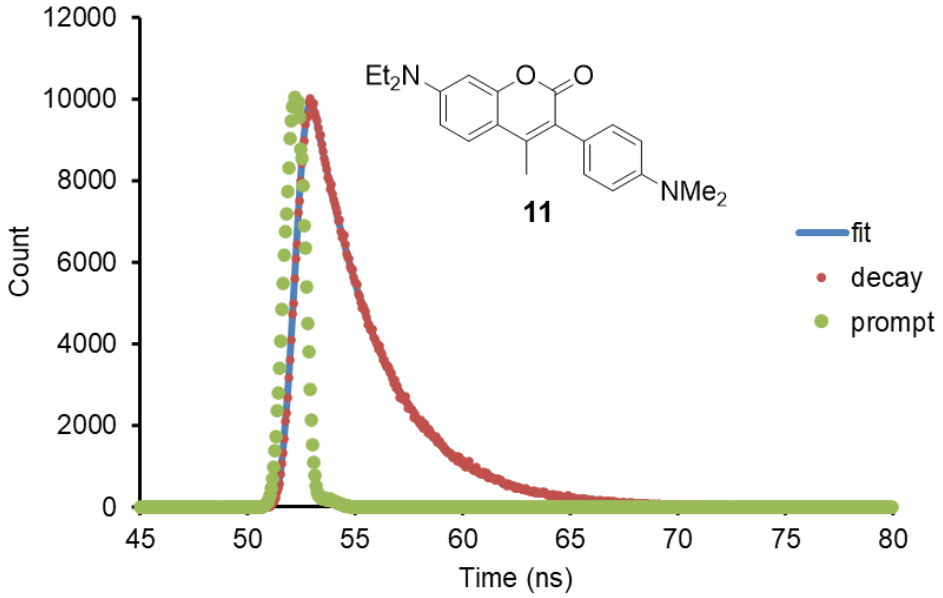

Figure S32. Fluorescence decay of compound **11** in DMSO (λ_{exc} = 390 nm, λ_{mon} = 540 nm).

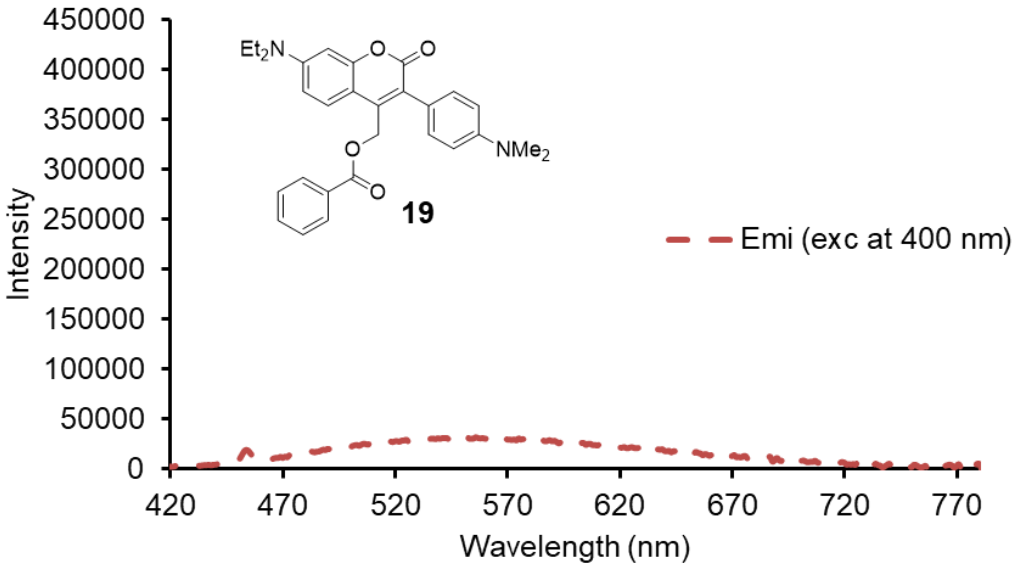

Figure S33. Fluorescence spectrum of compound **19** in DMSO (λ_{exc} = 400 nm).

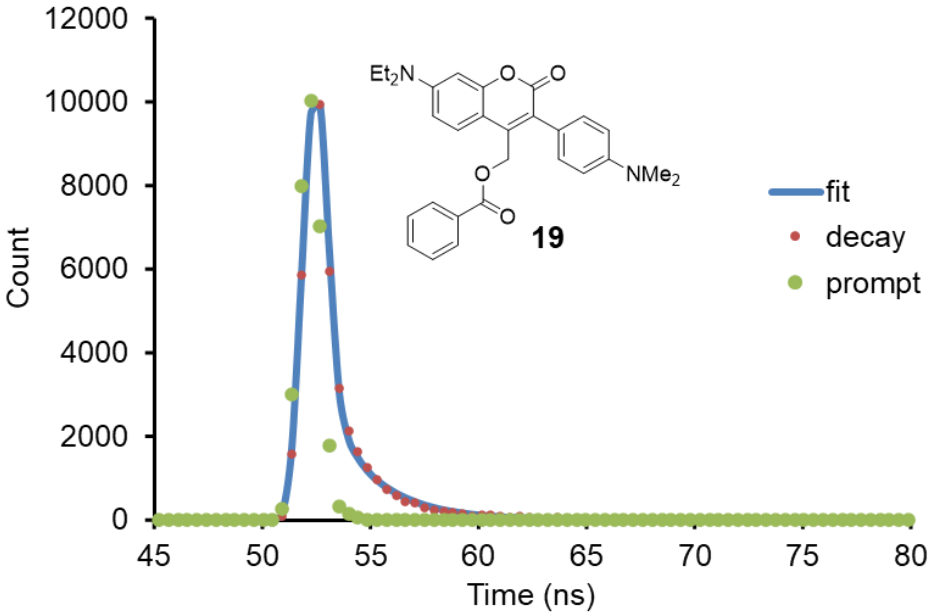

Figure S34. Fluorescence decay of compound **19** in DMSO (λ_{exc} = 390 nm, λ_{mon} = 550 nm).

Chemical actinometer for quantum yield measurement:

The rate of photoreaction of caged benzoate **19** can be quantified by quantum yield (ϕ).

$$\Phi = \frac{\text{number of reacted molecules per time unit}}{\text{number of photons absorbed per time unit}}$$

In this study, ferrioxalate was used as a chemical actinometer to measure photon fluxes. During the light irradiation, the potassium ferrioxalate gives three ion products as shown in the following equations.

$$Fe(C_2O_4)_3^{3+} \xrightarrow{h\nu} Fe^{2+} + C_2O_4^{-} + 2C_2O_4^{2-}$$

$$Fe^{2+} + 3phen \longrightarrow Fe(phen)_3^{2+}$$

The number of ferrous ions that were released by photoreaction is measured by the reaction of ferric ion with phenanthroline to afford the colored tris-phenanthroline compound which has peculiar absorption at 510 nm ($\varepsilon = 11100\ M^{-1}\ cm^{-1}$).

Caged benzoate **19** has absorption maxima around 400 nm. Therefore, we measured the light quantities at 400 nm using a xenon lamp with a monochromator as a light source. The equation is shown as below,

$$I(\text{mol/s}) = \frac{\text{moles of } Fe^{2+}}{\Phi_\lambda \times t \times F} = \frac{V_1 \times V_3 \times \Delta A(510\text{ nm})}{10^3 \times V_2 \times l \times \varepsilon(510\text{ nm}) \times \Phi_\lambda \times t}$$

V_1: the irradiated volume (mL)

V_2: the aliquot of the irradiated solution taken for the determination of the ferrous ions (mL)

V_3: the final volume (mL)

ΔA: the optical difference in absorbance between the irradiated solution and that taken in the dark

l: optical pathlength of the irradiation cell

ε (510 nm): ε of the complex $Fe(phen)_3^{2+}$
Φ_λ: the quantum yield of ferrous ion production at the irradiation wavelength
t: the irradiation time
F: mean function of light absorbed by the ferrioxalate solution

Procedure for measurement:
1) 117.7 mg of $K_3[Fe(C_2O_4)_3] \cdot 3H_2O$ was dissolved in 20 mL of 0.05 M H_2SO_4. (0.012 M Ferrioxalate was prepared)- solution A
2) 10.2 mg of 1,10-phenanthroline monohydrate and 2.25 gm of $CH_3COONa \cdot 3H_2O$ were dissolved in 10 mL of 0.5 M H_2SO_4- solution B
3) To a 3 mL solution A irradiated at 360 nm for 0, 10, 20 and 30 seconds, 0.5 mL of solution B was added. The absorption spectrum of each solution was measured to monitor the change in absorbance at 510 nm. The determined ΔA was used to calculate the light quantity.

The number of photons from Xe-lamp at 400 nm was determined to be I_{400} = 8.702×10^{-7} mol/min. (This value was obtained in previous work in our laboratory)

Procedure for Measurement:
Solution of **19** (0.48 mM in DMSO) was taken in a cell. Light irradiation was performed using a xenon lamp at 400 nm under ambient atmosphere and the reaction solution after irradiation was injected into HPLC and analyzed. Based on the integral value of peak area before and after light irradiation, the reaction rate was calculated using the following equation.
Reaction rate (%) = (integral value before light irradiation - integral value after light irradiation) ÷ integral value before light irradiation × 100.
The photoreaction quantum yield was calculated using the following equation,
Quantum yield Φ = number of molecules reacted by light irradiation (mol) ÷ amount of light absorbed by the compound (mol).

(HPLC condition)
Solvent : CH_3CN
Intersil ODS-3 5μm 4.6×250 mm

flow : 1.3 mL/min, press : 4.2 MPa, detect : 300 nm, range : 0.16

Computational details and additional results

We used density functional theory (DFT) and time-dependent (TD) DFT approaches, as implemented in the Gaussian 03 and 09 packages [1,2], to model the two chromophores of interest (Figure S35). Calculations have been performed in vacuum and were limited to properties related to the ground state geometry: geometry optimization, one and two-photon absorption related to the electronically excited states (ES). Optical spectra were obtained employing the density matrix formalism for non-linear optical responses as proposed by S. Tretiak and V. Chernyak [3,4]. One-photon absorption (OPA) and two-photon absorption (TPA) spectra were computed at the TD-B3LYP/6-31G(d)//B3LYP/6-31G(d) level of theory in conventional quantum chemical notation "single point//optimization level", including up to 20 singlet ES. This level of theory has been shown to provide good predictions for structure-TPA relationships [4-7]. The damping factor introduced to simulate the finite linewidth in the resonant spectra has been fixed to Γ=0.10 eV [4], except for a few points needed to extrapolate the experimental data at higher wavelengths (Table S4).

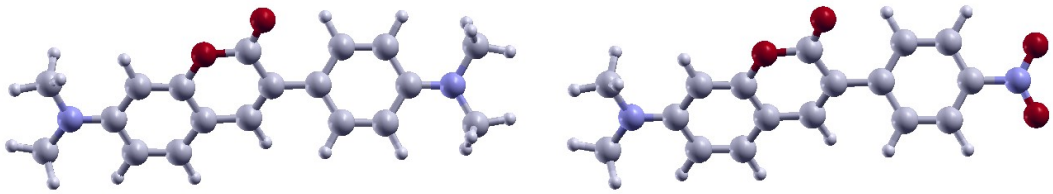

Figure S35. Optimized geometries of the compounds investigated in this work. (left) **D-π-D** coumarin derivative **12a** and (right) coumarin having a **D-π-A** character **12b**.

The ES structure was further checked for all chromophores at the TD-ωB97XD/6-31G(d)//B3LYP/6-31G(d) level, especially to check for possible spurious charge transfer states. In order to gauge the accuracy of our TD-B3LYP computed optical spectra, we have computed transition energies, state and

transition dipole moments at the TD-B3LYP and TD-ωB97XD levels of theory. First estimates of the TPA cross sections for push-pull chromophores may be obtained by using the two-level approximation, which is a standard approach. Within the two-level model, the TPA cross section σ_2 of a dipolar chromophore at the maximum ($\hbar\omega = \hbar\omega_{0i}/2$) reads [4]:

$$\sigma_2 = 2.0757 \times 10^{-3} \frac{\mu_{0i}^2(\mu_{ii}-\mu_{00})^2}{\Gamma} \text{(GM)} \quad (1)$$

where 0 and *i* label the ground and excited state of interest, respectively, and units of the input parameters are eV for Γ (vide supra) and Debye for dipole moments (μ_{ji}). For quadrupolar chromophores (push-push or pull-pull), one has to move to a three-state model considering an additional excited state (label *j*) and σ_2 at the maximum ($\hbar\omega = \hbar\omega_{0j}/2$) reads [4]:

$$\sigma_2 = \frac{2.0757\times10^{-3}}{4} \frac{\mu_{0i}^2\mu_{0j}^2}{\left(\omega_{0i} - {}^{\omega_{0j}}/_{2}\right)^2 \Gamma} \text{(GM)} \quad (2)$$

Noteworthy, these expressions highlight that σ_2 is inversely proportional to the average linewidth broadening parameter Γ, , which has been fixed arbitrarily 0.1 eV in our computations, except for a few points (Table S4).

For both chromophores of interest, the excited structure computed at the TD-B3LYP and TD-ωB97XD levels of theory agree, demonstrating the absence of low-lying spurious charge transfer states.

Computed TPA spectra are compared to the OPA spectra in Figure 15a and Figure 15b. Figure 15a reveals the quadrupolar nature (**D-π-D**) of the 7-dimethylamino-substituted coumarin (Figure S35, left), with low TPA responses for the first excited state for which the OPA response shows a clear maximum and a much larger TPA cross section related to the second excited state. This second band lies ~0.75 eV higher in energy, corresponding to a blue shift of the main TPA peak of about 80 nm. Its TPA amplitude is consistent with that derived from a three-state model (Table S3). Moreover, the two-state model significantly overestimates the TPA amplitude of the first band. Meanwhile, the value extracted from the model at the TD-ωB97XD level of theory (Table S3) shows

good qualitative agreement with the TPA cross-section obtained experimentally (Figure 19). This agreement becomes quantitative when extracting the linewidth broadening parameter Γ from the OPA spectra reported Figure 13 (compound **11**) and S15 (compound **19**). It corresponds to the half-width-at-half-maximum (HWHM) of a Lorentzian lineshape (see Ref. [4] for conversion factor between Lorentzian and Gaussian lineshapes) that is estimated to Γ = 0.2 eV. From equation (1), we deduce that the value is reduced by a factor of two, i.e. 5.5 GM, in nice agreement with the 5.6 GM measured experimentally at 680 nm from **11**.

Last, the marked difference between both levels of theory can be traced back to significant overestimation of the excited state dipole moment at the TD-B3LYP level.

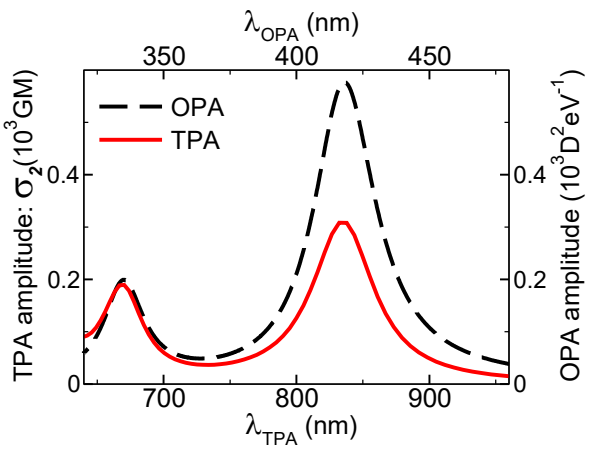

Figure S36. OPA (dashed lines) and TPA (straight lines) spectra of a D-π-A coumarin derivative **12b** (Figure S18, right) computed at the TD-B3LYP/6-31G(d)//B3LYP/6-31G(d) level of theory.

As expected, substitution of the dimethylamino group of the 4-(Dimethylamino)phenyl by a nitro group (Figure S35, right) leads to a chromophore with a clear dipolar nature, *i.e.* having a TPA maximum at twice the OPA maximum wavelength (Figure S36). This leads to an additional red-shift of the main TPA band, which shows up above 830 nm. For this **D-π-A** compound, the two-state model is in good agreement with the computed TPA amplitude at the maximum (Table S3). Such an agreement helps to further gauge effect of the level of theory on the TPA amplitudes. With ωB97XD, the TPA amplitude at the maximum is reduced by a factor of five, leading to a σ_2 of ~60 GM, which

remains sizeable as compared to other caged compounds already investigated.

Table S3. Calculated transition energies (ω_{0i} in eV), state and transition dipole moments (μ_{ij} in Debye) using the 6-31G(d) basis set and for geometries optimized at the B3LYP/6-31G(d) level of theory. The TPA cross section (σ_2 in GM) at the maximum is derived within the few-state models (Eq. (1) or (2)). Symbol *i* denotes the excited state of interest.

	TD-DFT functional	*i*	ω_{0i} (eV)	μ_{ii} (D) *x*	*y*	*z*	μ_{00} (D) *x*	*y*	*z*	μ_{0i} (D) *x*	*y*	*z*	σ_2[a] (GM)
12a	B3LYP	*1*	3,08	7,2	-4,4	0,8	2,2	-3,9	0,5	7,7	-0,7	0,2	**110**
	ωB97XD	*1*	3,64	-0,5	-4,1	0,7	2,2	-4,0	0,7	8,5	-1,1	0,2	**11**
12b	B3LYP	*1*	2,98	27,8	-2,9	0,5	11,7	-3,3	0,5	-7,6	0,3	-0,0	**309**
	ωB97XD	*1*	3,63	17,4	-3,4	0,7	11,2	-3,6	0,8	-8,7	1,0	-0,2	**60**
12a	B3LYP	*2*	3,84							15,6	0,1	0,2	**812**[b]

[a] *computed from the expression for a two-state model (1);* [b] *computed from the expression for a three-state model (2)*

As we cannot experimentally measure the TPA cross sections below 680 nm, i.e. in the region where the maximum is predicted to show up, we extrapolate the values based on the 18 GM experimentally measured for **11** at 680 nm (Figure 19). First, the position of the TPA maximum is predicted based on the calculated energy shift between the OPA maximum (i=1 in Table S3) and TPA one (i=2 in Table S3). Converting to wavelengths, TPA maxima are predicted at 624 and 651nm for **11** and **19**, respectively. Next, we use the energy shift between twice the experimental OPA maximum (2×386nm) and 680 nm, which amount to 0.21 eV, to compute the TPA cross section at an equivalent spectral position (3.08/2 + 0.21= 1.75eV). To ensure best possible extrapolation, we also use in our calculations Γ = 0.2 eV, as extracted from experimental OPA spectra (see above) and compute the TPA cross section at 1.75 eV (709 nm) and at the maximum 1.92 eV (646 nm). Computed values are reported in Table S4 and are used to estimate the TPA cross section of **11** at 624 nm (343×18/77=80 GM). The later

value can be further used to estimate the cross section of **19** at 651 nm, based on the 7 GM extrapolated at 750 nm and the 5.6 GM experimentally measured at 760 nm for **11** (80×7/5.6=100 GM).

Table S4. Calculated TPA cross section (σ_2 in GM) at the TD-B3LYP/6-31G(d)//B3LYP/6-31G(d) level of theory using a linewidth broadening parameter Γ = 0.2 eV extracted from the OPA spectra reported Figure 13 (**11**) and S15 (**19**). Experimental data recorded on compound **11** at 680 nm and extrapolated value at 624 and 651 nm for **11** and **19**, respectively.

	Calculated (12a)		**Experimental (11)**	**Extrapolated (11)**	**Extrapolated (19)**
***ω* (eV)**	1.75	1.92	1.82	1.99	1.91
***λ* (nm)**	709	646	680	624	651
***σ₂* (GM)**	77	343	18	80	100

TPA spectroscopic measurement of 11

Two-photon-excited fluorescence spectra of the studied model fluorophore **11** in solution phase (concentration: 1×10^{-4} M) were measured according to the protocol established by Xu and Webb using Fluorescein (0.1 N NaOH solution) as the standard.[8] The experimental setup is illustrated in Figure S37. In brief, the excitation light source was a mode-locked Ti:Sapphire laser (Chameleon Ultra II, Coherent Inc.) which delivers ~140 fs pulses with the repetition rate of 80 MHz and the beam diameter of 2 mm. The intensity level of the excitation beam was carefully controlled by the combination of a λ/2 wave plate and a polarizer in order to avoid the saturation of absorption and photodegradation. To minimize the effects of re-absorption, the excitation beam was focused as close as possible to the wall of the quartz cell (10 mm×10 mm cuvette) and the up-converted emissions were collected and induced by a fiber bundle into a CCD imaging spectrometer (USB-4000, Ocean Optics) for the spectra recording. This

optical system was also utilized for the characterization of the quadratic dependence of the TPA-induced up-conversion emission intensity on the pumping intensity for every data point.

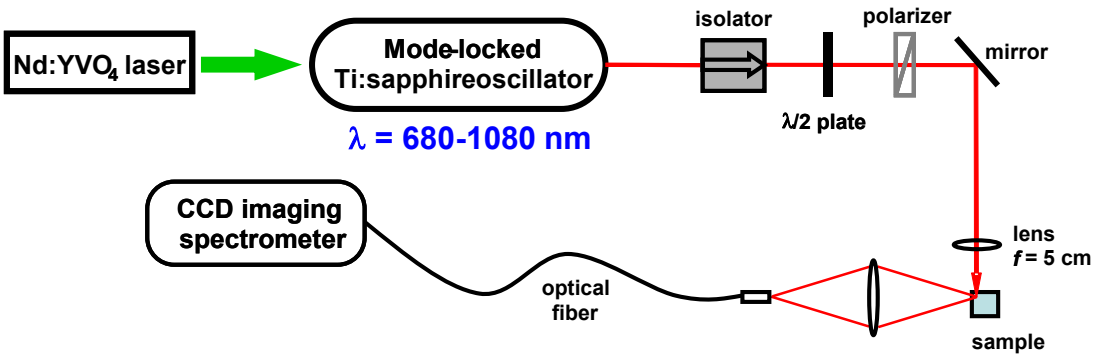

Figure S37. Optical setup for TPA spectrum measurement.

References of computational details

[1] Gaussian 03, Revision D.02, M. J. Frisch, G. W. Trucks, H. B. Schlegel, G. E. Scuseria, M. A. Robb, J. R. Cheeseman, J. A. Montgomery, Jr., T. Vreven, K. N. Kudin, J. C. Burant, J. M. Millam, S. S. Iyengar, J. Tomasi, V. Barone, B. Mennucci, M. Cossi, G. Scalmani, N. Rega, G. A. Petersson, H. Nakatsuji, M. Hada, M. Ehara, K. Toyota, R. Fukuda, J. Hasegawa, M. Ishida, T. Nakajima, Y. Honda, O. Kitao, H. Nakai, M. Klene, X. Li, J. E. Knox, H. P. Hratchian, J. B. Cross, V. Bakken, C. Adamo, J. Jaramillo, R. Gomperts, R. E. Stratmann, O. Yazyev, A. J. Austin, R. Cammi, C. Pomelli, J. W. Ochterski, P. Y. Ayala, K. Morokuma, G. A. Voth, P. Salvador, J. J. Dannenberg, V. G. Zakrzewski, S. Dapprich, A. D. Daniels, M. C. Strain, O. Farkas, D. K. Malick, A. D. Rabuck, K. Raghavachari, J. B. Foresman, J. V. Ortiz, Q. Cui, A. G. Baboul, S. Clifford, J. Cioslowski, B. B. Stefanov, G. Liu, A. Liashenko, P. Piskorz, I. Komaromi, R. L. Martin, D. J. Fox, T. Keith, M. A. Al-Laham, C. Y. Peng, A. Nanayakkara, M. Challacombe, P. M. W. Gill, B. Johnson, W. Chen, M. W. Wong, C. Gonzalez, and J. A. Pople, Gaussian, Inc., Wallingford CT, **2004**.

[2] Gaussian 09, Revision A.02, M. J. Frisch, G. W. Trucks, H. B. Schlegel, G. E. Scuseria, M. A. Robb, J. R. Cheeseman, G. Scalmani, V. Barone, B. Mennucci, G. A. Petersson, H. Nakatsuji, M. Caricato, X. Li, H. P. Hratchian, A. F. Izmaylov, J. Bloino, G. Zheng, J. L. Sonnenberg, M. Hada, M. Ehara, K. Toyota, R. Fukuda, J. Hasegawa, M. Ishida, T. Nakajima, Y. Honda, O. Kitao, H. Nakai, T. Vreven, J. A. Montgomery, Jr., J. E. Peralta, F. Ogliaro, M. Bearpark, J. J. Heyd, E. Brothers, K. N. Kudin, V. N. Staroverov, R. Kobayashi, J. Normand, K. Raghavachari, A. Rendell, J. C. Burant, S. S. Iyengar, J. Tomasi, M. Cossi, N. Rega, J. M. Millam, M. Klene, J. E. Knox, J. B. Cross, V. Bakken, C. Adamo, J. Jaramillo, R. Gomperts, R. E. Stratmann, O. Yazyev, A. J. Austin, R. Cammi, C. Pomelli, J. W. Ochterski, R. L. Martin, K. Morokuma, V. G. Zakrzewski, G. A. Voth, P. Salvador, J. J. Dannenberg, S. Dapprich, A. D. Daniels, Ö. Farkas, J. B. Foresman, J. V. Ortiz, J. Cioslowski, and D. J. Fox, Gaussian, Inc., Wallingford CT, **2009**.

[3] S. Tretiak, V. Chernyak, *J. Chem. Phys.* **2003**, *119*, 8809.

[4] F. Terenziani, C. Katan, E. Badaeva, S. Tretiak, M. Blanchard-Desce, *Advanced Materials* **2008**, *20*, 4641.

[5] S. Boinapally, B. Huang, M. Abe, C. Katan, J. Noguchi, S. Watanabe, H. Kasai, B. Xue and T. Kobayashi, *J. Org. Chem.*, **2014**, *79*, 7822.

[6] B. Xue, C. Katan, J. A. Bjorgaard, T. Kobayashi, *AIP Adv.*, **2015**, *5*, 12.

[7] Komori, N. and Jakkampudi, S. and Motoishi, R. and Abe, M. and Kamada, K. and Furukawa, K. and Katan, C. and Sawada, W. and Takahashi, N. and Kasai, H. and Xue, B. and Kobayashi, T., *Chem. Com.*, **2016,** *52*, 331.

[8] N. S. Makarov, M. Drobizhev and A. Rebane, *Opt. Express*, **2008**, *16*, 4029-4047.

Chapter 4

Conclusions and Outlook

Conclusions and Outlook:

In this research study, D-π-A and D-π-D based (coumarin-4yl)methyl type PPGs were synthesized. In terms of uncaging efficiency, D-π-D derivative is superior to the D-π-A analogues. According to the computational result, large MO coefficient on the carbon atom at 4-position in the LUMO seems to be an important factor for the design of (coumarin-4yl)methyl type PPG having efficient uncaging reaction. However, our D-π-D chromophore does not show high TPA cross-section over 700 nm, which is a remaining problem for TP uncaging reaction. To overcome this issue, π-extension on the 3-position will be one of the effective strategies. The detail investigation of photophysical and photochemical character of π-extended coumarin chromophore is the next interesting topic.

List of Publications

公表論文

(1) “Design, Synthesis, and Reaction of π-Extended Coumarin-based New Caged Compounds with Two-photon Absorption Character in the Near-IR Region”
Youhei Chitose, Manabu Abe,* Ko Furukawa, and Claudine Katan*
Chem. Lett. **2016**, *45*, 1186–1188.

(2) “Design and Synthesis of a Caged Carboxylic Acid with a Donor−π−Donor Coumarin Structure: One-photon and Two-photon Uncaging Reactions Using Visible and Near-Infrared Lights”
Youhei Chitose, Manabu Abe,* Ko Furukawa, Jhe-Yi Lin, Tzu-Chau Lin,* and Claudine Katan*
Org. Lett. **2017**, *19*, 2622−2625.

参考論文

(1) “Design and Synthesis of Two-Photon Responsive Chromophores for Near-Infrared Light-Induced Uncaging Reactions”
Manabu Abe,* Youhei Chitose, Satish Jakkampudi, Pham Thi Thu Thuy, Qianghua Lin, Bui Thi Van, Ayato Yamada, Ryoko Oyama, Miyu Sasaki, and Claudine Katan*
Synthesis, **2017**, *49* (5), 3337-3346.

(2) “２光子応答性ケージド化合物”
千歳　洋平，安倍　学*
光化学, **2017**, *48* (3), 130-138.

(3) “Design and synthesis of two-photon responsive chromophores for application to uncaging reactions”
Youhei Chitose, Manabu Abe*
Photochemistry, **2019**, *46*, 219-241.

(4) Convenient one-pot access to 2H-3-nitrothiochromenes from 2-bromobenzaldehydes, sodium sulfide and β-nitrostyrenes”
Thi Thu Huong Le, Chitose Youhei, Quy Hien Le, Thanh Binh Nguyen,* Dinh Hung Mac*
Org. Biomol. Chem., **2019**, *17*, 6355-6358.

Acknowledgement

All the research works described in this dissertation have been carried out under the guidance of Professor Manabu Abe at the Department of Chemistry, Graduate School of Science, Hiroshima University. My research work was supported by JSPS KAKENHI Grant Number JP18J20500.

I would like to express my sincere gratitude to my supervisor, Prof. Manabu Abe for his outstanding education, advice, support, guidance, and excellent encouragement throughout my research studies.

I wish to thank Dr. Sayaka Hatano and Dr. Ryukichi Takagi for their excellent support, discussions, and educations during my research work in our laboratory.

I am deeply grateful to Prof. Tzu-Chau Lin (National Central University), Dr. Claudine Katan (Université Rennes, France), and Dr. Ko Furukawa (Niigata University) for their excellent collaborations.

I also would like to express my appreciation to our lab members for giving me comfortable environment in laboratory.

Finally, I would like to express my heartfelt gratitude to my family and relatives for their excellent support, kindness, and giving birth to me.

February 2021

Youhei Chitose
Department of Chemistry, Graduate School of Science
Hiroshima University